AD-A133 735 RF SYTEMS IN SPACE VOLUME II SPACE-BASED RADAR ANALYSES 1/3
            (U) GENERAL RESEARCH CORP SANTA BARBARA CA
   A V MRSTIK ET AL. APR 83 RADC-TR-83-91-VOL-2
UNCLASSIFIED F30602-81-C-0119   F/G 17/9   NL
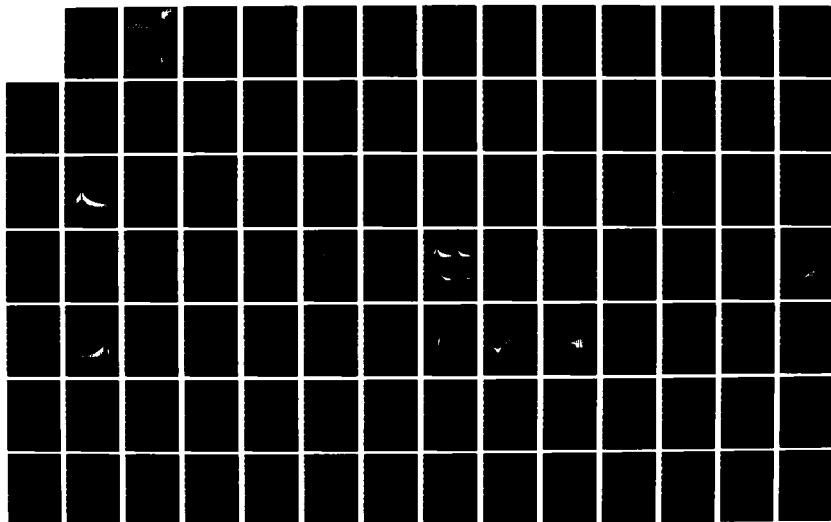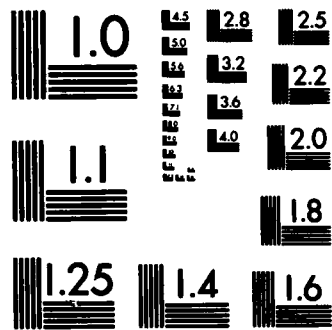
MICROCOPY RESOLUTION TEST CHART

NATIONAL BUREAU OF STANDARDS-1963-A

AD-A133735

RF SYSTEMS IN SPACE
Space-Based Radar Analyses

General Research Corporation

A. V. Mrstik, D. Beste, R. J. Bartek and P. M. Pazick

DTIC
SELECTED
OCT 18 1983
D

ROME AIR DEVELOPMENT CENTER
Air Force Systems Command
Griffiss Air Force Base, NY 13441

DTIC FILE COPY

This report has been reviewed by the RADC Public Affairs Office (PA) and is releasable to the National Technical Information Service (NTIS). At NTIS it will be releasable to the general public, including foreign nations.

RADC-TR-83-91, Volum II (of two) has been reviewed and is approved for publication.

APPROVED: *John C. Cleary*

JOHN C. CLEARY
Project Engineer

APPROVED: *Frank J. Rehm*

FRANK J. REHM
Technical Director
Surveillance Division

FOR THE COMMANDER: *John P. Huss*

JOHN P. HUSS
Acting Chief, Plans Office

REPORT DOCUMENTATION PAGE	READ INSTRUCTIONS BEFORE COMPLETING FORM

1. REPORT NUMBER	2. GOVT ACCESSION NO.	3. RECIPIENT'S CATALOG NUMBER
RADC-TR-83-91, Volume II (of two)	AD-A133736	

4. TITLE (and Subtitle)	5. TYPE OF REPORT & PERIOD COVERED
RF SYSTEMS IN SPACE Spaced-Based Radar Analyses	Final Technical Report
	6. PERFORMING ORG. REPORT NUMBER
	N/A

7. AUTHOR(s)	8. CONTRACT OR GRANT NUMBER(s)
A. V. Mrstik P. M. Pazick D. Beste R. J. Bartek	F30602-81-C-0119

9. PERFORMING ORGANIZATION NAME AND ADDRESS	10. PROGRAM ELEMENT, PROJECT, TASK AREA & WORK UNIT NUMBERS
General Research Corporation P. O. Box 6770 Santa Barbara CA 93111	62702F 45061450

11. CONTROLLING OFFICE NAME AND ADDRESS	12. REPORT DATE
Rome Air Development Center (OCSA) Griffiss AFB NY 13441	April 1983
	13. NUMBER OF PAGES
	214

14. MONITORING AGENCY NAME & ADDRESS(if different from Controlling Office)	15. SECURITY CLASS. (of this report)
Same	UNCLASSIFIED
	15a. DECLASSIFICATION/DOWNGRADING SCHEDULE
	N/A

16. DISTRIBUTION STATEMENT (of this Report)

Approved for public release; distribution unlimited.

17. DISTRIBUTION STATEMENT (of the abstract entered in Block 20, if different from Report)

Same

18. SUPPLEMENTARY NOTES

RADC Project Engineer: John C. Cleary (OCSA)

19. KEY WORDS (Continue on reverse side if necessary and identify by block number)

Simulation
Space-Based Radar
Space Fed Phased Array

20. ABSTRACT (Continue on reverse side if necessary and identify by block number)

The main objective of this effort was to develop a computer based analytical capability for simulating the RF performance of large space-based radar (SBR) systems. The model is capable of simulating corporate and space fed aperture. The model also can simulate multibeam feeds, cluster/point feeds, corporate feed and various aperture distributions. The simulation is capable of accepting Draper Labs structural data and antenna current data from Atlantic Research Corporation's (ARC) First Approximation Methods (FAM) and Higher Approximation Methods (HAM) models. In addition there is a routine to input various aper-

DD FORM 1473   EDITION OF 1 NOV 65 IS OBSOLETE
1 JAN 73

tures surface distortions which causes the elements in the array to be dis-
placed from the ideal location on a planar lattice.

There were analyses looking at calibration/compensation techniques for large
aperture space radars. Passive, space fed lens SBR designs were investigated.
The survivability of an SBR system was analyzed. The design of ground based
SBR validation experiments for large aperture SBR concpets were investigated.
SBR designs were investigated for ground target detection.

Accession For	
NTIS GRA&I	☒
DTIC TAB	☐
Unannounced	☐
Justification	

By	
Distribution/	
Availability Codes	
Dist	Avail and/or Special
A	

PREFACE

This final report presents results of an 18-month study on Radio Frequency (RF) Systems in Space. The study was performed for the Rome Air Development Center (RADC) by General Research Corporation (GRC). The work performed under this contract is presented in the following five reports:

1. A.C. Ludwig, J. Feeman, A.V. Mrstik, and J. Gardner, RF Systems in Space—Interim Report, General Research Corporation CR-1-1048, September 1982.

2. A.C. Ludwig, J. Feeman, and J. Capps, RF Systems in Space—Final Report, Vol. I, Space Antenna Radio Frequency (SARF) Simulation, General Research Corporation CR-2-1048, December 1982.

3. A.V. Mrstik, D. Beste, R. Bartek, and P. Pazich, RF Systems in Space—Final Report, Vol. II, Space-Based Radar Analyses, General Research Corporation CR-2-1048, December 1982.

4. J.R. Feeman and J.D. Capps, SARF User's Manual, General Research Corporation CR-3-1048, December 1982.

5. J.R. Feeman and J.D. Capps, SARF Sample Computer Simulation Runs, General Research Corporation CR-4-1048, December 1982.

The objectives of the study are:

1. To develop and validate a space-antenna RF (SARF) simulation for modeling the RF performance of large, space-based radar systems

2. To develop calibration/compensation techniques for large-aperture space radars

3. To investigate passive, space-fed lens, space-based radar designs

4. To analyze the survivability of space radar

5. To design ground-based validation experiments for large-aperture space radar concepts

6. To investigate space radar designs for ground target detection

The first objective represents 2/3 of the total effort, and is covered by reports 1, 2, 4, and 5. The remaining objectives, 2 through 5, are covered by report 3. The technical sections of the Interim Report are reproduced as Appendix A of Vol. I.

CONTENTS

CONTENTS (Cont.)

ILLUSTRATIONS

ILLUSTRATIONS (Cont.)

ILLUSTRATIONS (Cont.)

ILLUSTRATIONS (Concl.)

TABLES

TABLES (Cont.)

3   ANTENNA CALIBRATION AND COMPENSATION

3.1   INTRODUCTION AND SUMMARY

The antenna calibration and compensation task was undertaken with three principal objectives:

1. **Performance Monitoring**—Investigate approaches for measuring the structural and electronic state of the system.

2. **Error Compensation**—Develop compensation techniques to obtain the optimum RF performance given the state of the system.

3. **Technology Needs**—Identify technical areas needing advancement in order to accomplish calibration and compensation.

The motives for pursuing these objectives are evident. The SBR is a very large, complex electronic system which must operate in the hostile environment of space in spite of mechanical and electrical failures or natural and man-made disturbances. Furthermore, once in orbit, the system will be inaccessible; it cannot be recalled for further ground testing and modification to correct problems and to compensate for failures. The system performance must be monitored in space; any compensation for failures or other sources of degradation must be performed within the system itself or under remote control from the ground.

Performance Monitoring

Some types of failures will be detectable without special performance monitoring techniques: it will be immediately apparent that the system is malfunctioning. Special testing will be required, however, to detect failures that cause more subtle degradation in system performance. For example, if the radar's effective radiated power were only slightly degraded, the system could continue to detect and track the manned aircraft normally seen, and it might not be apparent that a number of problems exist, including the following: (1) inadequate

11

sensitivity to detect the smaller targets of interest (e.g., cruise missiles), (2) degraded tracking accuracy, or (3) erroneous RCS estimates.

Alternative methods for monitoring each of the critical functions are discussed, with a brief note on the advantages and disadvantages of each method. Promising candidates are identified.

The bottom line of this study of performance monitoring is that because of the unique functions performed by the SBR, some special test procedures will be necessary. Additional electronic equipment may have to be developed to implement some of these tests. However, the requirements are well within the state-of-the-art; with adequate planning and attention to detail, they can easily be provided for.

Error Compensation

In Secs. 3.2-3.4 we examine techniques to detect and compensate for antenna errors. The intent is to maintain antenna performance in the presence of component failure and degradation which should be anticipated in the space environment.

In pursuing this task, we focused on those compensation techniques which are unique to a large-aperture spacecraft antenna. Three generic types of degradation were of concern:

1. Array Distortions--Deviations of the array element positions as a result of distortions in the array surface

2. Module Failures--Failures of the elements to control the phase and/or amplitude of their radiation

3. Feed Failures--Failures of the feed system to properly deliver the signal energy to the radiating elements, or collect the signal energy from the receive elements

12

One should not infer that these are the only important types of degradation, nor the only ones for which compensation techniques might be desired. Other types of failures such as blown-out power amplifiers, failed digital processors, failed signal processors, etc., are of course also possible and will have to be considered. However, these types of failures are not unique to the large-aperture radars of interest here. They are a problem for many systems, and have been dealt with on many existing systems.

After considering the three generic types of degradation, we elected to focus our efforts on the first type, array distortions. We selected this one for a number of reasons. First, we had reason to suspect (as later borne out in our detailed analysis) that the nominal thermally-induced distortions in the proposed membrane arrays would seriously degrade the radar performance. Some compensation would be required. Second, despite the need for aperture compensation, little thought had previously been given to how to accomplish it. Finally, we had some ideas as to how the required compensation could be achieved.

The following questions were addressed:

1. What distortions can be expected?

2. What is the effect of these distortions on the antenna radiation pattern?

3. What methods can be used to detect the distortions?

4. What methods can be used to compensate for distortions?

5. How effective are the compensation methods?

Two general types of errors were examined: (1) random errors, which are uncorrelated element-to-element, and (2) systematic errors, which are correlated across the aperture. The effects of these types of errors on the antenna gain and sidelobe levels were quantified as a

13

function of the amount of distortion. This quantitative data is presented in Sec. 3.2 and can be used to determine the maximum acceptable distortion consistent with a beam pattern of specified quality. In the absence of distortion compensation, these specifications define the mechanical limits to which the array must be designed.

Estimates of the expected distortion of the membrane array due to thermal effects were derived independently by Draper Laboratories and General Dynamics. Both companies arrived at similar results which predict a radial stretching and contraction of the membrane as it passes in and out of the earth's shadow and changes its orientation with respect to the sun. Using the predicted radial distortions as input to our antenna pattern simulation SARF, we found that the antenna pattern degradation will be unacceptable. Unless some form of compensation is employed, the antenna will not meet its design specification over the required field-of-view.

Section 3.2 also evaluates the effectiveness of phase compensation to correct for the aperture distortions. Two forms of phase compensation are considered: one at the individual element level, the other at an aggregate level in which a large number of nearby elements are treated as a single unit for compensation. This latter approach is of interest since it could be implemented within the feed of a multiple-beam feed without disturbing the array elements within the lens.

While investigating phase compensation we came across a very interesting fact. The textbooks and papers in the literature seem to lump together their discussions of the effects of array element position errors with their discussion of element phase errors. When considering displacement errors, the authors invariably translate the displacement errors into phase errors and then proceed from that point on by modeling the effects as entirely due to phase errors. Although this is an acceptable approach for considering a given direction of radiation (such

14

as in the mainbeam direction), it is not useful for evaluating the effects on the total radiation pattern (i.e., in other directions). The problem is that an array element displacement error produces a phase error which is direction-dependent. Thus, a displacement cannot be treated solely as a phase error. The analyses in Sec. 3.2 recognize this problem and account for the fundamental distinction between phase errors and displacement errors. Space-fed and corporate-fed arrays are individually considered, since the effects of distortions are quite different for these two cases.

Another very interesting and related observation is the fact that phase compensation alone cannot totally compensate for any displacement error. If an element is shifted from its desired location, a correcting phase shift could be introduced by the element. However, the amount of the phase correction would be a function of the direction of the element displacement <u>relative to the direction in which the antenna pattern is to be corrected</u>. In other words, we can use phase compensation to restore the beam in one specified direction, but we cannot restore the antenna pattern in all directions simultaneously. Phase compensation will be less and less effective as we move away from the "preferred direction" (i.e., the direction for which the correcting phases were selected).

In Sec. 3.2 we determine the residual antenna pattern degradation after phase compensation has been applied. Both random and systematic distortions are considered. The results can be briefly summarized by the following:

1.   Phase compensation can substantially reduce the sensitivity to random and systematic errors. When using the anticipated thermally produced distortions predicted by Draper Laboratories and General Dynamics, we find that the resulting radiation pattern does not meet the SBR specifications. However, by using phase compensation, the specified performance can be achieved.

15

2.   If the distortion errors are uncorrelated element-to-element
      or of high spatial frequency, the correction must be done at
      the individual elements and thus would impact the design of
      the array lens.

3.   If the distortion errors vary slowly across the lens, the
      correction can be done entirely within the feed without dis-
      turbing the lens components.

4.   A great deal of effort has been devoted by Grumman and
      others to developing a lens structure which has minimum dis-
      tortion due to thermal and other effects. If one started
      off recognizing the possibility of phase compensation, it
      might be possible to alleviate some of the tight structural
      requirements and arrive at a more efficient and cost-
      effective design.

5.   Although phase compensation appears adequate to compensate
      for the anticipated array distortions, in light of (4)
      above it might be desirable to design for even greater
      amounts of distortion than previously considered. In this
      way it might be possible to further reduce the structural
      requirements. As the amount of distortion is increased, the
      point will eventually be reached at which phase compensation
      alone will no longer be adequate to restore the beam. For
      these larger distortions, amplitude correction as well as
      phase correction may be necessary. The effectiveness of
      phase/amplitude compensation should be examined further. A
      question which needs to be addressed is as follows: Can
      phase/ amplitude compensation totally compensate for arbi-
      trary displacement errors? To the authors' knowledge, this
      question has not been addressed in the literature to date.

Distortion Sensing

Up to this point, we have been addressing the impact of distortion
errors and the effectiveness of phase compensation. If distortion is to

16

be compensated, it must of course first be sensed. Section 3.3 describes a spectrum of distortion sensing methods ranging from "indirect" methods which depend heavily on the use of models which estimate the distortion on the basis of a few temperature or strain measurements, to "direct" methods which measure the position of each element. A number of the methods investigated continue to appear promising and deserve further consideration.

One particularly attractive method is based on the use of a phase detector and small amount of digital logic within each array module. With this method, described further in Sec. 3.4, each array element is self surveying and computes the desired phase correction to compensate for distortion-induced errors. By building this capability into each module, the lens could be self-correcting and substantially more tolerant to lens displacement errors. The digital logic to implement this scheme is minimal and of little consequence. The required phase detector should likewise not be a major problem. In fact, General Electric has already designed a phase detector for use in the array modules to detect and correct for errors in the module phase shifters.[1] This same phase detector could also be used to compensate for displacement errors.

Recommendations

As a result of this study, we recommend that the following technical issues be pursued on future programs to assess and develop promising calibration and compensation techniques:

1. Additional Sources of Failure—As noted earlier, we have focused on one source of error (array distortions) which appears to have been given little attention in the past. Other types of failures and errors within the array modules and the feed should also be investigated further.

---

[1] R.J. Naster et al., *Adaptive Transmitter Techniques*, General Electric Company, RADC-TR-80-344, November 1980.

One particular area which should be addressed is failure or loss of control of individual or groups of array modules. Some work has been done in the past on this subject, although this has not received as much attention as it merits. One promising method of compensating for module failures would be to increase the power radiated by adjacent modules. A paper by A.C. Ludwig[1] suggests that large regions of outage could be compensated by proper amplitude control of the remaining elements.

2. Structural Analyses—The results of this work clearly show that the requirement for compensation as well as the effectiveness of the various compensation techniques depends highly on both the magnitude and the functional form of the array distortions. Because of this sensitivity, we recommend that further structural analyses be undertaken to predict the expected array distortions of candidate SBR designs of key interest.

In addition, the structural analyses should be integrated with the electronic analyses so as to allow tradeoffs between the mechanical requirements and the requirements for electronic compensation. It seems to us that, to date, the mechanical designers have not been free to take advantage of electronic compensation to lessen their design burden. The key questions are: how would the mechanical design change if electronic compensation were used, and what would be the payoff?

3. Phase and Amplitude Compensation—The current analysis focused on phase compensation techniques. If larger mechanical errors are to be tolerated, it will be necessary to

---

[1] A.C. Ludwig, "Low Sidelobe Aperture Distributions for Blocked and Unblocked Circular Apertures," IEEE Transactions on Antennas and Propagation, AP-30, No. 5, September 1982.

18

use both amplitude and phase compensation. Before pursuing this path, a very basic but apparently unexplored issue must be addressed: Is it possible to use phase and amplitude compensation to simultaneously preserve both mainbeam gain and low sidelobes in all regions of interest?

4. Implementation of Compensation Techniques--The RF distortion sensing and compensation techniques identified in this report should be investigated further. Specific designs should be considered. General Electric has a preliminary design for a phase detector which could be used with each module for self-location and self-compensation. GE's development of this phase detector should be continued and integrated with the basic module designs. Logic and algorithms for self-compensation should be developed along with a detailed investigation of the accuracy, advantages, and disadvantages of the alternative self-surveying techniques. Similar work should be done for the feed compensation schemes.

The following four subsections present the technical considerations leading to the above conclusions and recommendations. Section 3.2 considers the impact of various types of lens distortions and how these distortions might be compensated. Section 3.3 describes various methods of sensing the presence of lens distortion. Section 3.4 considers some promising methods of implementing the distortion compensation techniques. Finally, Sec. 3.5 describes various means of monitoring the performance of an SBR.

3.2 ERROR COMPENSATION

The expansion and contraction of the SBR array face and its supporting structure due to thermal effects in orbit will cause the array elements to shift from their nominal positions. In this section we address two key questions, as follows:

19

1. What is the expected impact of these distortions on the antenna radiation pattern?

2. How effective could electronic compensation be in restoring the desired pattern?

Since the effects of distortion will depend on the functional form of this distortion, we have investigated two generic types of distortion: Random and Systematic (Table 3.1). "Random" distortions refer to those which are random and uncorrelated element-to-element. These errors would probably be the natural result of manufacturing tolerances and most likely would be quite small. The "Systematic" errors could be considerably larger and might result from thermal effects and deployment errors, as well as manufacturing errors. The error types listed in Table 3.1 are discussed in the following subsections, where quantitative estimates of the degradation of the antenna pattern are derived as a function of the amount of distortion.

In this investigation, we depend heavily on the use of the antenna pattern generation program SARF. The program is used first to compute the pattern of an undistorted array, second to compute the pattern with

TABLE 3.1

DISTORTION TYPES INVESTIGATED

Random
>   In-Plane Errors
>   Out-of-Plane Errors
>   Simultaneous In- and Out-of-Plane Errors

Systematic
>   Parabolic
>   Sinusoidal
>   In-Plane Linear Stretch

the specified distortions, and finally to compute the resulting pattern
after various types of electronic compensation (discussed later). In
addition to generating the radiation pattern for each of the above con-
ditions, the program computes three performance parameters, as follows:

1. Peak Gain

2. RMS Sidelobe Level

3. Peak Sidelobe Level

These three parameters are useful tools for characterizing the pattern
quality in simple terms. For a given antenna pattern, there is a single
peak gain and a single peak sidelobe. However, the sidelobes will gene-
rally vary substantially with direction. Thus, the "RMS Sidelobe Level"
is computed as a function of angle off the direction of peak gain. The
root-mean-square (RMS) value is computed over a region extending ± 1
degree about this angle. At L-Band this 2 degree region includes about
ten sidelobe phase reversals of an ideal antenna of 71 m diameter.

A major problem in investigating the effects of distortions on the
large antennas of interest[1] is that hours of computer time would be
needed to compute the radiation pattern for any one set of conditions.
Since we were interested in parametrically investigating many different
conditions, some other approach had to be found. The approach that we
eventually settled on was to use the simulation to compute the patterns
of linear arrays and then scale the results to the planar arrays of
interest. A linear array model was selected consisting of 422 elements
with a 0.7λ spacing and a 45 dB Taylor illumination taper.

This approach was selected for a number of reasons, including the
following:

1. The square root reduction in number of array elements and
    radiation directions reduced the computing time from impos-
    sible to insignificant.

_____

[1] The normal design of primary interest to RADC has circular aperture of
71 m diameter and approximately 131,000 elements.

2. The beamwidth and sidelobe structure of the 71 m linear array would be comparable to that of the 71 m diameter planar array of primary interest.

3. Although the linear array's maximum gain of 24.9 dB is a long way from the 56 dB gain of the planar array, the gain loss for small random displacement errors will be comparable for the two cases. In the case of random displacement errors the loss in peak gain can be shown (see later discussion in Sec. 3.2.1.2) to be independent of the number of array elements. Thus, the performance of the 422 element linear array, with various amounts of random element displacement, should be useful for evaluating the gain loss which would be experienced for the 71 m diameter planar array with its 131,000 elements.

4. Although the sidelobes relative to peak gain will be radically different for the planar and linear arrays, the RMS sidelobes relative to isotropic will be comparable for situations in which the sidelobe level is dominated by random displacement errors. With a 45 dB Taylor illumination, the 422 element linear array yields sidelobes 20 dB or more below isotropic in the absence of displacement errors. Thus, the effects of any degradation which brings the sidelobes within 5 or 10 dB of isotropic (as specified for the 71 m planar array) will be immediately apparent.

As noted above, the linear array model is desirable from the computational standpoint and can be theoretically shown to yield useful data on gain loss and RMS sidelobe levels relative to isotropic for random displacement errors. However, there remains the question of its merit when the displacement errors are systematic rather than random. The answer must of course depend on the amplitude and functional form of the displacement errors; but for small errors the linear array is probably a reasonable analysis tool. With this caution in mind, we have

22

used the linear array. For some cases of particular interest (as noted later in Sec. 3.2.4), we have checked the results by computing the radiation pattern for a planar array as well.

Figure 3.1 shows the ideal pattern for the 422 element linear array in the absence of distortion errors. This error-free pattern is given here for later comparison with the patterns for distorted arrays.

3.2.1 Random Element Position Errors

The impact of random element positions before and after phase compensation is addressed in the following subsections. Both corporate and space-fed arrays are examined.

3.2.1.1 Phase Errors

Figure 3.2 depicts the geometries for corporate and space-fed arrays. An example element is shown which is displaced a distance Δx in the plane of the array and a distance Δy out of plane. In the case of the corporate feed, a ray from the displaced element will be shifted relative to its error-free length by an amount

$$\Delta P = \sin \theta \Delta x + \cos \theta \Delta y \tag{3.1}$$

where θ is the direction of radiation measured as an angle off of the array axis. Thus in the direction θ , the displaced element will introduce a phase error

$$\Delta \phi = \frac{2\pi}{\lambda} \Delta P \tag{3.2}$$

where λ is the signal wavelength.

For normally distributed random displacement errors which are uncorrelated in the x and y directions, Eqs. 3.1 and 3.2 can be used to derive the variance of the phase error in direction θ as follows:
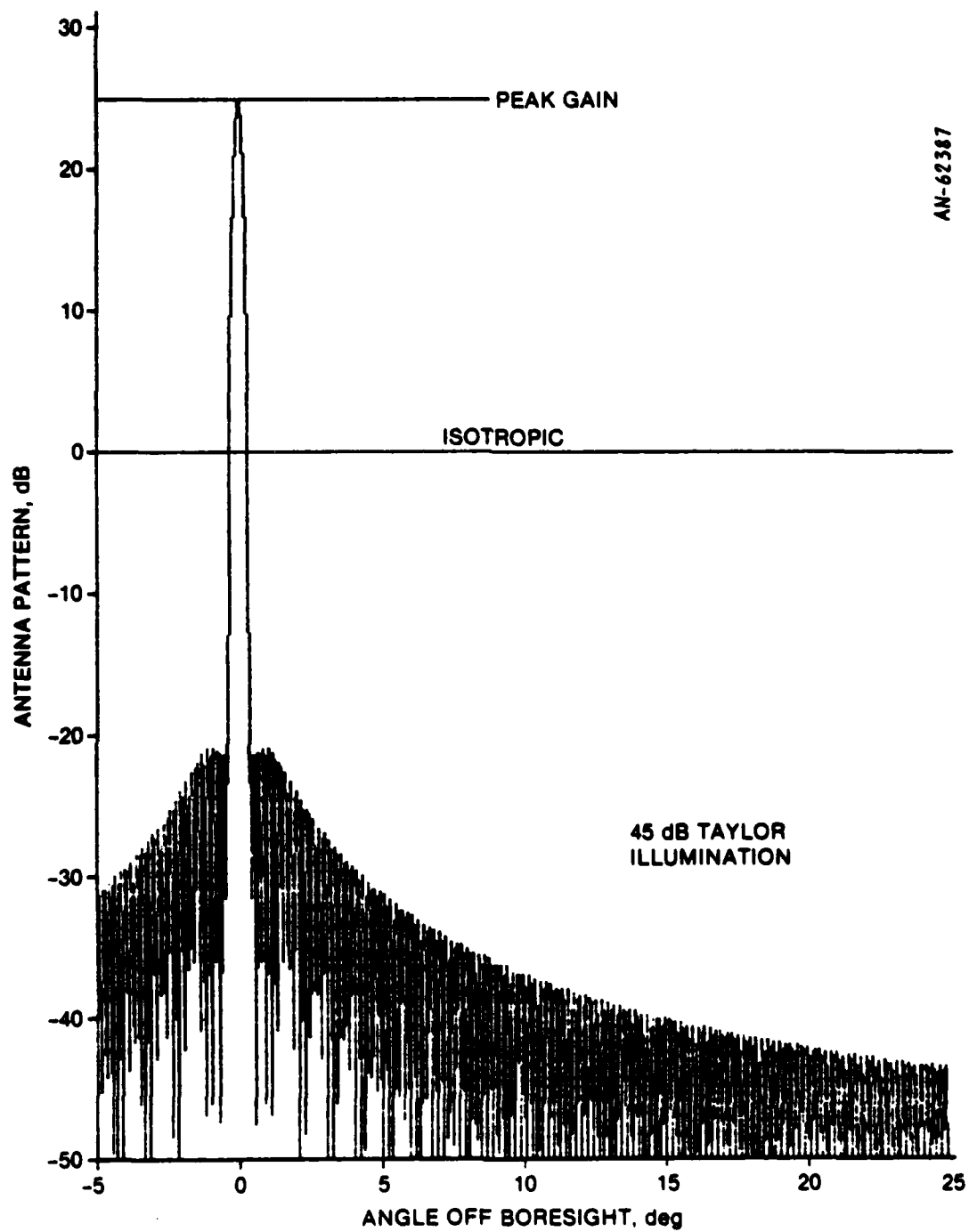
Figure 3.1.   Error-Free Radiation Pattern

CORPORATE FEED

EXAMPLE
DISPLACED
ELEMENT

UNDISTORTED
ELEMENT
LOCATIONS

PATH LENGTH
ERROR, ΔP

$\Delta P = \sin \theta \, \Delta X + \cos \theta \, \Delta Y$

SPACE FEED

AN-63640

FEED

$\Delta P = \sin \theta \, \Delta X + \cos \theta \, \Delta Y + \ell_D - \ell_A$
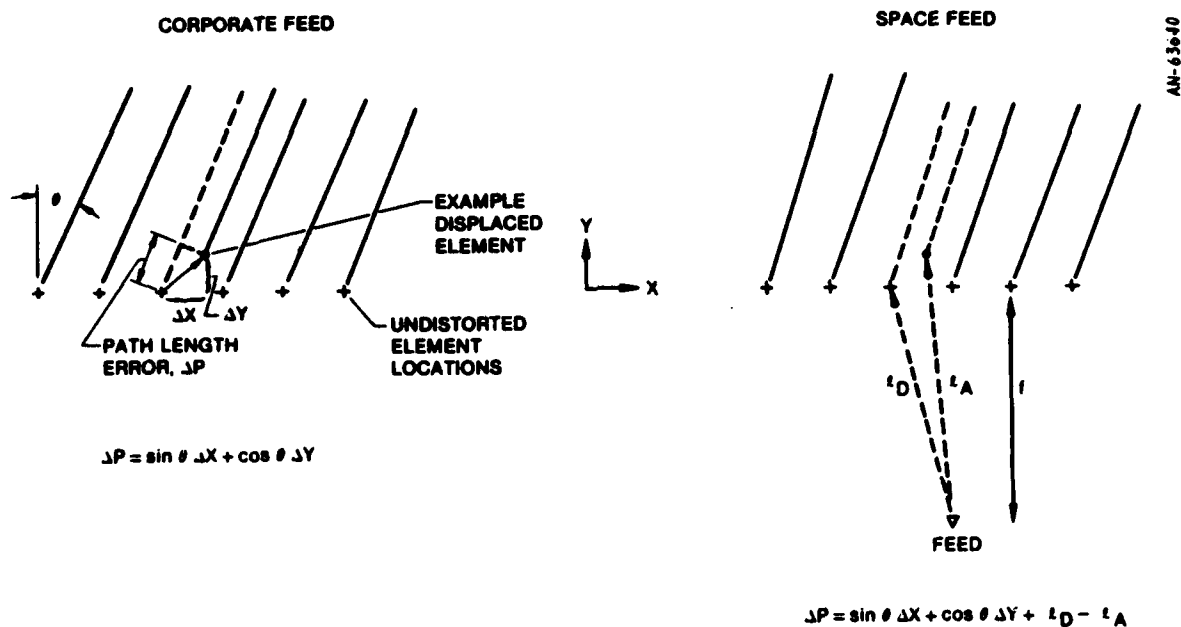
Figure 3.2. Element Position Errors

$$\sigma_\phi^2 = \left(\frac{2\pi}{\lambda}\right)^2 \left[\sigma_x^2 \sin^2 \theta + \sigma_y^2 \cos^2 \theta\right] \qquad (3.3)$$

where σ_x^2 and σ_y^2 are the variances of the displacement error in the x and y directions. If the x and y distortions have the same variance, Eq. 3.3 reduces to the following simple expression:

$$\sigma_\phi^2 = \left(\frac{2\pi}{\lambda}\right)^2 \sigma_x^2 \qquad (3.4)$$

Comparable expressions for a space-fed array are slightly more complicated since any displacement of the element also changes the phase of the element excitation (see Fig. 3.2). The composite shift in path length for a ray at an angle θ with aspect to the array axis is given by

25

$$\Delta P = \sin \theta \Delta x + \cos \theta \Delta y + \ell_D - \ell_A$$

where ℓ_D is the distance between the feed and the undisturbed element location, and ℓ_A is the distance between the feed and the displaced element. The above equation can be approximated by

$$\Delta P \approx \left(\sin \theta - \frac{x}{\sqrt{x^2 + f^2}} \right) \Delta x + \left(\cos \theta - \frac{f}{\sqrt{x^2 + f^2}} \right) \Delta y \qquad (3.5)$$

where f is the perpendicular distance from the feed to the array. Again, assuming the x,y displacement errors are uncorrelated and normally distributed, Eq. 3.5 leads to the following phase variance:

$$\sigma_\phi^2 = \left(\frac{2\pi}{\lambda} \right)^2 \left[\sin \theta - \frac{x}{\sqrt{x^2 + f^2}} \right]^2 \sigma_x^2 + \left(\frac{2\pi}{\lambda} \right)^2 \left[\cos \theta - \frac{f}{\sqrt{x^2 + f^2}} \right]^2 \sigma_y^2 \qquad (3.6)$$

If σ_x and σ_y are equal, Eq. 3.6 reduces to the following expression:

$$\sigma_\phi^2 = 2 \left(\frac{2\pi}{\lambda} \right)^2 \left[1 - \frac{x \sin \theta + f \cos \theta}{\sqrt{x^2 + f^2}} \right] \sigma_x^2 \qquad (3.7)$$

3.2.1.2 Gain Degradation

The loss of antenna gain due to phase errors has been investigated by Ruze and others.[1] For small phase errors, the relative gain (i.e., the gain with errors relative to the error-free gain) is given by

$$\frac{G}{G_o} \approx 1 - \overline{\delta^2} \qquad (3.8a)$$

---

[1] John Ruze, "Antenna Tolerance Theory—A Review," _Proceedings of the IEEE_, Vol. 54, No. 4, April 1966, pp. 633-640.

where $\overline{\delta^2}$ is the RMS phase error across the aperture weighted by the illumination taper. For an N element linear or planar phased array

$$\overline{\delta^2} = \frac{\sum_{n=1}^{N} A_n \sigma_{\phi_n}^2}{\sum_{n=1}^{N} A_n} \qquad (3.8b)$$

where A_n is the illumination amplitude (voltage or current) on the nth element, and $\sigma_{\phi_n}^2$ is the variance of the phase error of the nth element.

Figure 3.3 shows the relative gain computed using Eq. 3.8 with the phase errors given by Eq. 3.4 (Corporate Fed Arrays) and Eq. 3.7 (Space Fed Arrays). For both antenna types, the displacement errors are normally distributed and uncorrelated in both the in-plane and out-of-plane directions. For the space-fed design, it was assumed that the distance f between the feed and the array plane was 1.4 times the array width (i.e., f = 100 meters for the nominal 71 m diameter aperture).

Referring to the figure, one can see that the relative gain of the corporate feed, which is independent of scan angle, drops rapidly for position errors beyond a few hundredths of a wavelength. The space-fed array is substantially more tolerant of position errors: when focused on axis it can tolerate position errors of several tenths of a wavelength before the relative gain drops precipitously. The reason for this greater tolerance can be seen easily by referring back to Fig. 3.2. Note that an element located at the center of the array can move forward or backward (in the y direction) without generating any phase error for a beam directed on-axis. The phase change for the path on the feed
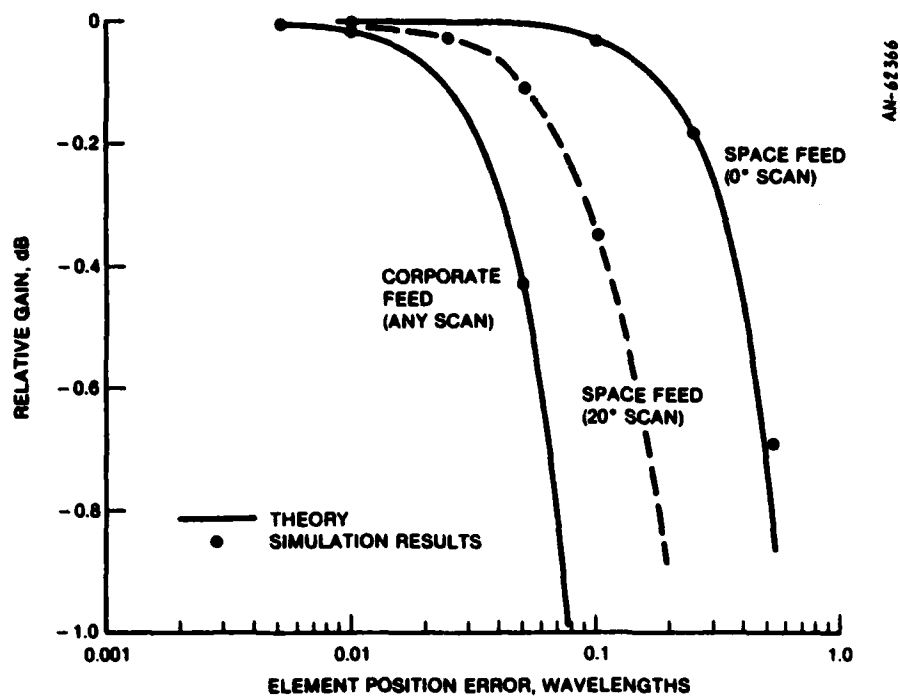
Figure 3.3. Gain Loss--Sensitivity to Random Element Position Errors

side is exactly compensated by the phase change on the target side. In-plane variations do cause a slight phase error, but for elements near the center and normal feeds which are many wavelengths behind the array, the resulting phase error is negligible. As one moves toward the edge of the array, the self-compensation is not as effective, although the error is always substantially less than that for a corporate feed.

The tolerance of a space-fed design to displacement errors decreases as the array is scanned off-axis. The results for a 20° scan angle are shown in the figure.

The lines in the figure were computed using conventional array theory and the equations cited earlier. The solid dots are sample points which were computed with the antenna pattern program SARF. As

can be seen from the figure, the theoretical results and the simulation results are indistinguishable for all test cases except the one computed for the space feed at 0° scan with 0.5λ position errors. The slight disagreement between the two results no doubt reflects the fact that the theory assumes the phase errors are small. At 0.5λ displacements, the phase errors are no longer small and the theory begins to break down.

The curves in Fig. 3.3 along with the equations given earlier can be used to relate gain loss to element position errors. Thus, in the absence of any electronic compensation (discussed in the next section), these results could be used to specify how much random element displacement could be tolerated, while remaining within a specified gain loss budget.

3.2.1.3 Gain Degradation After Phase Compensation

Equations 3.1 and 3.5 given previously relate the path length error in a given direction to the element displacement. For a given frequency, this path length can be equated to a phase delay which could, in principle, be compensated for by electronically advancing or retarding the phase of each element by an amount dependent on its displacement. If we assume for the moment that an appropriate means of implementing such a scheme could be found,[1] it would be possible to compensate for the displacement errors in a preferred direction. The correcting phase would have to be adjusted as the antenna is scanned. In the absence of such an adjustment, the phase error of each element would increase as the antenna is scanned off the "preferred" direction for which the compensating phases were computed.

It can be shown that the element phase error after compensation is given by

---

[1] Methods of sensing the element displacement and inserting the compensating phases are discussed in some detail later in Secs. 3.3 and 3.4.

$$\Delta\phi = \frac{2\pi}{\lambda}(\sin\theta - \sin\theta_o)\Delta x + \frac{2\pi}{\lambda}(\cos\theta - \cos\theta_o)\Delta y \qquad (3.9)$$

where $\Delta x, \Delta y$ are the element displacement errors and θ_o is the scan angle at which the compensating phase is computed (i.e., $\Delta\phi = 0$ at $\theta = \theta_o$).

It is interesting to note that Eq. 3.9 applies equally well for both space-fed and corporate-fed arrays. After phase compensation, the degradation at directions off the preferred direction is the same for both types of arrays.

Figure 3.4 shows the gain of an example space-fed array with fairly large position errors σ_p of 0.5 wavelengths (although not shown in the figure, the gain loss of a corporate-fed array with position errors of this magnitude would be very large). Note that in the absence of compensation, the gain falls off with increasing scan angle.[1]

The figure also shows the resulting gain after compensation for two preferred directions: 0 degrees and 20 degrees off-axis. The curves show the expected result that the full gain is achieved at the preferred directions and that it drops off as the array is scanned off the preferred direction. If the compensating phases were adjusted at each angle, the full gain could be achieved everywhere. However, as discussed in the following section, preserving the gain does not insure that the desired low sidelobes are preserved.

3.2.1.4 Sidelobe Degradation

In addition to decreasing the antenna gain, element displacement errors also increase the antenna sidelobes. For the case of normally distributed small phase errors, the RMS sidelobe level of planar and

---

[1] The data in the figure was computed using the SARF simulation at scan angles of 5, 10, 15 and 20 degrees. Straight lines were used to connect these computed points in the figure.
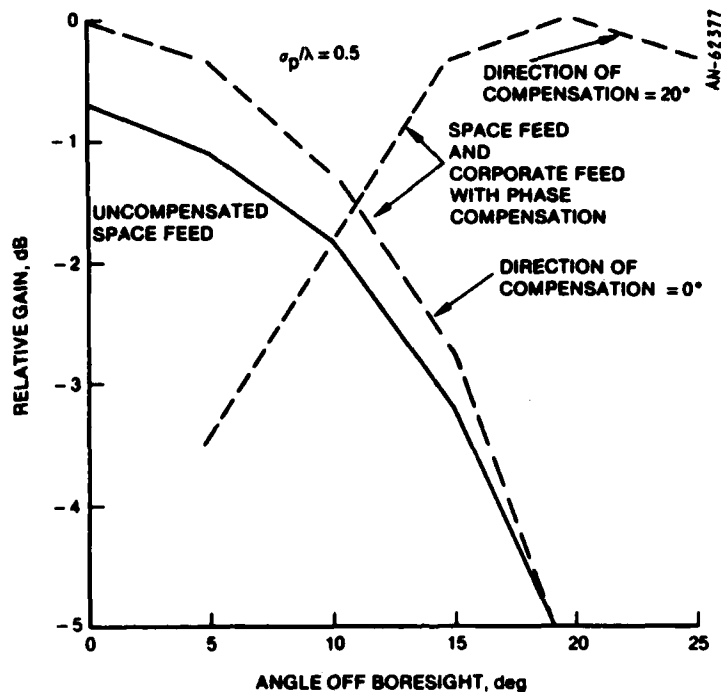
Figure 3.4. Gain Loss After Phase Compensation—Random Element Position Errors

linear arrays relative to isotropic is given by the following expression:

$$SLL = \frac{\sum\limits_{n=1}^{N} A_n^2 \sigma_{\phi_n}^2}{\sum\limits_{n=1}^{N} A_n^2}$$

(3.10)

where N is the number of array elements, A_n is the illumination amplitude of the n<u>th</u> element, and $\sigma_{\phi_n}^2$ is the phase variance of the n<u>th</u> element.

For corporate arrays, the translation from displacement errors to phase errors is invariant with element position within the array. Thus, $\sigma^2_{\phi_n}$ is independent of n and can be removed from the summation to yield

$$SLL = \sigma^2_{\phi}$$

Using Eq. 3.4, we arrive at the following simple expression for the sidelobe level of a corporate array with normally distributed and uncorrelated element displacement errors:

$$SLL = \left(\frac{2\pi}{\lambda} \sigma_p\right)^2 \qquad (3.11)$$

where σ_p is the standard deviation of position error. It is interesting to note that this expression is independent of scan angle as well as the number of elements in the array. This second attribute is particularly important since it supports the use of smaller arrays to simulate the effects of displacement errors on much larger arrays.

Figure 3.5 shows the RMS sidelobe levels of a number of corporate arrays with element position errors ranging from 0.005 to 0.1 wavelengths. The dashed lines were computed using Eq. 3.11 above; the solid lines were generated by connecting samples computed at 1 degree increments with the antenna pattern simulation SARF. As can be seen from the figure, the theory and simulation results agree very well.[1] The fluctuations in the simulation results are the result of the fact that we computed a single radiation pattern for one randomly selected set of element displacement errors. Selection of another set would yield a

[1]The data is presented for a mainbeam focused on the antenna boresight. For the cases shown, the results at a different scan angle would be no different.

0° SCAN ANGLE
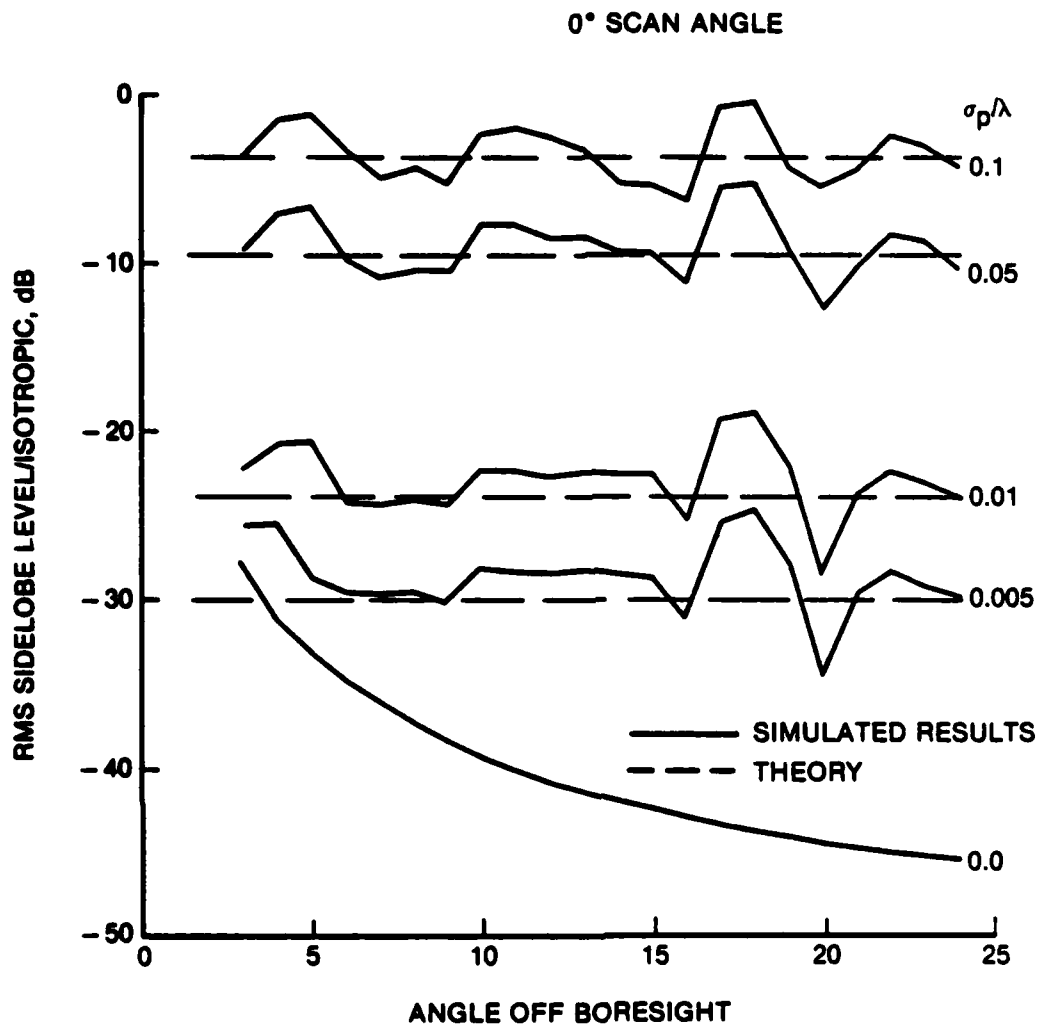
Figure 3.5. RMS Sidelobes—Random Element Position Errors, Corporate Feed

different curve. The average of many such cases would converge to the dashed straight lines given as the theoretical result.

Figure 3.6 shows the radiation pattern derived with the simulation for one set of normally distributed displacement errors having a standard deviation of 0.01 wavelength.
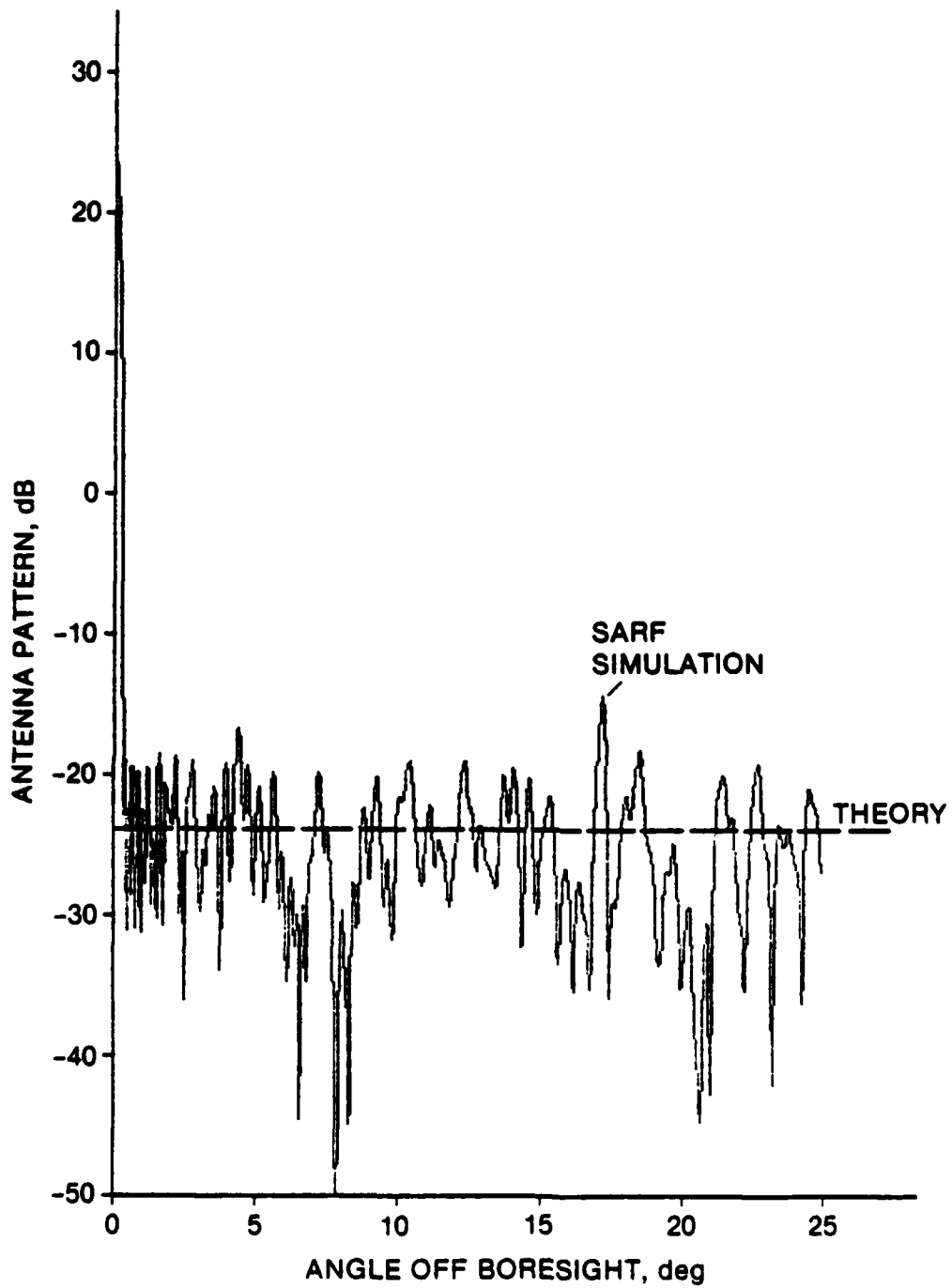
Figure 3.6.   Sample Radiation Pattern for Corpora.. Feed—Random
              Element Position Errors, $\sigma_p/\lambda = 0.01$

34

The sidelobe behavior of space-fed arrays in the presence of displacement errors is substantially different in two respects: (1) the relationship between element displacement and phase error varies with the position of the element in the array, and (2) the phase errors vary with scan angle. Equation 3.7 gives the phase errors of a space-fed array as a function of scan angle and element position. Substitution of Eq. 3.7 into Eq. 3.10 yields the desired expression for the RMS sidelobe levels of a space-fed array.

The dashed line in Fig. 3.7 shows the computed sidelobes for $\sigma_p/\lambda = 0.1$ using Eqs. 3.7 and 3.10. The solid lines were generated with the SARF simulation in an analogous manner to those previously presented for the corporate-fed array. The figure demonstrates the close agreement between the theoretical and simulation results for an example displacement of 0.1 wavelength; and shows the expected increase in sidelobe level with increasing off-axis angle. (Although the sidelobes increase with increasing angle off boresight, they never grow to the point that they exceed those of a corporate feed with equivalent element displacement errors. This can be verified by comparing Figs. 3.5 and 3.7.) Figure 3.8 shows the actual pattern generated by the SARF simulation for 0.1 wavelength displacements.

The preceding results were derived for an array on which the displacement errors of each element were normally distributed but uncorrelated in both the in-plane ("x" coordinate) and out-of-plane ("y" coordinate) directions. Figure 3.9 shows the sidelobe levels for two additional cases: (1) in-plane element displacements only, and (2) out-of-plane displacements only. For the purpose of the illustration, the displacements were assumed to have a standard deviation of 0.1 wavelengths.

In the case of out-of-plane displacements, denoted by (0.0, 0.1), the near-in sidelobes hardly differ from the no-error case (0.0, 0.0).
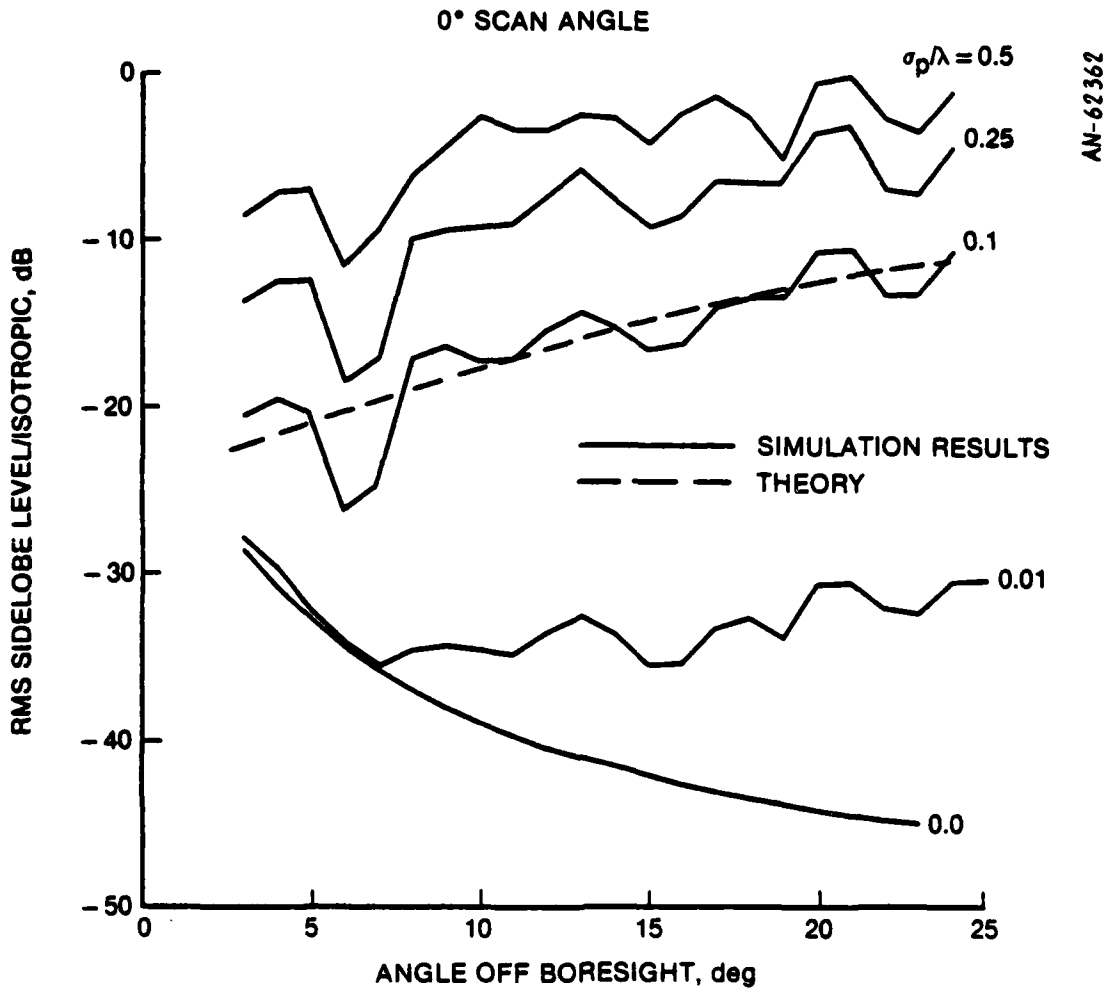
Figure 3.7. RMS Sidelobes--Random Element Position Errors, Space Feed

The effects of out-of-plane displacements do not become evident until about ten degrees off axis. The in-plane case, denoted as (0.1, 0.0), shows that the sidelobes are much more sensitive to in-plane errors.

Figure 3.10 shows the sensitivity of sidelobe level to scan angle for a space-fed array. The figure illustrates the interesting fact that
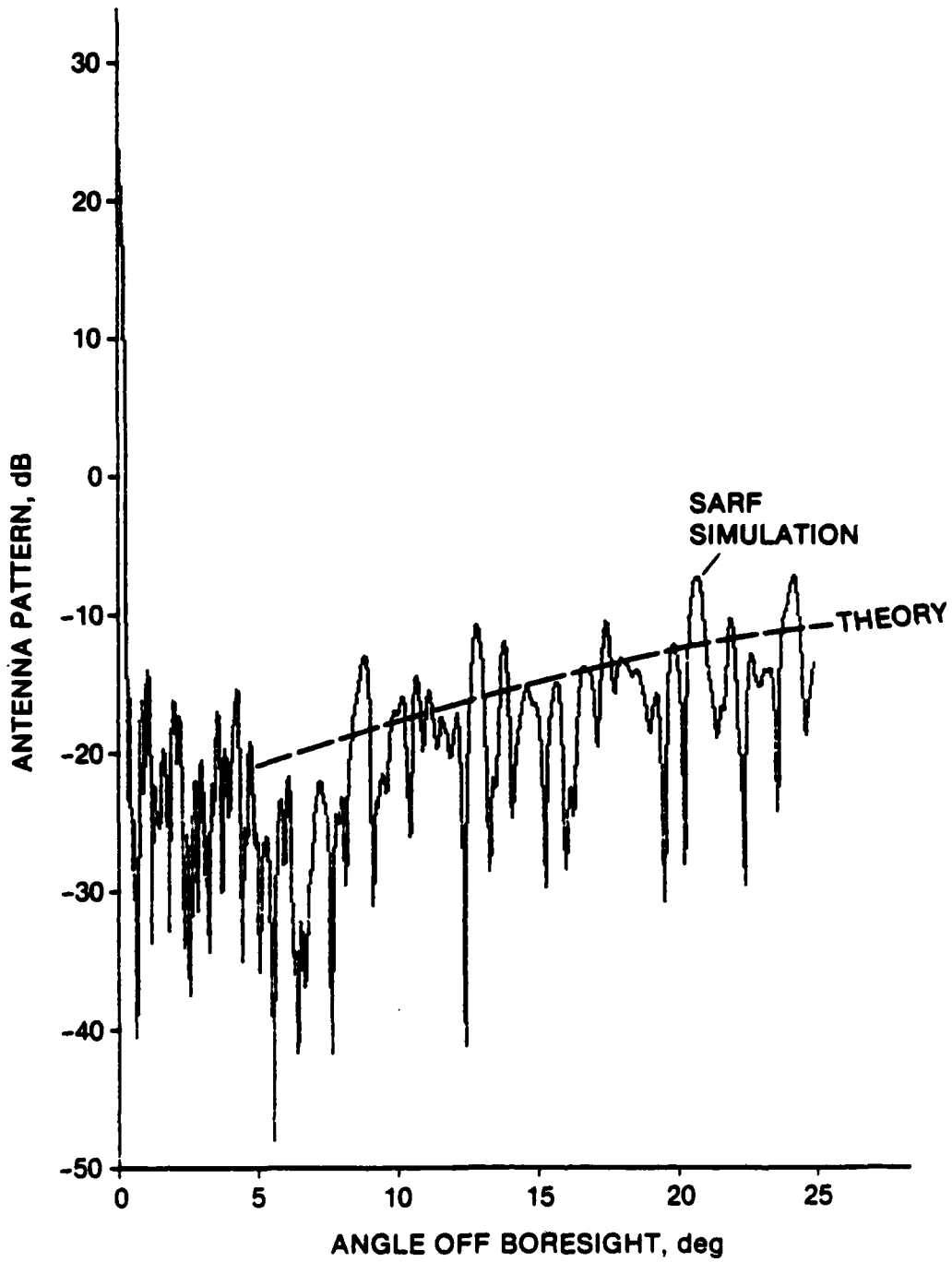
Figure 3.8. Sample Radiation Pattern for Space Feed--Random Element Position Errors, $\sigma_p/\lambda = 0.1$
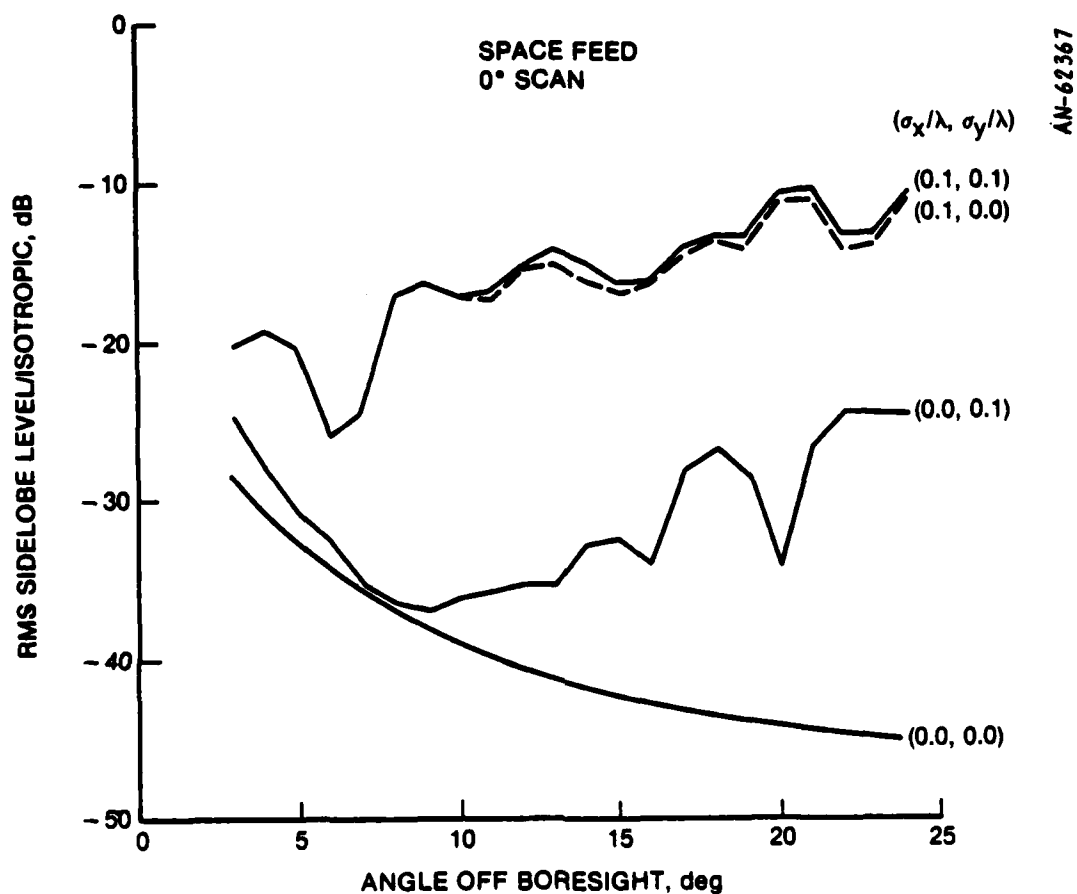
Figure 3.9. RMS Sidelobes--Sensitivity to Direction of Random Element
Position Errors

the RMS sidelobes are invariant with scan angle. The sidelobes of
corporate-fed arrays are likewise invariant with scan angle, but in the
case of corporate-fed arrays, the sidelobes do not increase with
increasing angle off the antenna boresight.

As noted earlier, we have been using the SARF antenna simulation
with a 71 m linear array in the belief that the sidelobe levels due to
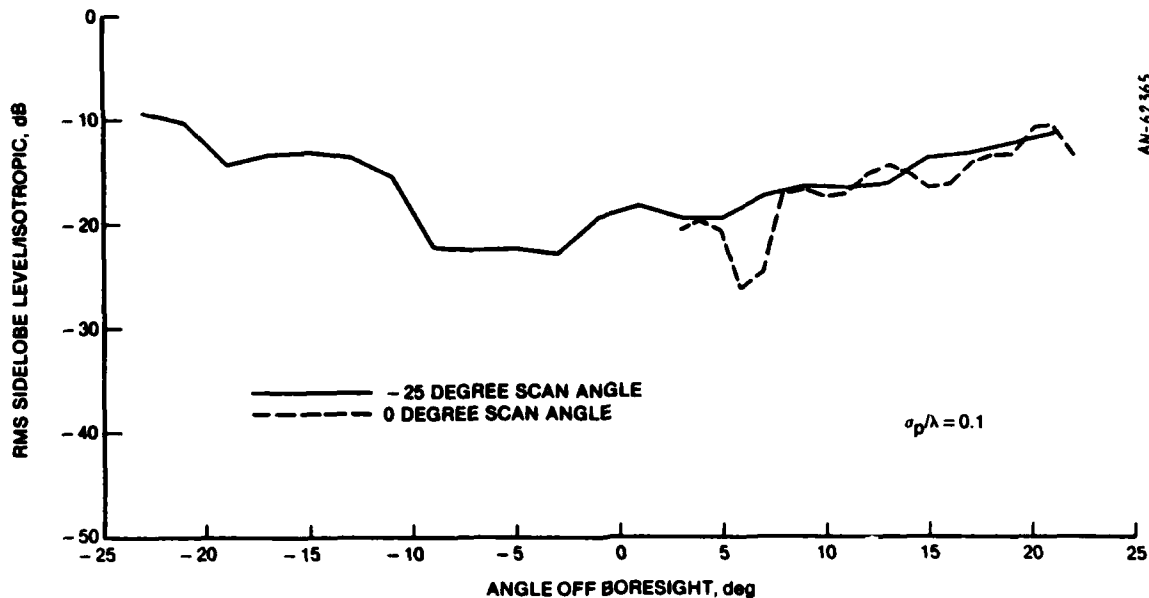
Figure 3.10. RMS Sidelobe Sensitivity to Scan Angle--Space Feed

random displacement errors (when referenced to isotropic) are invariant
with the number of array elements. Thus, the results for the 71 m
linear array with its 422 elements are assumed to be representative of
the full 131,000 element planar array of key interest. This assumed
invariance with number of elements is further supported by the data
shown in Fig. 3.11, which compares the sidelobes computed using SARF for
a 7 m and 71 m array. As one can see from the figure, there is no sig-
nificant difference for these two arrays, which differ in number of ele-
ments by an order of magnitude.

3.2.1.5 Sidelobe Degradation After Phase Compensation

The discussion in Sec. 3.2.1.3 showed that the phase errors intro-
duced by displacement errors could be compensated for entirely in any
desired single direction. However, the phase error would grow rapidly
when moving away from the preferred direction. The residual phase error
after compensation was given by Eq. 3.9 as a function of the element
displacement errors, and the preferred direction in which the phase
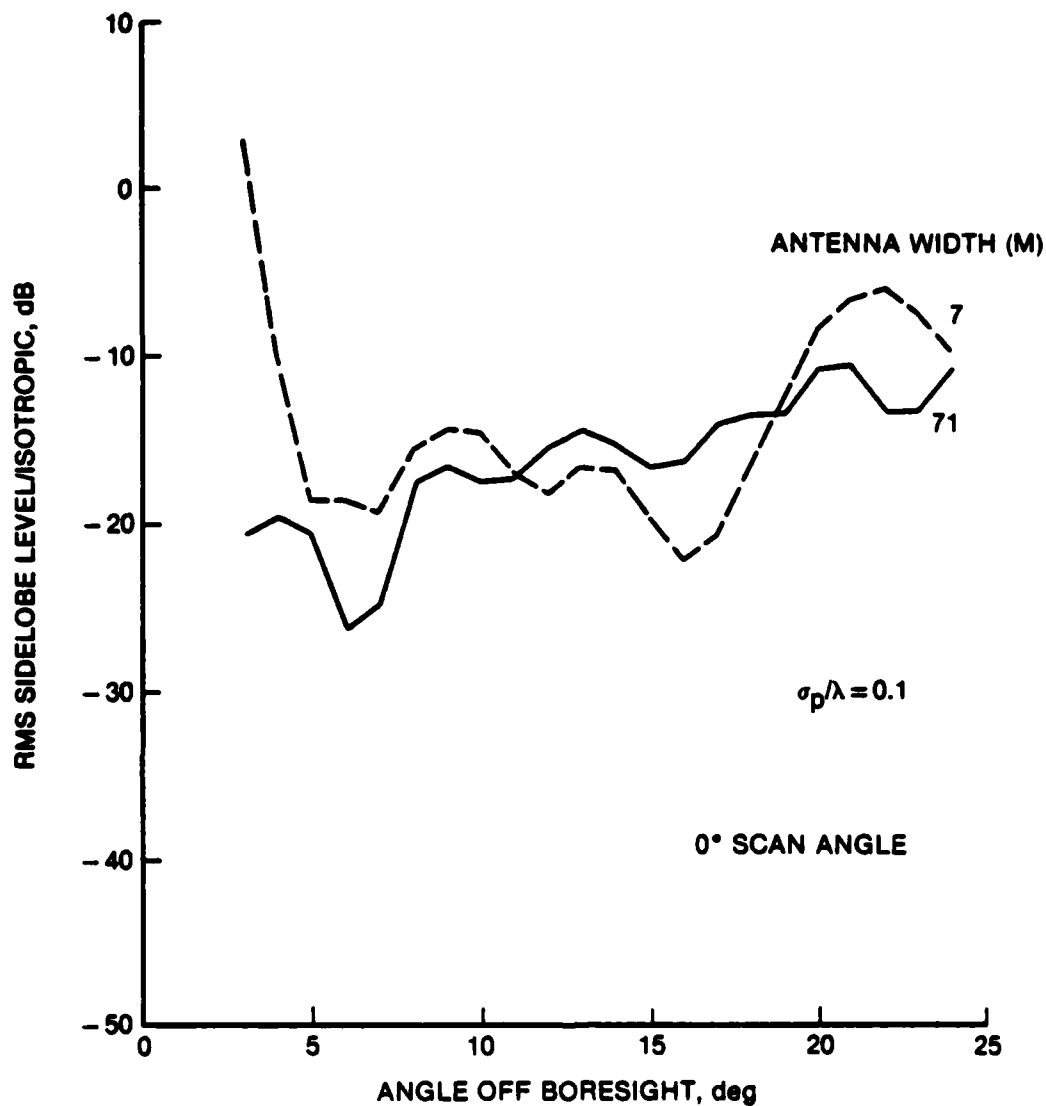
Figure 3.11. Sidelobe Sensitivity to Antenna Size--Space Feed

errors were removed. Substitution of Eq. 3.9 into Eq. 3.10 gives the desired expression for the RMS sidelobe levels after compensation. Figure 3.12 shows the computed results for two element displacement errors and antennas of arbitrary size.
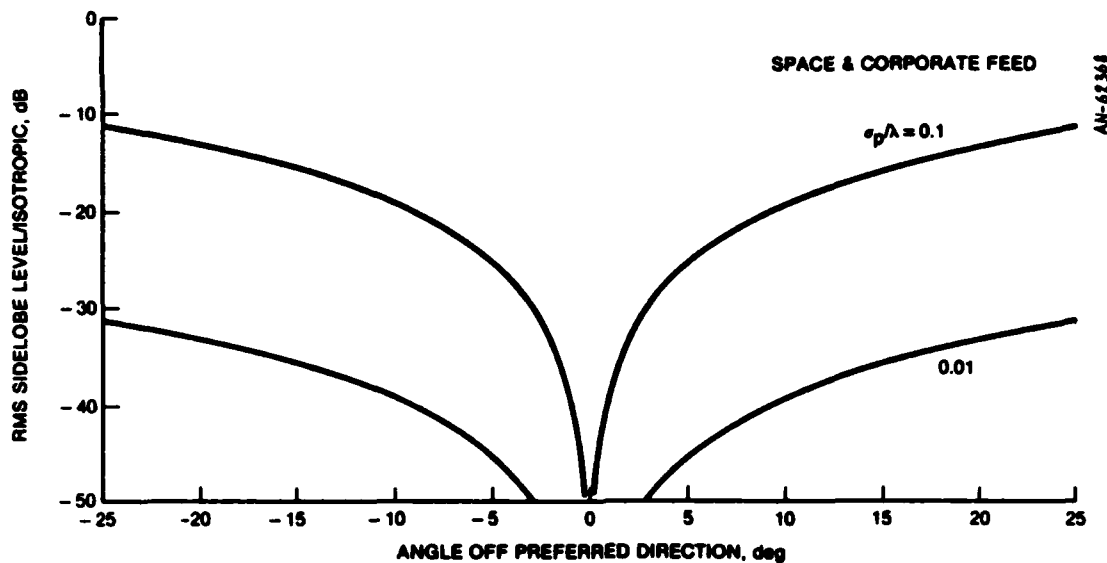
Figure 3.12.   Residual RMS Sidelobe Level After Phase Compensation—
Theoretical Results

The theoretical and simulation results are compared in Fig. 3.13, which depicts a case in which phase compensation is used to remove the displacement-induced phase errors at a scan angle of -10 degrees while simultaneously scanning the beam to +10 degrees. This figure illustrates clearly the fact that although we can eliminate the effects of phase errors on the gain or the sidelobe level in some specified direction, we cannot simultaneously eliminate the effects in all directions. If we elect to adjust the phase shifters to correct in the direction of the main beam, we can eliminate the gain loss and significantly improve the near-in sidelobes. The resulting far-out sidelobes will in many cases be improved relative to their pre-correction values, but they will by no means be improved as much as the near-in sidelobes. Alternatively, we could control the sidelobes in some specified direction of key importance, and accept the degradation of mainbeam gain.
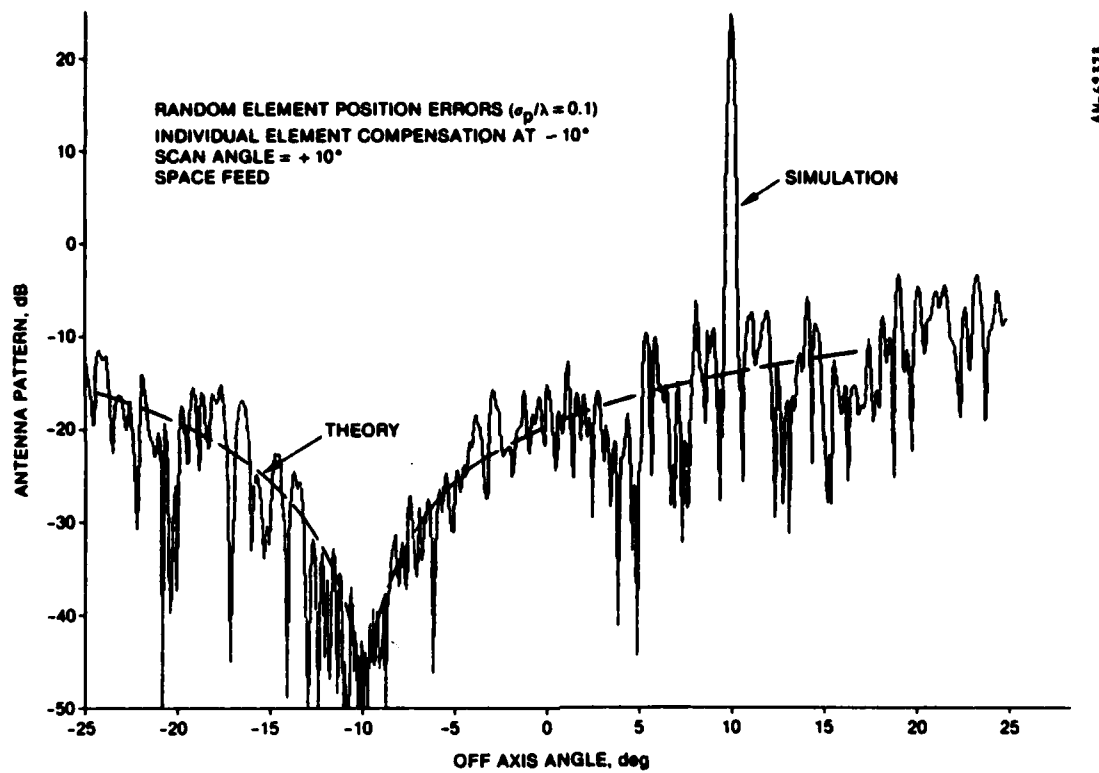
Figure 3.13. Residual RMS Sidelobe Level After Phase Compensation--
Example Simulation Result

3.2.2 Parabolic Displacement Errors

Figure 3.14 depicts an array in which the elements are paraboli-
cally displaced and out of plane. This displacement is assumed to be
symmetric about the center of the array and to have a maximum displace-
ment of D_{max} . In addition, the elements are displaced slightly in the
x direction to maintain a constant element-to-element spacing along the
distorted array face.

Figure 3.15 shows the radiation pattern of this distorted array as
a function of D_{max} . By comparing the patterns for the distorted array
with that of the error-free array (Fig. 3.1), one can immediately see
that parabolic distortion does not appreciably affect the far-out side-
lobes. The principal degradation is in the form of reduced mainbeam
gain and altered near-in sidelobes.
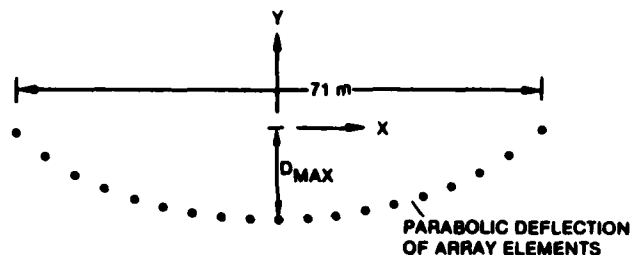
Figure 3.14. Parabolic Displacement Errors

Figure 3.15 suggests that parabolic distortions as large as ten wavelengths (i.e., $D_{max}/\lambda = 10$) will have little impact on the radiation pattern, except perhaps on the mainbeam gain. Figure 3.16 shows the relative gain as a function of D_{max}. The figure shows that displacements of a couple of wavelengths result in less than two tenths of a dB loss in gain, even at scan angles as much as 20 degrees off-axis. At 10 wavelength displacement the loss on-axis is still only about 0.7 dB; however, at 20 degrees, the loss is much greater.

The rectangular box at 10 wavelengths displacement indicates the relative gain computed for an array in which the elements are parabolically distorted only in the out-of-plane direction. The elements are not shifted in the in-plane direction and thus the spacing between adjacent elements varies across the aperture. This modified form of "parabolic" distortion results in somewhat less gain loss.

43
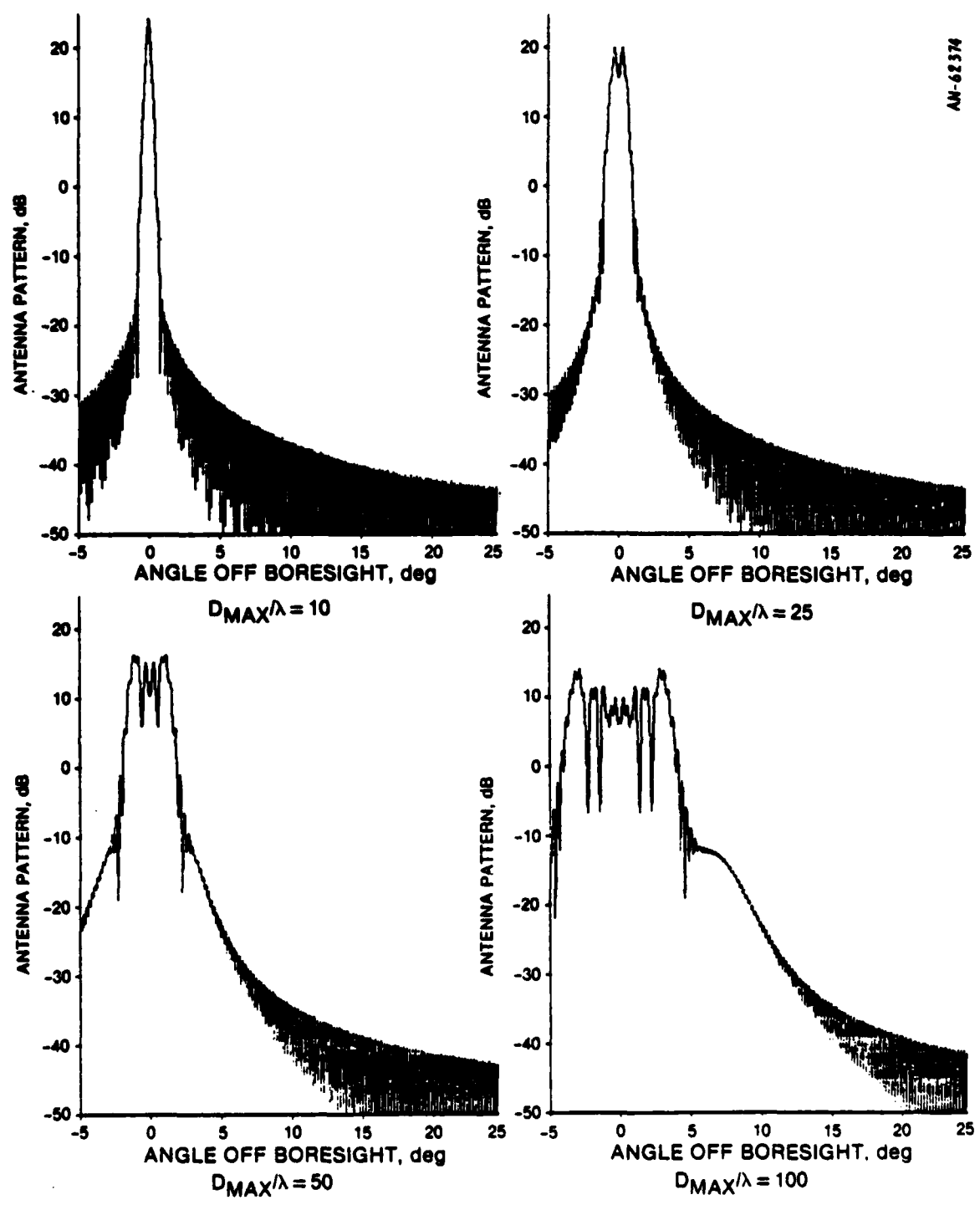
Figure 3.15. Space Feed Antenna Sensitivity to Parabolic Distortions
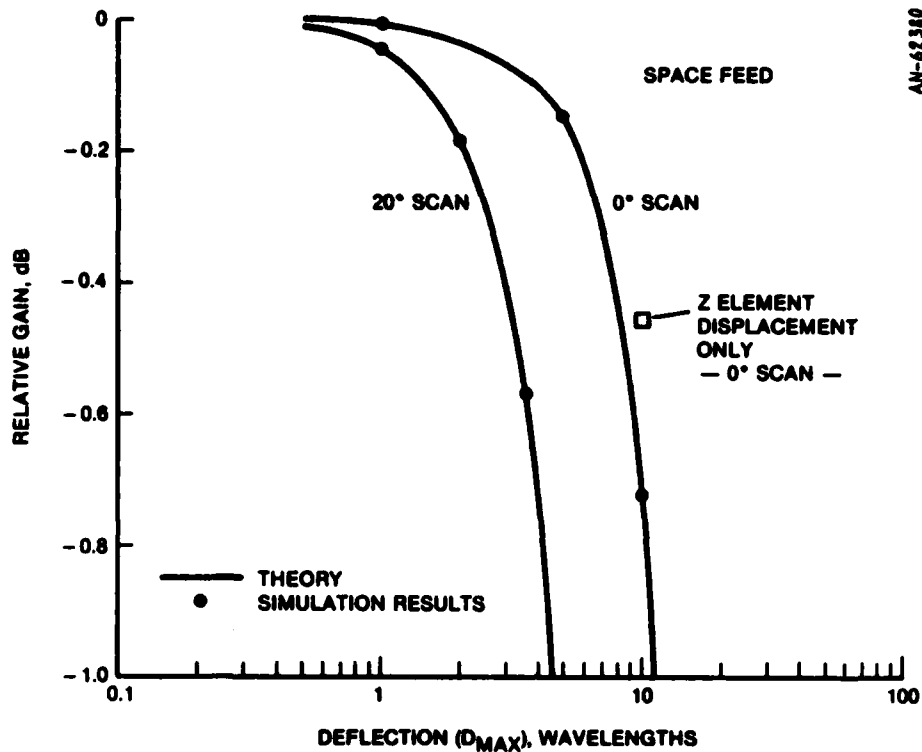
Figure 3.16. Gain Loss—Sensitivity to Parabolic Deflection

The solid line in Fig. 3.17a shows the relative gain as a function of scan angle for D_{max} = 10 wavelengths. As would be expected, the space-fed antenna is less tolerant of displacement errors at higher scan angles.

Figure 3.17 also shows the relative gain after each of two types of compensation: (1) individual element compensation, and (2) feed compensation. For the "individual element compensation," the phase of each array element was shifted to compensate for the displacement error in some preferred direction of radiation (0° was the preferred direction in Fig. 3.17a; 20° in Fig. 3.17b). This is exactly the same form of compensation discussed in the preceding sections for dealing with random element displacement errors.

45
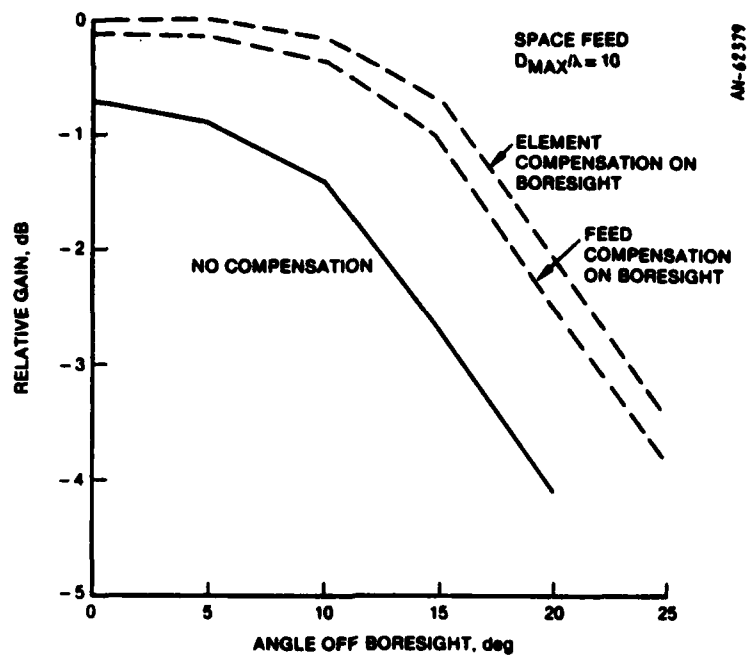
(a) Compensation On-Axis
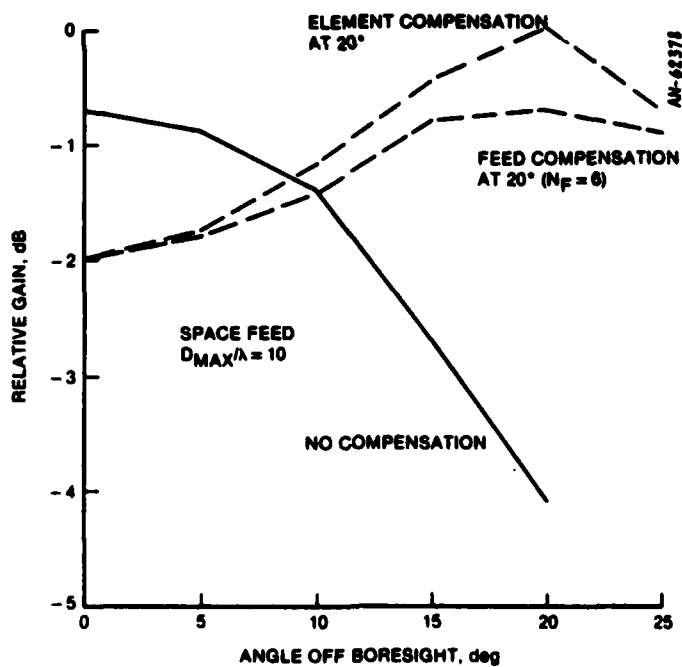
(b) Compensation at 20 degrees

Figure 3.17. Gain Loss After Phase Compensation—Parabolic Deflection Errors

46

Since the parabolic errors cause systematic smoothly varying phase errors across the aperture, there is some promise of using one compensating phase to correct more than one adjacent element. This approach has the attractive feature that it could potentially be implemented entirely within the feed with no modification of the array lens. Figure 3.18 shows a multiple beam feed illuminating a distorted array lens. By adjusting the phase of the feed beams, it would be possible to insert a correction for a large number of adjacent elements. Since the distortion is correlated element-to-element, adjacent elements will need similar correcting phase shifts. To first order the multiple beam feed correction scheme can be viewed as dividing the lens into N segments and applying an independent correction to each of the segments where N is the number of independent feed beams.
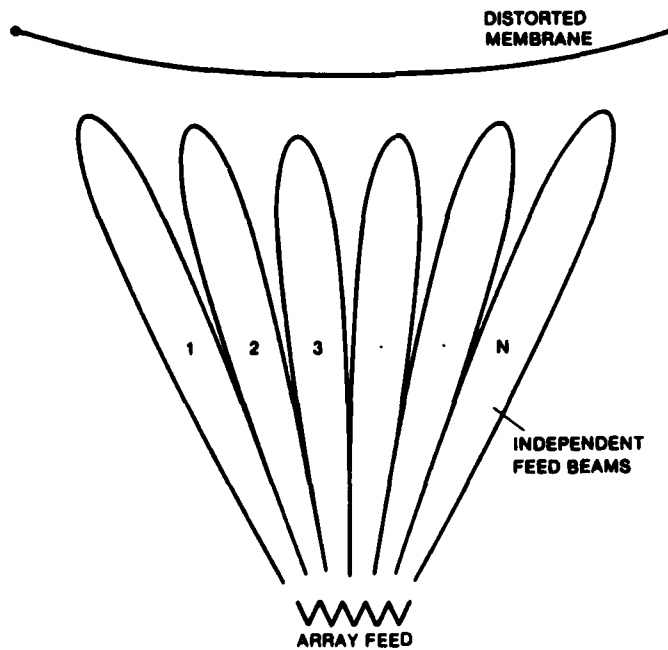
Figure 3.18. Feed Compensation

The baseline two-dimensional array uses a feed with about 36 independent beams. Thus, for our one-dimensional linear array, a six-beam feed is of interest. Figure 3.17 shows the resulting performance with six feed beams ($N_F = 6$).

Figure 3.17a shows that compensation within the feed yields on-axis relative gains that are only a few tenths of a dB below that achievable with individual element phase compensation. However, this difference is appreciably higher off-axis. At 20 degrees off-axis, the gain is about eight tenths of a dB below that achievable with individual element compensation.

Varying the number of feed beams can significantly affect the performance of the feed compensation scheme. Figure 3.19 shows the relative gain as a function of number of feed beams for an example parabolic distortion of $D_{max} = 25$ wavelengths.

On the basis of the above considerations, we arrive at the following conclusions with respect to parabolic distortions:

1. The primary impact of these distortions is on gain; the impact on all but the near-in sidelobes is slight.

2. The gain loss is very small for distortions as high as one wavelength.

3. Individual element phase correction is very effective in restoring full gain.

4. The effectiveness of feed compensation depends on the amount of distortion and number of independent feed beams.

3.2.3 Sinusoidal Displacement Errors

The antenna pattern simulation SARF was used to briefly investigate the impact of sinusoidal distortions of the type depicted in Fig. 3.20. Figure 3.21 shows the computed radiation pattern of a space-fed

48
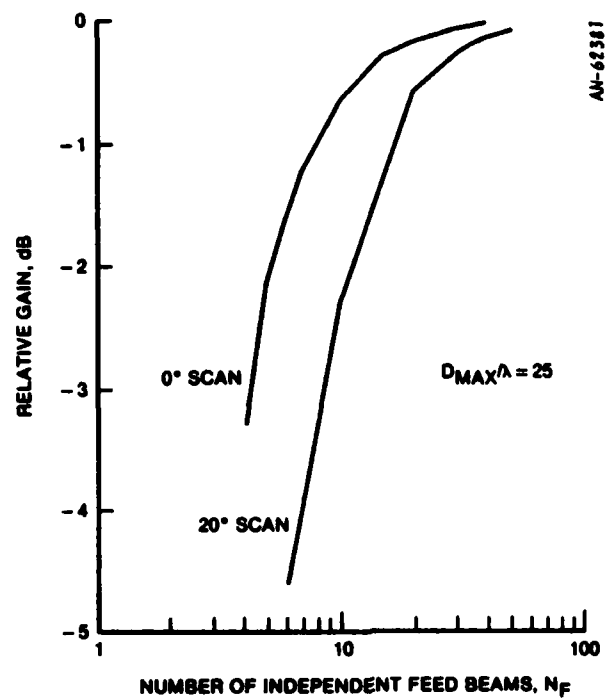
Figure 3.19. Gain Loss After Phase Compensation--Dependence on Number of Feed Beams
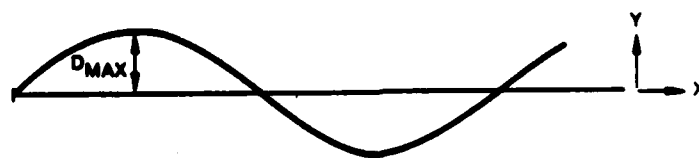
$$\Delta Y = D_{MAX} \, SIN \left(2\pi \, \frac{XN_c}{L} \right)$$

N_c = NUMBER OF CYCLES ACROSS APERTURE

L = APERTURE WIDTH

Figure 3.20. Sinusoidal Distortion
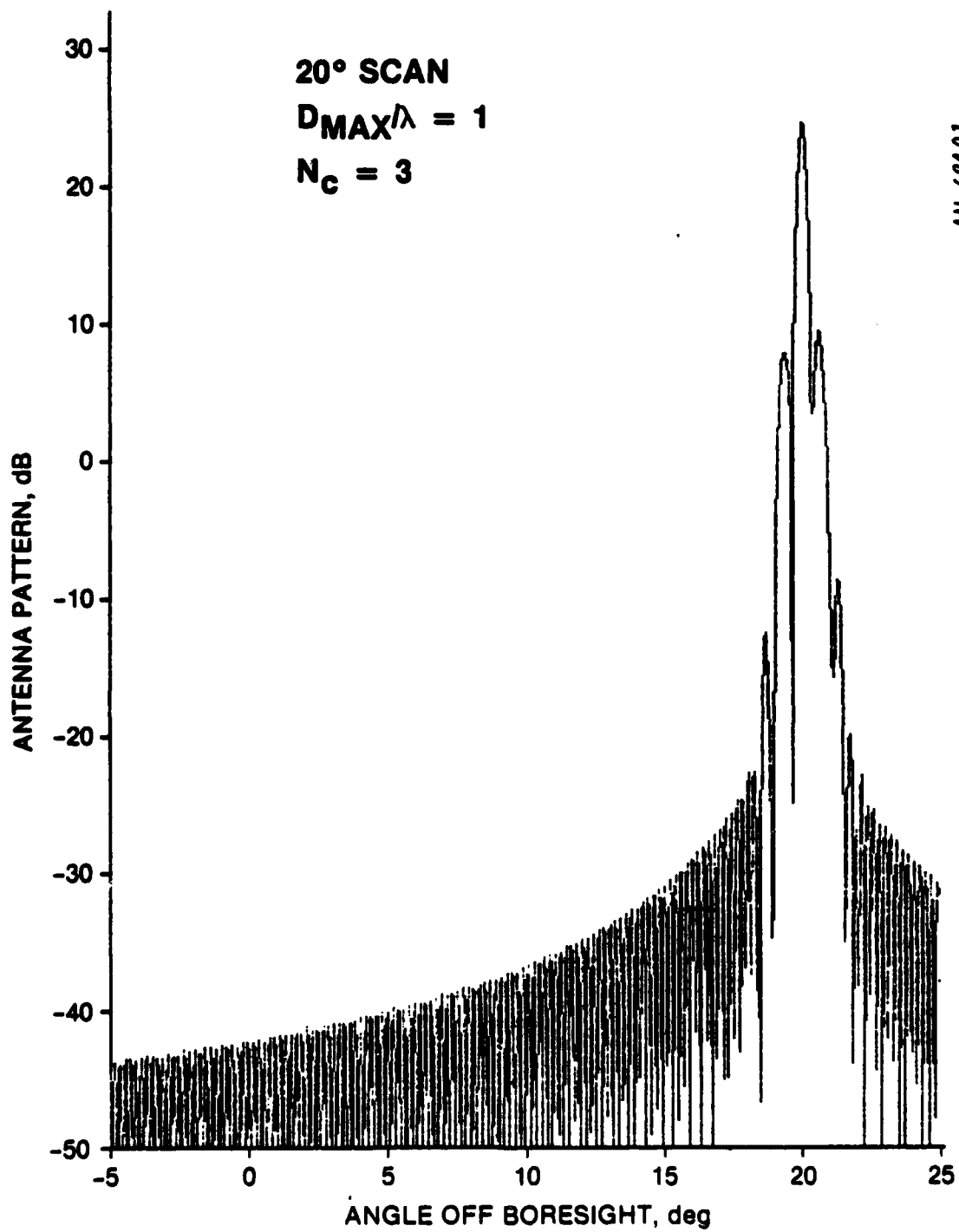
Figure 3.21. Sinusoidal Distortion--No Compensation

array with three cycles of sinewave across the aperture with a peak
deviation of one wavelength.

From the computed radiation pattern, one can see that the side-
lobes are generally unaffected except near the mainbeam. The near-in
lobes appear to be periodic with a period of about 0.6 degrees, which is
consistent with what one might expect for a 71 m aperture which has a
three-cycle periodic distortion across it.[1]

Figure 3.22 shows the improvement with individual element phase
compensation. Figure 3.23 shows the improvement with feed compensation,
assuming six independent feed beams. Although both compensation tech-
niques appear to be effective in reducing the high near-in sidelobes,
the feed-compensation approach introduces additional grating lobes with
a period of about 1.2 degrees.

3.2.4 In-Plane Linear Errors

By definition, these displacement errors occur only in the plane
of the array; there are no errors in the "y" direction. Figure 3.24
illustrates the in-plane errors. Each element is assumed to be shifted
an amount $\Delta X = \alpha X_n$ where α is a constant defining the distortion
level and X_n is the "x" coordinate of the nth array element. The
element displacements thus increase linearly along the radius of the
aperture.

---

[1]The lobe structure of elements spaced 71/3 meters apart is periodic at
an incremental angle θ_o given by

$$\frac{71}{3} \sin \theta_o = \lambda$$

Using $\lambda = 0.24$ meters and solving the above expression yields
$\theta_o = 0.6$ degrees.
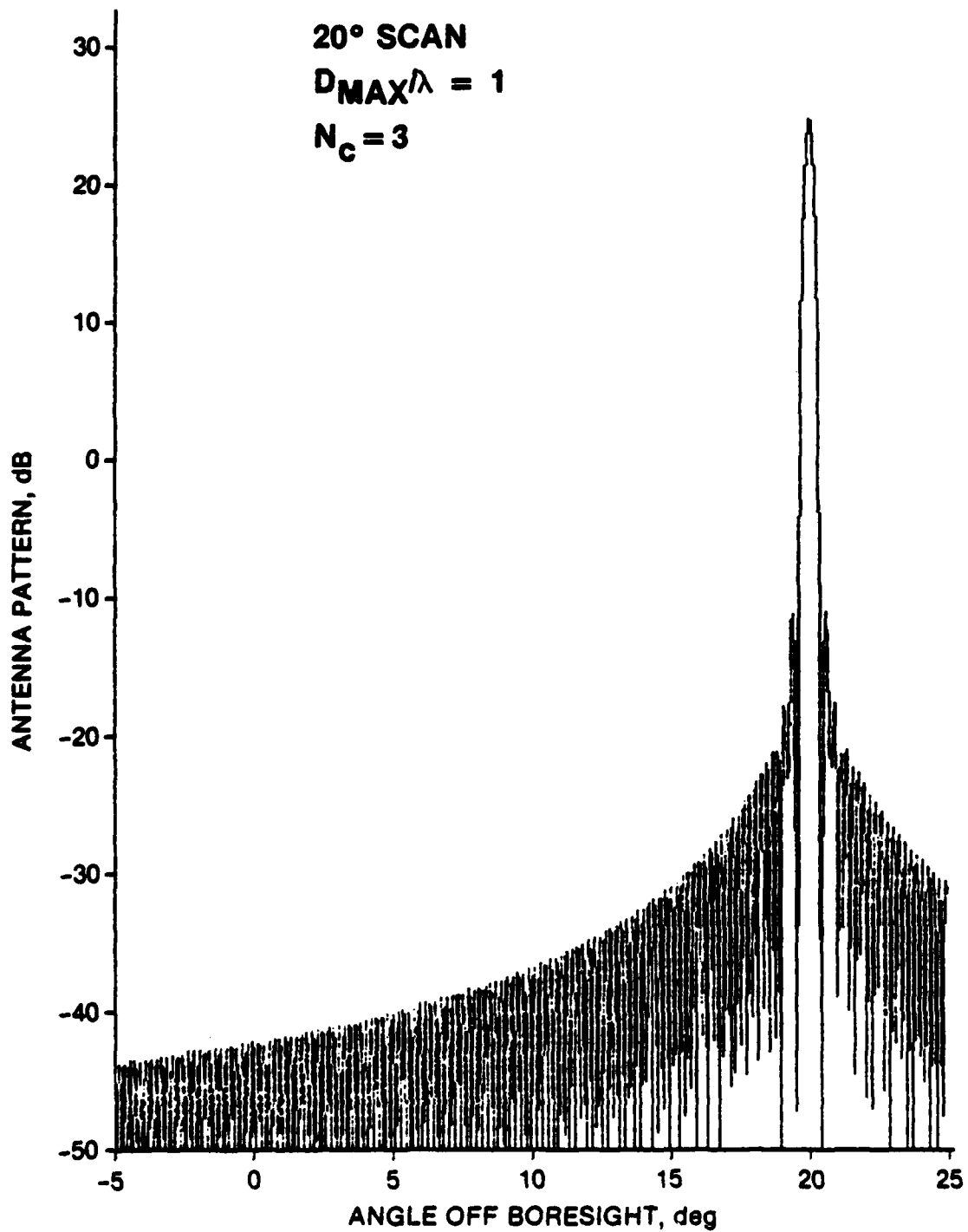
Figure 3.22. Sinusoidal Distortion--Individual Element Phase Compensation

20° SCAN
$D_{MAX}/\lambda = 1$
$N_C = 3$
$N_F = 6$

AN-62399
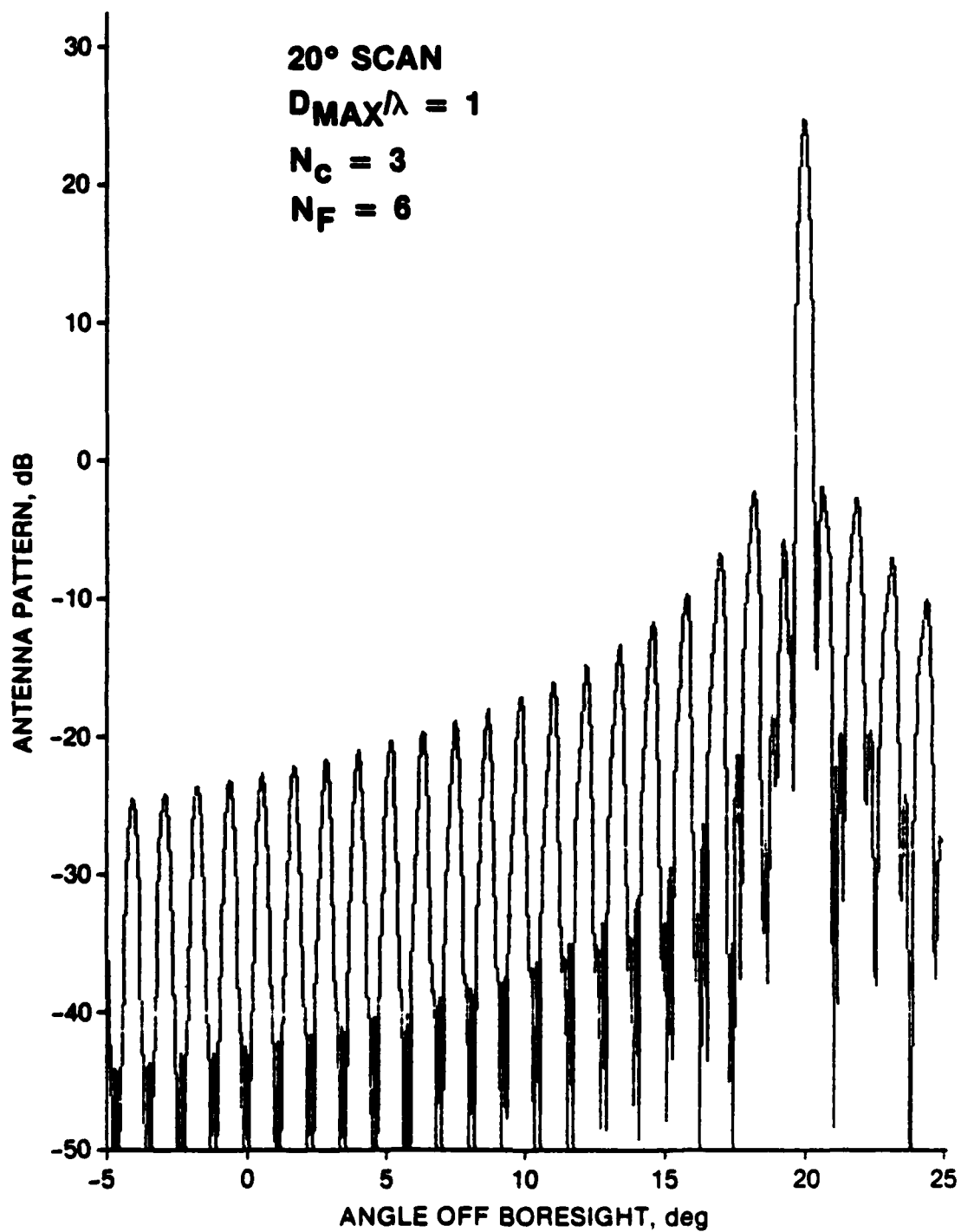
Figure 3.23.   Sinusoidal Distortion--Feed Port Phase Compensation

AN-65642
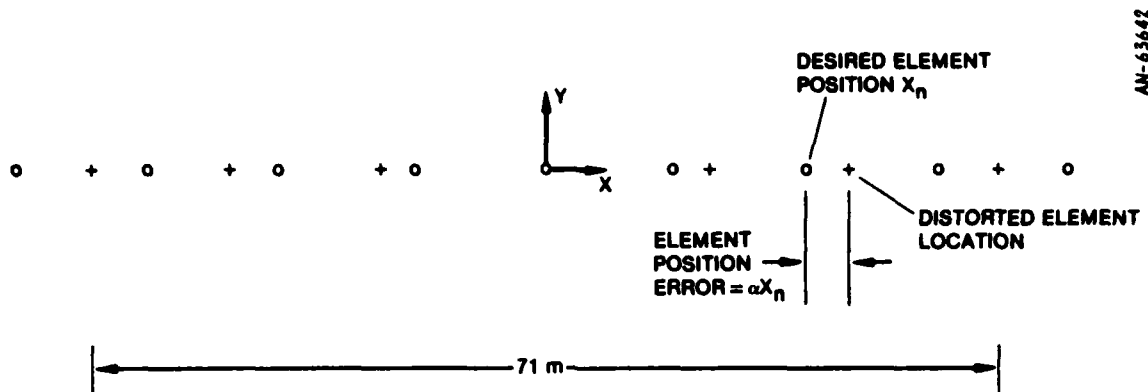
Figure 3.24. In-Plane Linear Displacement Errors

In-plane linear errors are especially interesting since thermal analyses by both Draper Laboratories[1] and General Dynamics[2] indicate that the expected thermal loading of the bicycle-wheel design will produce a linear in-plane shifting of the array elements. The Draper and General Dynamics results are briefly discussed below.

Draper Laboratories under the direction of RADC examined in considerable detail the rim, mast, stays, and membrane of the 71 m diameter bicycle-wheel concept. Their objective was to determine the thermally induced distortions of the antenna surface and feed support as a result of solar illumination at different aspect angles. Their approach was to use a finite element model of the antenna including the rim-mast-stay assembly and a 32 section (gore) membrane, and to determine the temperature histories of a large number of thermal nodes as the earth pointing

[1] Space Radar Large Aperture Simulation/Analysis, The Charles Stark Draper Laboratory, Inc., Rome Air Development Center, Final Technical Report RADC-TR-82-33, March 1982.

[2] Design and Development of a Microstrip Antenna Single Layer Membrane Lens for Space Radar, General Dynamics, Final Technical Report under USAF Contract No. F30602-80-C-0094.

54

satellite progresses along one entire orbit. Five orbital times at which the thermal conditions would be critical were examined in detail:

1. Sun perpendicular to the array plane

2. Sun parallel to the array plane

3. Satellite entering eclipse

4. Satellite emerging from eclipse

5. 45 minutes after end of eclipse where temperature difference between upper and lower stays is at its maximum

The array distortions at 3,264 points on the array were computed for each case and stored on magnetic tape. GRC was later given this tape to use as input to our analyses of the effects of distortions on the antenna pattern.

Case 5 was selected for further study after preliminary investigation indicated it gave the greatest thermal distortions. Further examination of the tape showed that the distortion was entirely radial with the location error of each element increasing linearly along the radius. The errors are shown in Fig. 3.25. The Draper model assumed that the edge of the array was fixed and that the center of each membrane gore was spring-loaded in a way which would keep the tension constant while creating or taking up any slack due to thermal contraction or expansion. Thus, the errors are zero at the edge and increase toward the center of the array. The direction along the radial in which the errors increase is of no consequence to us; what is important is the slope "α" of error growth. Referring to the figure, one can see that according to the Draper data $\alpha = 0.04 \text{ m}/35 \text{ m} = 1.1 \times 10^{-3}$.

A similar analysis was performed by General Dynamics[1] which also included the thermal effects of heat dissipation from the module

---

[1] Design and Development of a Microstrip Antenna Single Layer Membrane Lens for Space Radar, General Dynamics, Final Technical Report under USAF Contract No. F30602-80-C-0094.
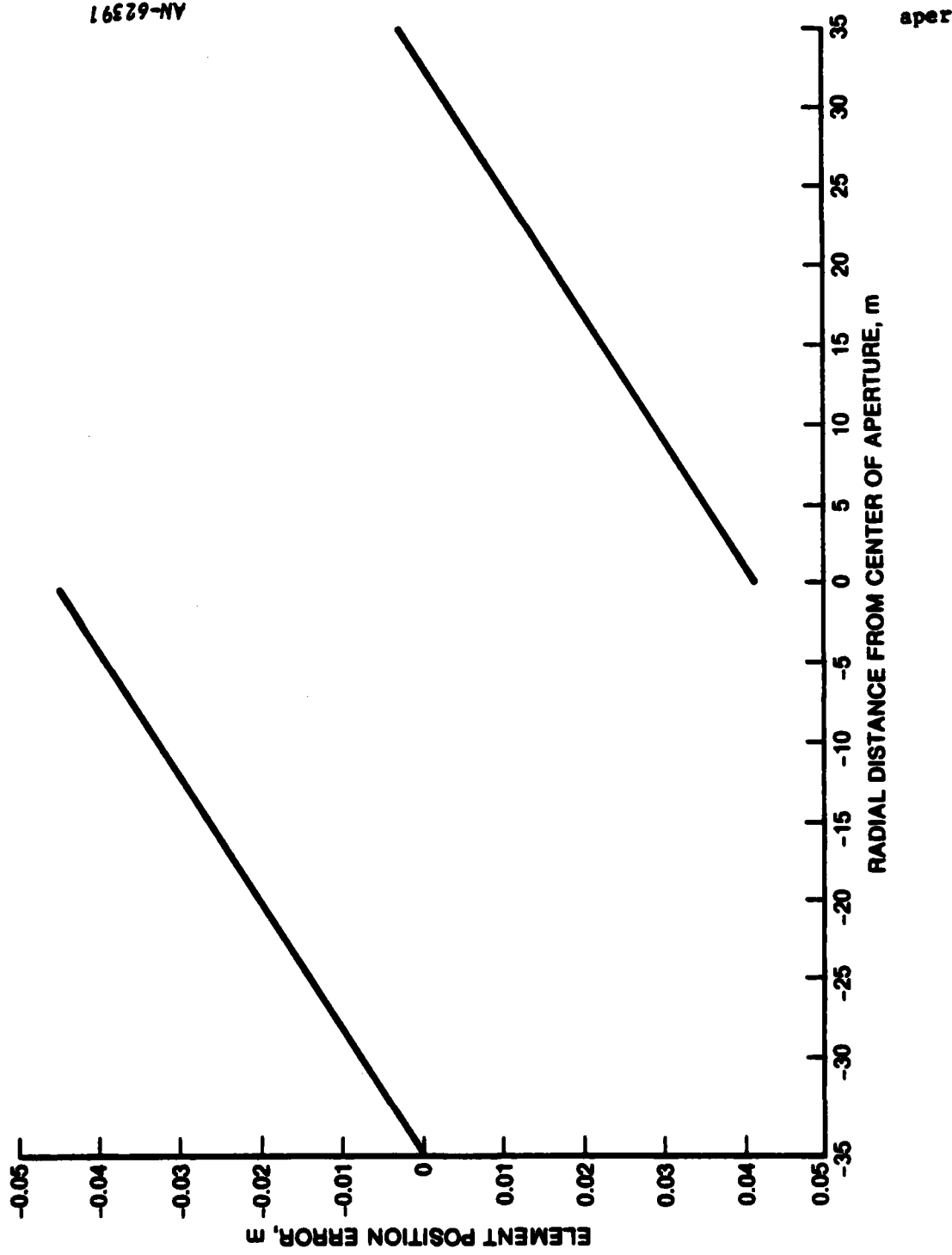
Figure 3.25. Element Position Errors Across Aperture From Draper Laboratories Data

elements. In contrast to the Draper work, the General Dynamics work assumed that the centers of the membrane gores were rigidly attached and that the outer edges of the gores were spring-loaded to absorb the expected thermal expansion and contraction. However, aside from this minor difference in the attachment method, the Draper and General Dynamics results are remarkably similar. They both predict an in-plane radial error linearly varying with radius from the center of the aperture. The rate of increase, quantified by the parameter α used by General Dynamics, was as follows:

$$\alpha = \begin{cases} 1.7 \times 10^{-3} & \text{for 1/4 watt module dissipation} \\ \\ 0.8 \times 10^{-3} & \text{for 1 watt module dissipation} \end{cases}$$

The Draper result of $\alpha = 1.1 \times 10^{-3}$ falls between the General Dynamics results for the two cases. Thus, we selected the Draper number to use for our investigation of the effects on the antenna pattern.

Figure 3.26 shows the computed pattern for the nominal 71 m wide linear array, with the Draper linear stretching of the element positions across the aperture. One can see that on axis (0° scan) the space feed is very successful in suppressing the effects of the distortion. However, at 20 degrees of scan, the space feed is much less tolerant of these errors. Although the far-out sidelobes are far below the level of concern, the near-in sidelobes are unacceptable.

Figures 3.27a-b show the patterns at 20 degrees scan after phase compensation. Phase compensation at the individual element level totally restores the pattern; phase compensation at the feed with a six beam feed does not totally eliminate the distortion effects, but suppresses the effects to the point that they are no longer significant. (The lobing structure with a period of about 1.2° is what one should expect for a 71 m array segmented into six parts.)
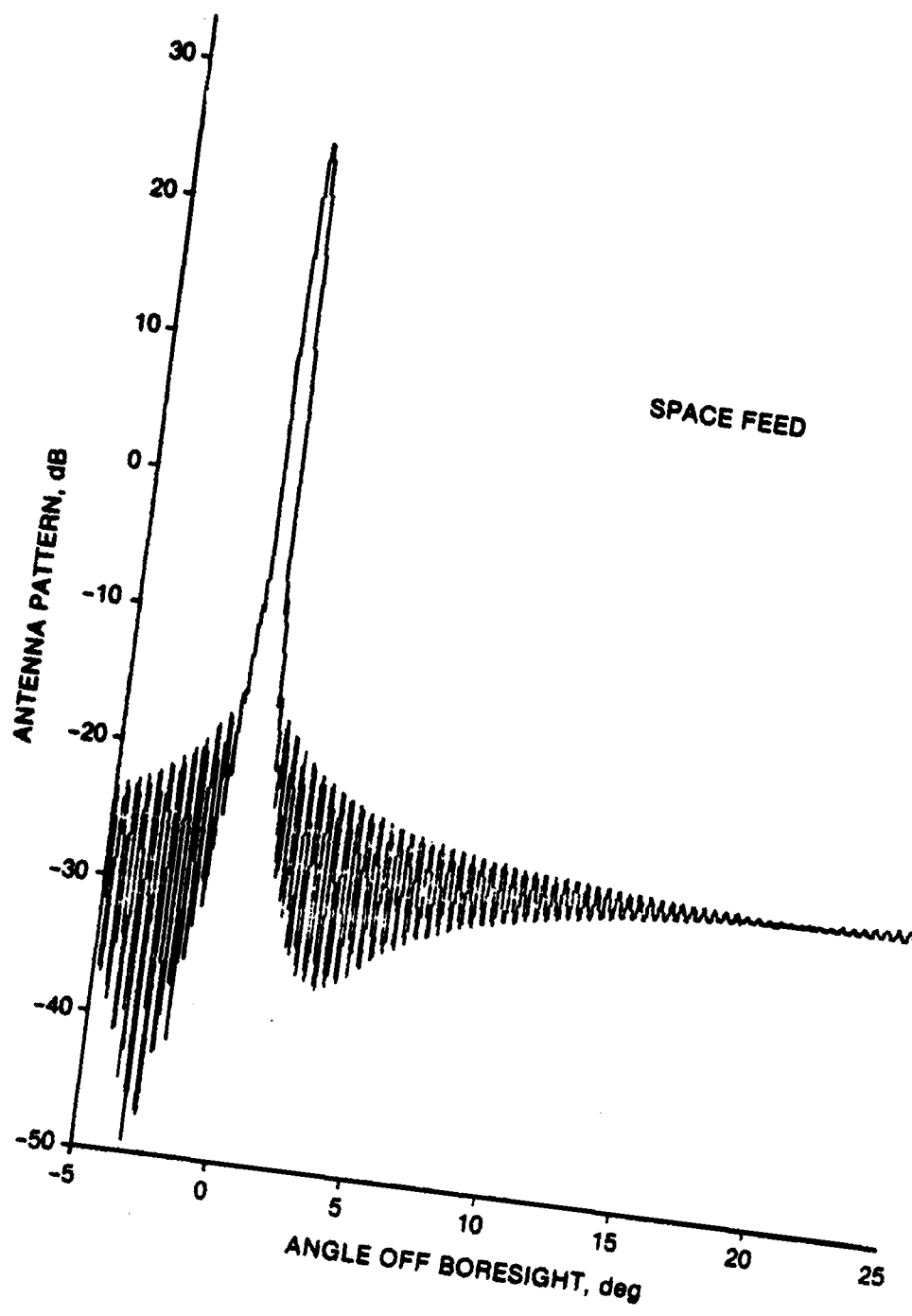
(a) 0° Scan

Figure 3.26. Antenna Pattern With Draper Position Errors

58

SPACE FEED

AN-62390
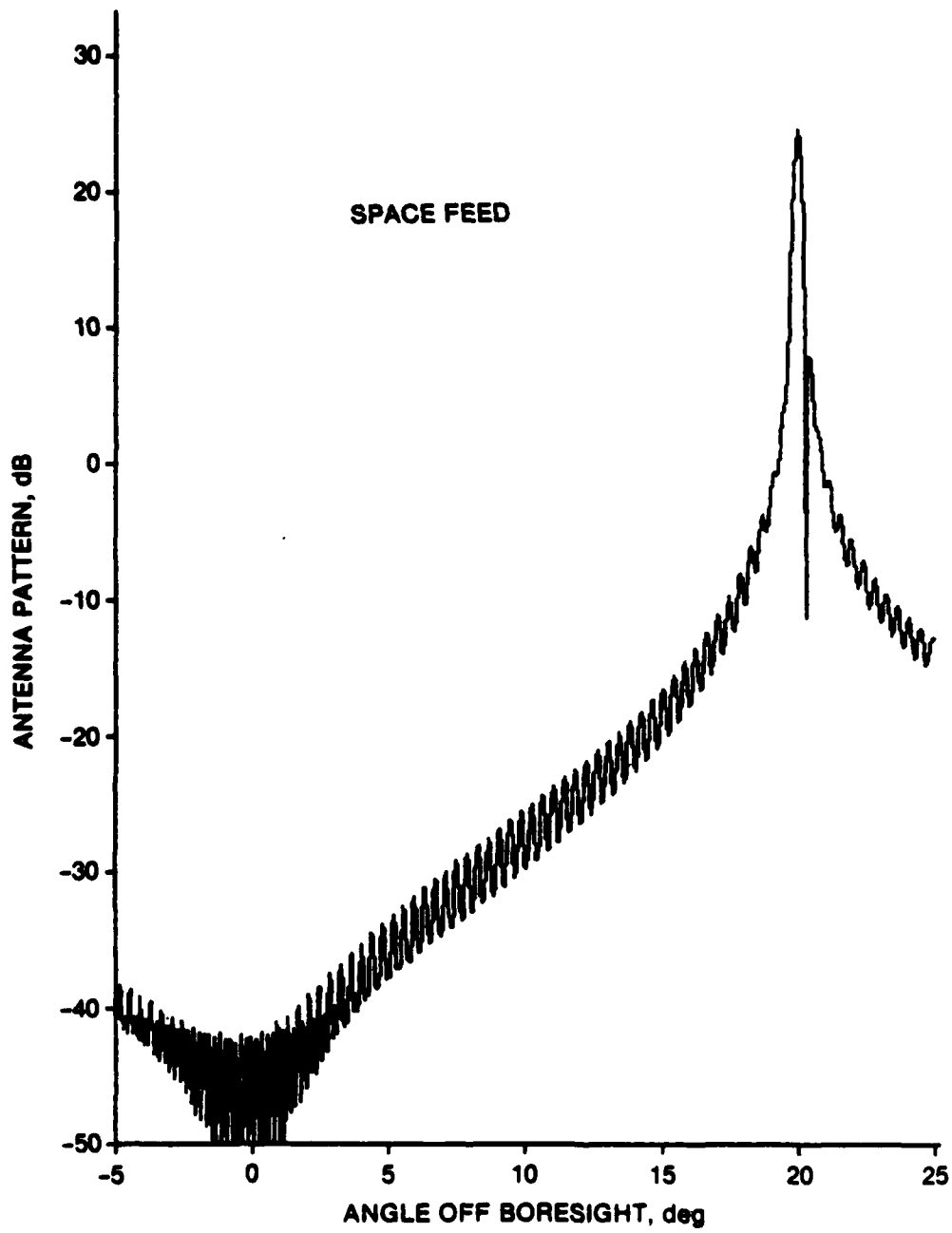
(b) 20° Scan

Figure 3.26 (Concl.)

AN-62389
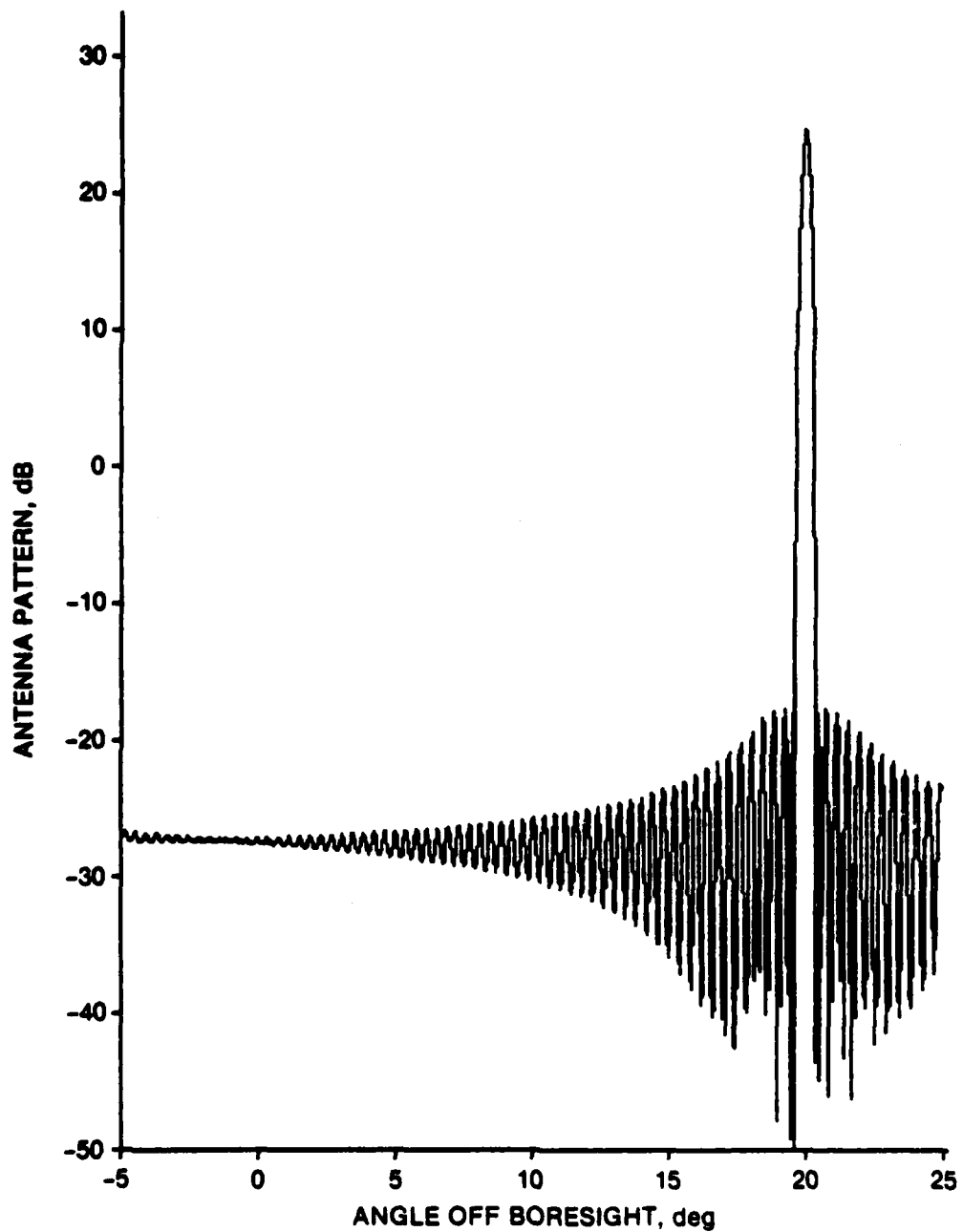
(a) Individual Element Phase Compensation

Figure 3.27. Compensated Antenna Pattern With Draper Position Errors at 20° Scan

60
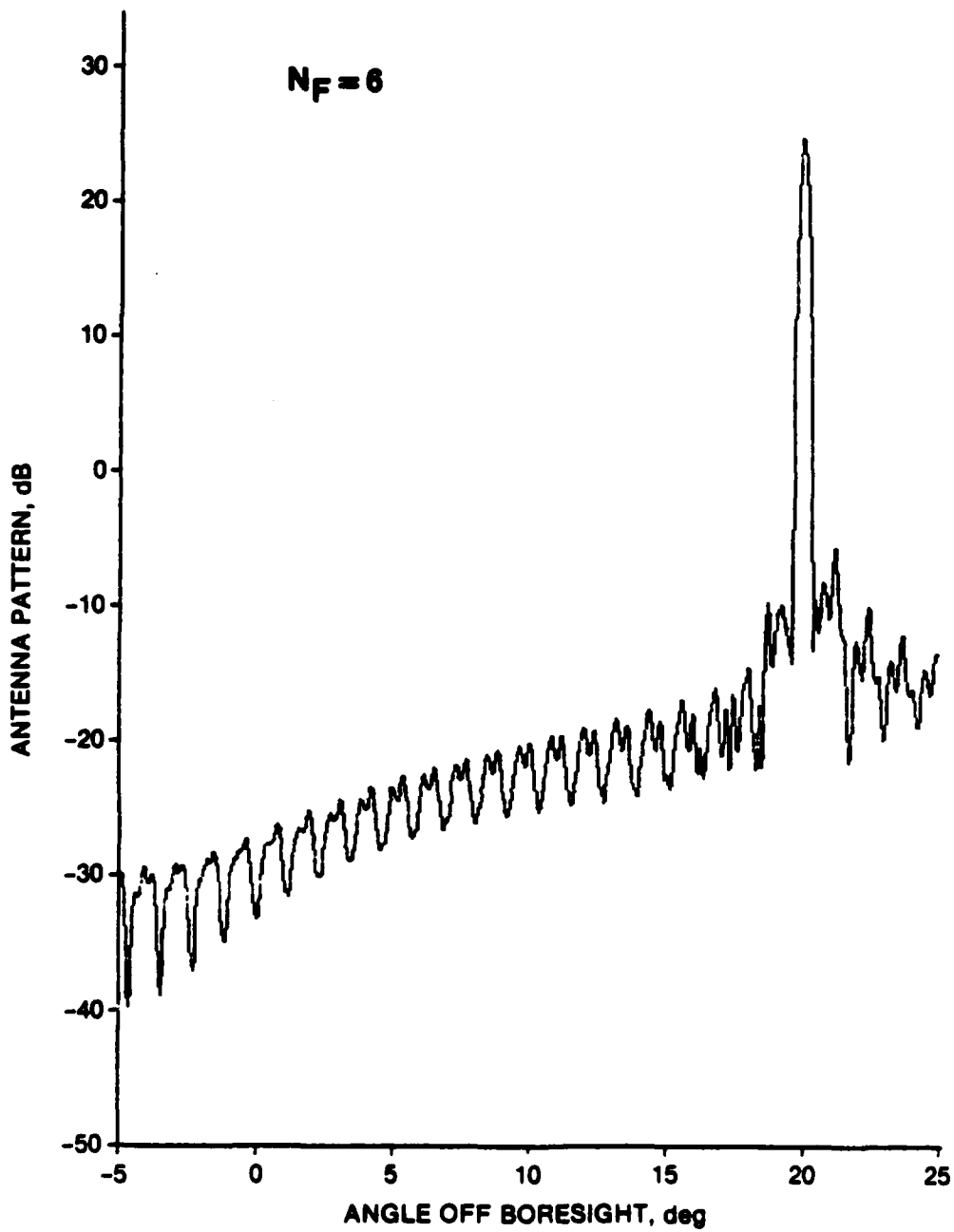
(b) Feed Phase Compensation

Figure 3.27 (Concl.)

The preceding results were generated using the SARF simulation with a 71 meter linear array. As discussed earlier in Sec. 3.3, we believe that the performance of a 71 meter linear array can be used to predict the performance of a 71 meter diameter planar array with random distortions. However, this extrapolation is less certain for distortions other than random. Thus, we must be cautious in drawing final conclusions from the above.

In order to increase our confidence in the use of the linear array model, SARF was also exercised to compute the pattern of a full 71 m diameter planar array with 131,000 elements. The Draper tape with the predicted distortions was used as input for the distorted element positions. The resulting pattern is shown in Fig. 3.28.

Although the full planar array pattern differs somewhat from the model linear array, the basic shape and overall conclusions are unchanged: the predicted thermal distortion significantly alters the near-in lobes but does not impact the pattern beyond a few lobes from the mainbeam.

3.3 DISTORTION SENSING TECHNIQUES

The discussion in the preceding section tacitly assumed that the locations of the displaced array elements were known. This section describes some of the methods which might be used for determining the element locations. Table 3.2 lists the possibilities considered; each is discussed in the subsections which follow.

3.3.1 Indirect Measurement

The "indirect" techniques listed at the top of Table 3.2 are those which depend on models to compute the displacements rather than directly measuring the displacement of the array face or individual elements. For example, strain gauges and/or thermometers located at key points on the antenna might be used to derive inputs to models which would predict

62
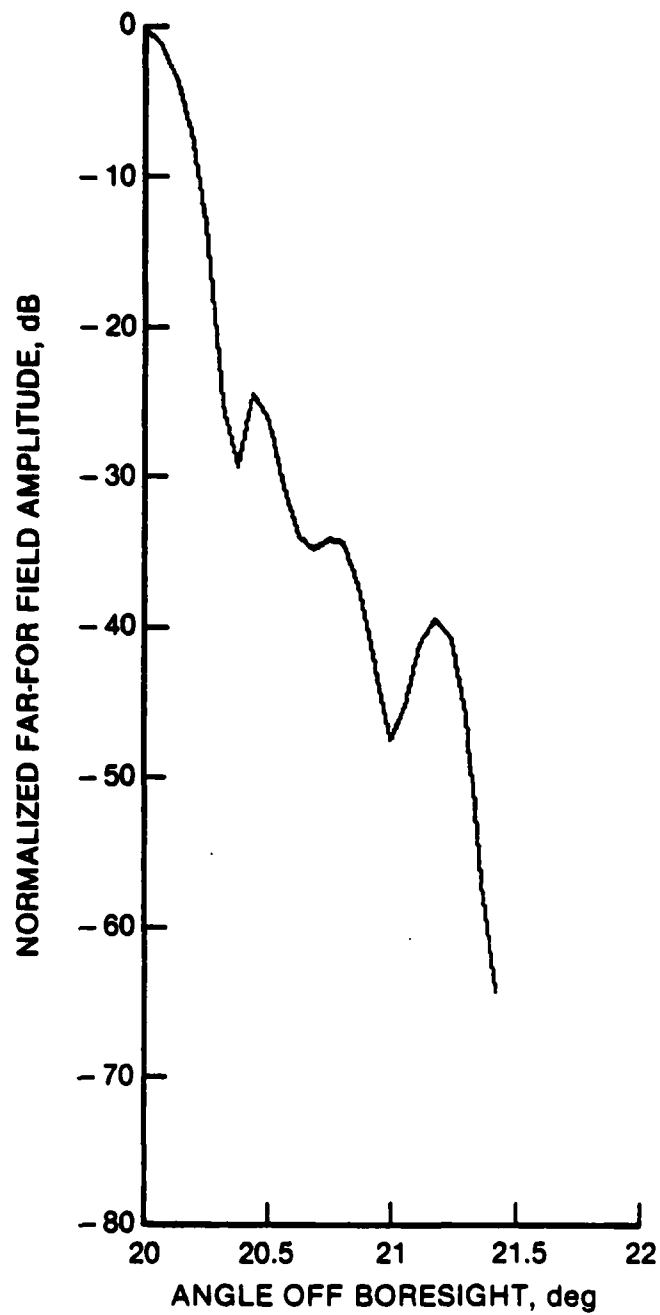
Figure 3.28. Antenna Pattern With Draper Position Errors, 20° Scan,
Full 2-D Array With 131,000 Elements

TABLE 3.2

DISTORTION SENSING TECHNIQUES

Indirect Measurement of Membrane Position

      Temperature Measurements

      Strain Measurements

      Radar Orbit Location/Orientation

Direct Measurement of Position of Array Face

      Pulsed Laser Range Finder

      Modulated CW Laser Range Finder

      Two-Color Heterodyne CO_2 Interferometry

      Self-Pulsed Frequency Detection

      Optical Triangulation

Direct Measurement of Individual Array Element Positions

      Pulsed Laser Range Finder

      Modulated CW Laser Range Finder

      Two-Color Heterodyne CO_2 Interferometry

      Self-Pulsed Frequency Detection

      Optical Triangulation

RF Phase Measurements of Individual Elements

RF Phase Measurements of Aggregate Elements

---

the distortions at any given time. Conceivably, distortions in the membrane could be calculated from knowledge of the temperature and strain measurements at key points. One might even consider making no measurements at all and relying entirely on models which precompute the antenna distortions as a function of the radar's orientation and position in orbit.

The indirect methods require good predictive knowledge of the structure's thermal behavior. Whether or not a predictive model of adequate accuracy could be developed and confidently fielded is unknown.

The temperature distribution, especially during the shadow crossings, varies rapidly and asymmetrically across the structure. Factors such as deformations in support structure shape, flaws or degradation of the array face, etc., make it exceedingly difficult to accurately model the array distortion.

3.3.2 Direct Measurement

The direct measurements listed in Table 3.2 have the potential advantage of being considerably more tolerant to modeling uncertainties and material flaws than the indirect methods. Measurements could be made of the position of either the array face, or the individual elements within the face. In the former case, measurements of the array face at selected points would have to be translated into estimates of the element positions.

In the following subsections direct methods are described for locating the array face and/or array elements. The key factors which affect the selection of a measurement technique are accuracy, data rate, and sensor positioning. At low data rates (~1 Hz), millimeter accuracy can be achieved by state-of-the-art surveying rangefinders. Extending this technology to higher data rates or more accuracy would need custom systems development, but no new development in optical or electronic components. The optical and electronic components currently used in military laser radars and in optical communication systems would be quite appropriate to use in an upgraded laser rangefinder.

For accuracies better than 100 microns and higher data rates, interferometry becomes more appropriate. Again, all the components already exist, and successful laboratory devices have been demonstrated. The basic issues center around developing compact and stable systems.

Optical triangulation techniques can be fast and accurate. They do require coordination with some type of distance-measuring device.

However, a fast triangulation sensor could measure a large number of sample points simultaneously, while a slower distance-measuring device measured only the reference legs. Implementation of such a system depends strongly on the ability to obtain a set of suitable viewing angles.

In an actual system, it might be best to use more than one type of measurement device. This could lead to greater flexibility and reliability. Since all three of the techniques described above could be implemented with semiconductor diode lasers, an individual sensor could be quite compact. This would make it feasible to use a large number of sensors which do the data processing in a parallel manner.

3.3.2.1 Pulsed Laser Rangefinding

In order to operate in full sunlight at a range of 100 to 200 m, a laser rather than an incoherent light source will be required. A pulsed laser can be used with a gated incoherent detector and spectral filters so that the sunlight received during the pulse is an insignificant contributor to the measurement noise compared to the noise generated by the optical detector and electronics. Surveying instruments now in use have ranges on the order of a kilometer, using diode lasers. This long range is, in large part, made possible by the use of retroreflecting targets and by the small beamwidth of a laser compared to an incoherent source. In space the performance of a rangefinding laser is still better because there is no atmospheric loss or aberration factor. Terrestrial precision commercial rangefinders can now measure to 3 mm accuracy at one-kilometer range. This accuracy should be more than adequate for the SBRs now being considered.

However, the current rangefinders require 7 s for the initial measurement and 1 s per measurement to follow the target as it is continuously moved. This rate is clearly too slow to support measurement of all one hundred thousand plus elements, but would support measurements at a fewer number of key points. The basic way to speed up the

66

measurement process is to shorten the laser pulse. This can best be
seen from the equation for the range accuracy of a measurement in which
a series of pulses is averaged:

$$\overline{\delta R} = \frac{c}{2} \frac{t_p}{\sqrt{N(SNR)}}$$

where $\overline{\delta R}$ = measurement accuracy averaged for N pulses

c = speed of light in free space

t_p = pulse duration

N = number of pulses

SNR = power signal-to-noise ratio

This equation is graphed in Fig. 3.29. The parameter is the pulse dura-
tion. Commercially available GaAs laser diodes can generate 1-ns
pulses. Pulse-train laser systems using Nd-Yag, mode-locked laser
devices with 200-ps pulse length are commercially available as labora-
tory instruments. There are other laser technologies which can achieve
even shorter pulses, but these two systems are the closest to field
applications. From the figure we see that a 200-ps pulse duration would
require only two pulses to attain 3 mm accuracy with an SNR of 10.
Since the Nd-Yag laser is quite powerful, the actual SNR could be
increased, so that 1 mm accuracy is a realistic figure. It may be
harder to obtain the accuracy with a GaAs laser unless it is operated at
a high repetition rate.

There are tradeoffs between the diode and Nd-Yag lasers in terms
of repetition rate, size, power, and weight. The diode laser can oper-
ate at a higher repetition rate, is smaller, draws less power, and
weighs less. It also has less output energy, poorer beam quality, and
longer pulses. It should be noted that experimental diode lasers have
been fabricated with shorter pulses, but these are still laboratory pro-
totypes or restricted technology.

SNR = 10 dB

AN-61179

$t_p = 5 \times 10^{-8}$

2×10^{-8}

5×10^{-9}

2×10^{-9}

1×10^{-9}

5×10^{-10}

2×10^{-10}

1×10^{-10}

5×10^{-11}

2.5×10^{-11}

NUMBER OF AVERAGED PULSES (N)

1000

100

10

1

0.1   1.0   100

MEASUREMENT ACCURACY ($\overline{\delta R}$), mm
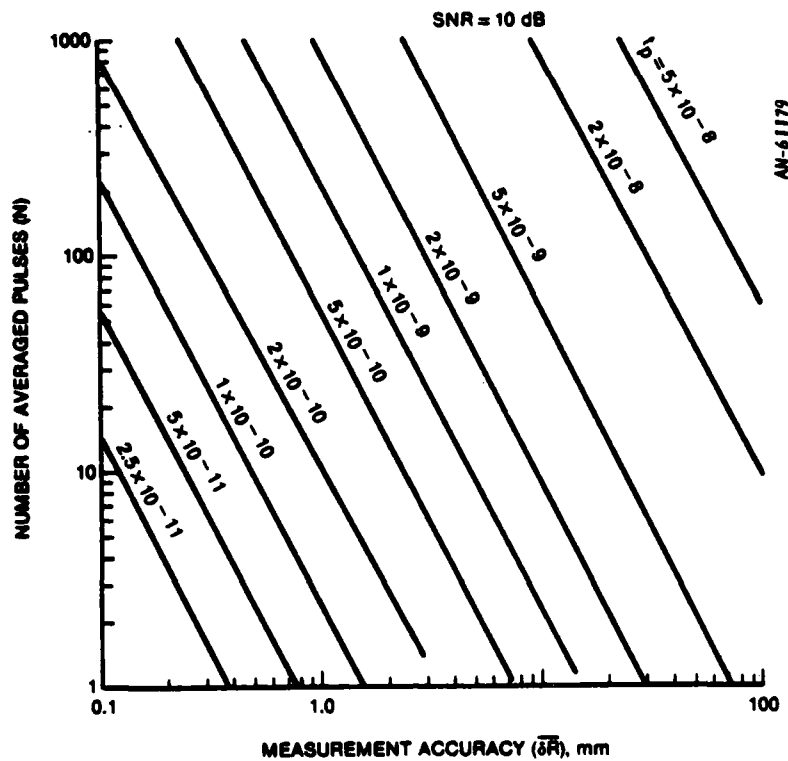
Figure 3.29. Rangefinder Performance

Since both the communications industry and the military are
strongly supporting research and development on short-pulse diode
lasers, it is quite probable that a 100-ps to 500-ps diode laser would
be field-deployable within a short time. In that case, the preference
would fall to the diode system, at least for applications where compact-
ness, low weight, and low power requirements are important. At present,
however, the Nd-Yag laser, operating in a mode-lock pulse-train mode, is
closest to attaining measurement accuracy of 1 mm in one pulse train.
The limited repetition rate is a significant problem: thermal effects
limit the standard rod laser to only 10 pulse trains per second. There
are alternative lasers which would meet the requirement, but they have
other problems, especially with triggering. More details on specific
systems are given in the references listed in the bibliography.

For measurement accuracy of a few millimeters, it should be possible to use currently available diode laser systems with only minor modifications, provided that the repetition rate can be increased or that the pulse width can be reduced to 200 or 500 ps.

There are commercial silicon avalanche detectors which have been developed for measuring mode-locked laser signals. These detectors have rise times less than 50 ps.

3.3.2.2 Modulated CW Laser Rangefinding

In a modulated CW laser rangefinder, the optical carrier is amplitude-modulated and the modulation phase is compared to that of the detected return signal. If the target range exceeds the modulation wavelength, then multiple frequencies of modulation must be used to remove the ambiguity. The measured target range is given by:

$$R = \lambda_m \left[\frac{\Delta\phi}{4\pi} + N_m \right]$$

where
R = measured range

λ_m = modulating wavelength

$\Delta\phi$ = phase difference between the reflected signal and the modulation signal

N_m = number of modulation wavelengths

Some surveying systems use modulated lasers (see Fig. 3.30), especially helium-neon, to achieve accuracies comparable to the state-of-the-art in pulsed lasers. It is also possible to use modulated diode lasers in this type of system.

Sunlight may be something of a problem with this system if direct detection is used. Provided that the sun is not exactly behind the laser, and that spectral filters are used, then direct detection with
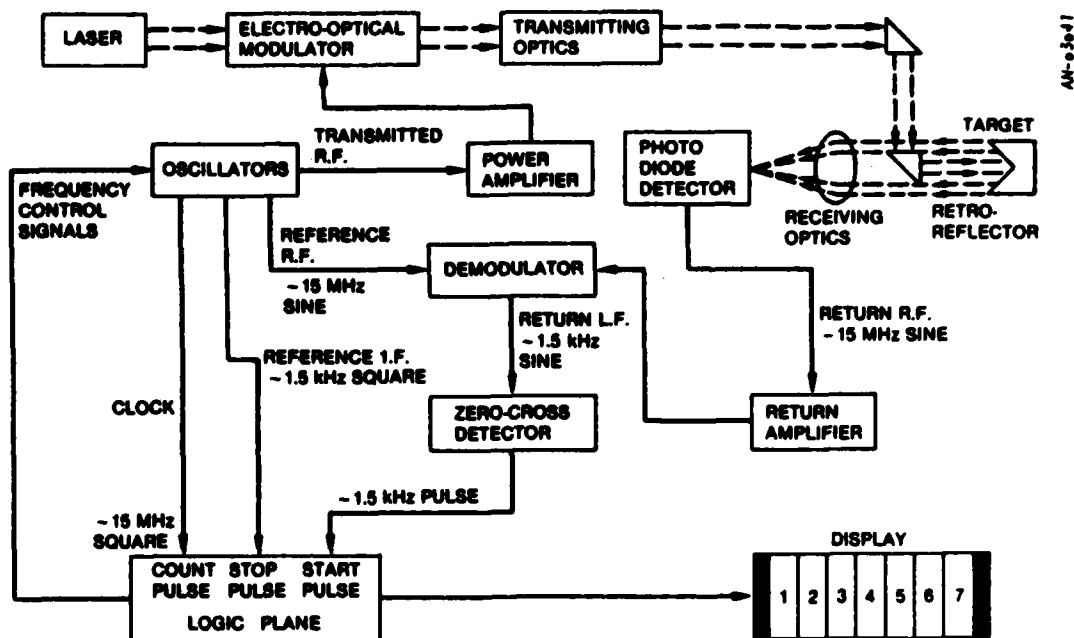
Figure 3.30. Laser Ranging

photo-detectors would be feasible. Direct detection is preferable to heterodyne detection, because angular alignment must be extremely stringent for heterodyne detection.

The limiting factor in extending this technology to sub-millimeter accuracy is likely to be the phase measurement technology. There are commercially available electro-optical modulators which operate around 1 GHz, which is a modulation wavelength of 30 cm. If sufficient phase stability can be maintained with two-color modulation, then this technology could achieve sub-millimeter accuracy.

3.3.2.3 Two-Color Heterodyne CO_2 Interferometry

This is a type of measurement system, shown in Fig. 3.31, which has been designed for measuring to micron accuracies. It is similar to a modulated CW rangefinder except that a heterodyne detection scheme is used. Since the wavelength of a CO_2 stabilized laser can be tuned in
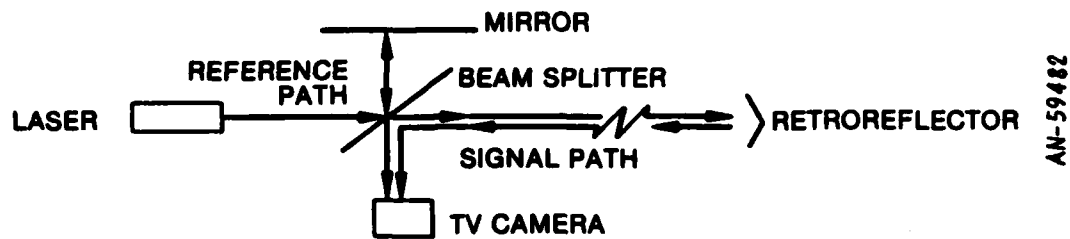
Figure 3.31. Optical Interferometry

---

discrete steps around 10 μm, the "modulation" is provided by running the laser at two nearby frequencies and using the beat frequencies of the detected return signal. The heterodyne detection, although complex and sensitive, is more feasible at the longer optical wavelengths than it is at visible and near-infrared wavelengths (the angular tolerances are proportional to the wavelength). Another advantage of heterodyne detection, besides providing an inherent "modulation" mechanism, is that quantum-limited detection is possible. However, at the measurement ranges of 100 to 200 m, this level of detection is not required. Again, phase stability may prove to be a limiting factor, since the signal must maintain phase coherence with the reference beam during the transit time. A stabilized, multi-color CO_2 laser is a complex device and may be inherently non-robust.

This technology is more applicable to sub-millimeter measurement accuracies where the rangefinding technologies begin to fail.

3.3.2.4 Self-Pulsed Frequency Detection Rangefinding

In many ways, this system is similar to a pulsed rangefinder. However, instead of measuring the time of flight of the pulse, which requires high-speed electronics, the returned laser pulse is used simply as a trigger for the laser to send out another pulse. The range accuracy of this system is

71

$$R = \frac{c}{2PRF}$$

where
R = range

c = speed of light

PRF = pulse repetition frequency

To make ten measurements per second to millimeter accuracy would require at least a 10 MHz pulse repetition rate. The membrane should be stable during the measurement time or the triggering might be disrupted, possibly spoiling the whole cycle.

The limiting factor in this technology may prove to be the requirement for a high repetition rate. Although communication-system lasers can meet this condition, they may not have adequate robustness. The technology question for this system should be left open until more research is done.

3.3.2.5 Optical Triangulation

For calibration, it will be necessary to have at least one optical ranging system. However, the finite measurement time of the ranging system might not be compatible with the required data rate, if absolute measurements are made on every target. Triangulation may be referenced to the rim structure, provided rim motion is small or can be compensated for during data reduction.

Consequently, optical triangulation measurements are of interest since they can, at least in theory, be made quickly. It will be assumed that all optical triangulation measurements are made from small targets, essentially the same types used for the optical ranging; e.g., Scotch-lite tape. Probably it would be feasible to equip each optical triangulation sensor with a small diode laser which would illuminate the target.

72

Optical triangulation systems determine the spatial coordinates of a target by measuring from three (or more) angles.[1] Consequently, it is important that measurements can be made from the appropriate angles. This can be a limiting factor if there are restrictions on where the sensors can be located. To some extent, this limitation can be reduced if the triangulation targets maintain a predictable spatial relationship to key calibration targets which can be measured with a ranging sensor. Then, what would otherwise be an underdetermined two-angle measurement could (theoretically) be completed by data processing. Another constraint on triangulation is that the relative locations of all the sensors must be accurately known so that their measurements can be electronically correlated.

The technology of optical triangulation has three mainstream applications: photogrammetry, surveying with optical theodolites, and military angle-only tracking systems. Although new products which use electronic signal processing are rapidly being developed, at present only the military applications have fully electronic systems. They are generally based on optical arrays or vidicons, which have much lower resolution than film. Consequently, it is necessary to compensate for the small resolution by decreasing the field of view. Other ways to compensate are to scan the sensor, to use a reticle pattern, or to arrange the "target" into a special pattern. All these compensation techniques permit the use of interpolation and centroid processing algorithms to effectively "resolve" within a sensor resolution cell (pixel).

3.3.2.6 Close-Range Photogrammetry

Commercial systems are available which can achieve millimeter accuracy at a range of 100 m (1 part in 10^5). However, these instruments use high-resolution film and manual processing. An advantage of

---

[1] In practice, more angles are desired for statistical averaging.

one particular type, the Geodetic Services system, is that it permits self-calibration algorithms to be incorporated into the measurement. This system might be implemented rather easily with the use of thin lines stretched across the rim.

It would be necessary to incorporate electronic sensor technology into this system. However, by using a narrow field of view on the order of 0.1 mrad, a high-resolution TV camera would have between 5 and 10 pixels covered by a 1 mm target. This should be sufficient for the required measurement accuracy. If not, then a small dither of the camera scan would permit interpolation. However, the cameera must have zoom capability since the target acquisition requirement is for the target to be anywhere within a 1 m circle.

3.3.3 RF Phase Measurements

The final two distortion sensing techniques listed in Table 3.2 are based on the concept depicted in Fig. 3.32. In this concept, the array is illuminated with a reference RF source (within the array's frequency band). A phase detector is then used to measure the phase difference between the signal at a reference element and an arbitrary element under test. If the RF source is in the far field, and if the array is phased so that the elements should be coherent in the direction of the source, then the measured phase difference will be given by

$$\Delta\phi = \frac{2\pi}{\lambda} (\Delta X + \Delta L)$$

where ΔX is the element displacement along the direction of the incoming reference signal, and ΔL is the electrical path length difference between the array elements and the phase detector.

This expression can be inverted to determine the element displacement ΔX within some multiple number of wavelengths.

74
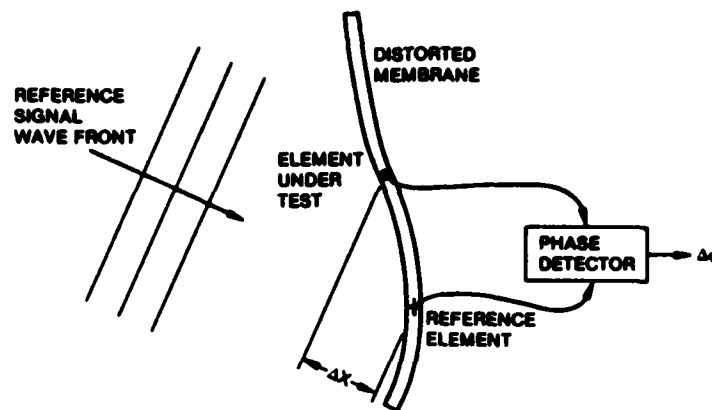
$$\Delta X = \lambda \left(\frac{\Delta \phi}{2\pi} + N \right) - \Delta L$$

Figure 3.32. RF Phase Sensing Concept

$$\Delta X = \lambda \frac{\Delta \phi}{2\pi} + N\lambda - \Delta L$$

where $N = 0,1,2,3,\ldots$ represents the ambiguity in number of wave-
lengths that the element may have been displaced to produce the observed
phase shift $\Delta \phi$. If the array distortion is known to be less than one
wavelength, then N can be set equal to zero. If not, a measurement of
the phase difference for a couple of different frequencies will resolve
the ambiguity. The uncertain parameter ΔL could also be determined
with multiple frequency measurements.

In order for the phase detector to make the necessary phase meas-
urement in a reasonable amount of time, the reference source must be
sufficiently strong. Figure 3.33 shows the time necessary to make phase
measurement accurate to 0.11 radians as a function of the peak power of
a ground-based beacon. The beacon is assumed to have a diameter of 1 m
(42 wavelengths). Referring to the figure, one can see that a 100 watt
beacon would be adequate to make a phase measurement in less than 10

BEACON DIAMETER: 1 m
PHASE MEASUREMENT ERROR: 0.11 RAD
SYSTEM TEMPERATURE: 600° K
SYSTEM LOSS: 3 dB
ELEMENT GAIN: 3 dB

AN-61558

5600 n mi SBR
(R = 11,000 km)

600 n mi SBR
(R = 3000 km)

PHASE MEASUREMENT TIME, µs

BEACON PEAK POWER, watts
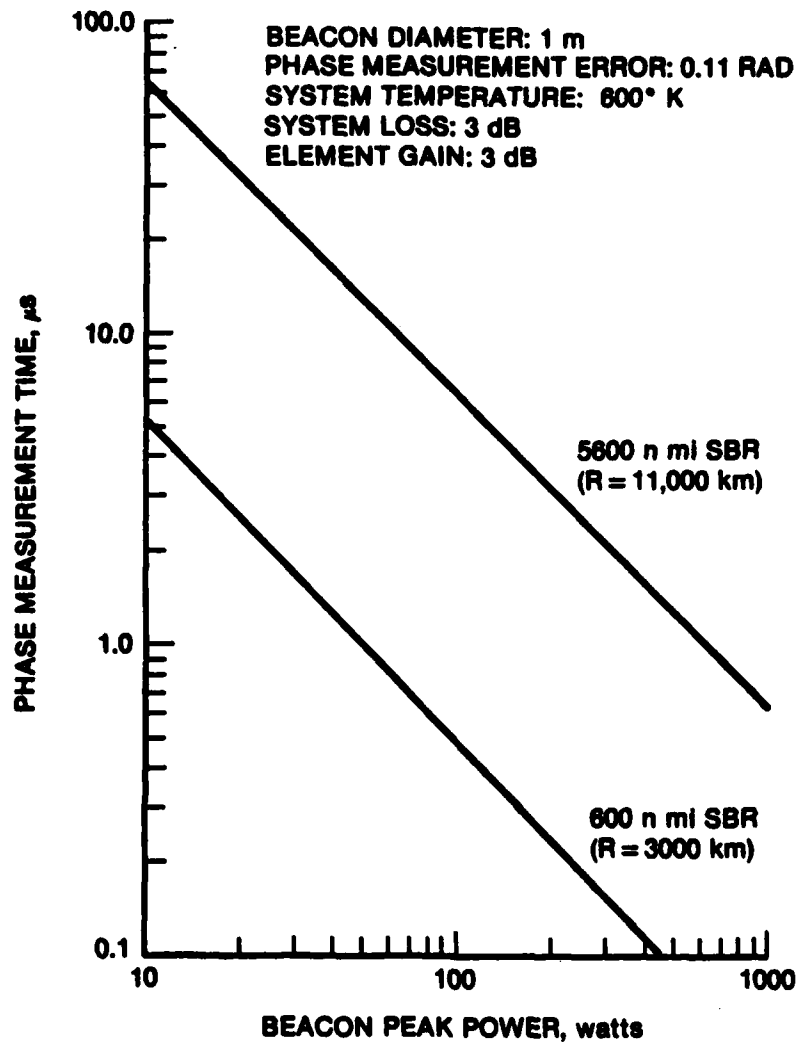
Figure 3.33.   Phase Measurement Time--Ground-Based Beacon

µsec on-board a radar in a 5,600 n mi orbit. Thus, all 131,000 elements
of the 71 m diameter array of interest could be sequentially processed
in less than 1 second. These low power beacons could easily be distri-
buted as necessary to support phase measurements.

76

The arrangement shown in Fig. 3.32 would allow one to measure an element displacement in the direction of the beacon. By using two or more additional beacons in different directions, the element could be located in three dimensions.

The beacon source does not necessarily have to be located on the ground nor in the far field, but in fact, could as well be located on the spacecraft structure itself. Some possibilities for this are explored in the next section, which addresses various methods of implementing phase compensation.

3.4   IMPLEMENTATION OF DISTORTION COMPENSATION

This section is intended to outline some of the methods which might be used to implement the compensation techniques described in the earlier sections. Table 3.3 lists the possibilities considered. The first method, reshaping the array, is a mechanical approach. The remaining three are electronic responses which are pursued in the following paragraphs.

Figure 3.34 shows three generic methods in which the information derived by a distortion sensor (such as any of those described in Sec. 3.3) might be used to compensate for distortion. Figure 3.34a depicts how phase compensation could be implemented entirely within the feed. Under this approach, the measurements taken by the distortion sensor are

---

TABLE 3.3

DISTORTION COMPENSATION TECHNIQUES

1.   Reshape Array
2.   Adjust Phase of Individual Array Elements
3.   Adjust Phase of Feed Array Elements
4.   Adjust Phase and Amplitude of Array and/or Feed Elements
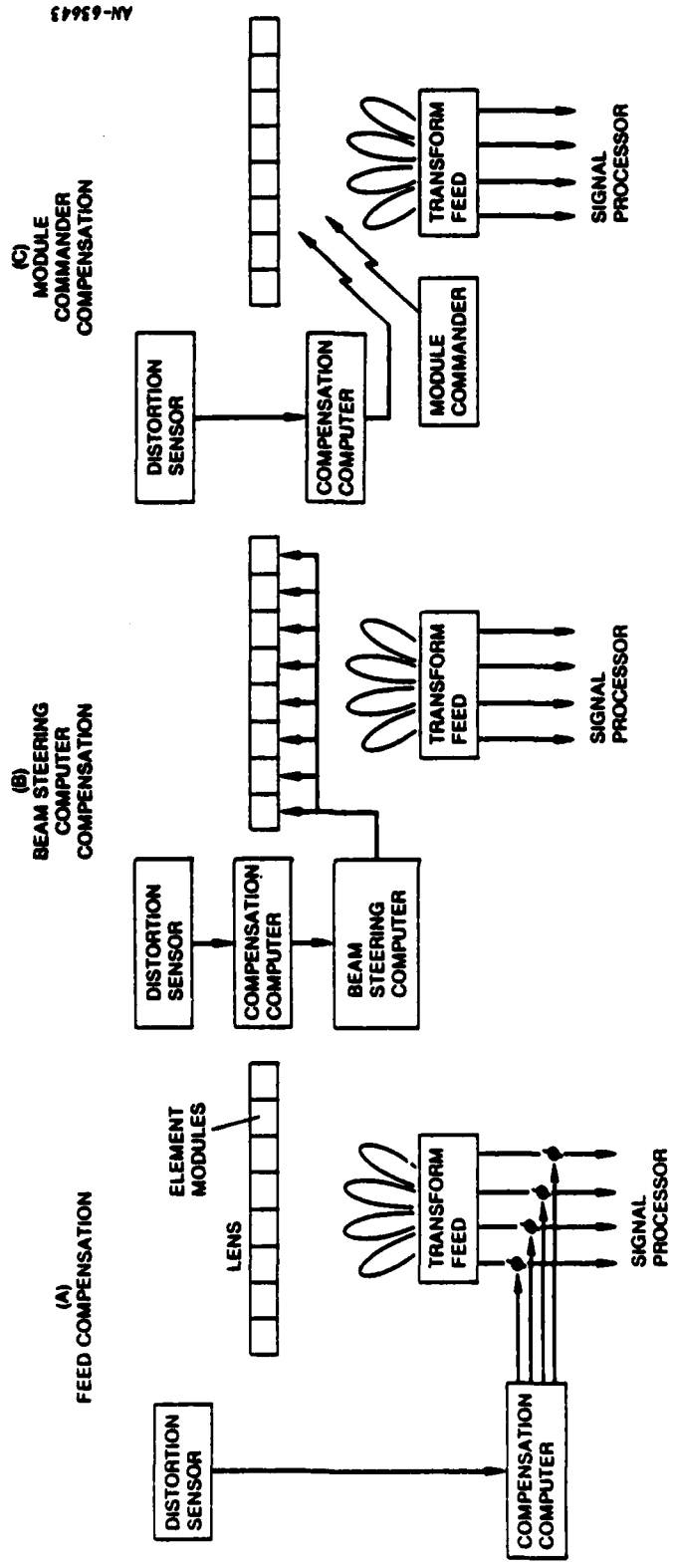
Figure 3.34. Alternate Compensation Methods

used to derive estimates of the mean phase distortion in each of the
feed beams. This mean distortion is then extracted at the feed ports as
shown with the adjustable phase shifters. The effectiveness of feed
compensation depends on the correlation distance of the distortions
across the aperture as well as on the number of feed beams which can be
independently adjusted (see discussion in Sec. 3.2).

Figure 3.34b depicts a different situation for the case in which
the array modules are controlled by a centralized beam steering com-
puter. (The beam steering commands are relayed to the modules via hard-
ware.) In this implementation, the distortion sensor measurements are
fed into a compensation computer which in turn provides inputs for the
beam steering computer to use in adjusting the phases of the individual
elements. The phase shift command given to each module is thus a compo-
site of the phase shift for the nominal beam steering plus a phase shift
to account for the displacement of the module.

Figure 3.34c shows the beam steering architecture originally pro-
posed by the Grumman/Raytheon team. Under this scheme, there is no cen-
tralized beam steering computer. A "module commander" simultaneously
sends to all modules a single command defining the direction of the
desired beam. Each module has a small computer which can take the com-
mand and, with knowledge of its own location, compute its own phase
shifter setting. In order for this approach to work in the presence of
distortion errors, each module's knowledge of its own position must be
updated. Thus, the module must be modified to accept revised coordi-
nates to be used in computing its phase shift. The "compensation compu-
ter" depicted in the figure would use the outputs from the distortion
sensor to compute the coordinates of each module. These new coordinates
would then be radio-linked to the modules. The coordinate updating can
be done at a much lower rate than the beam steering and thus, although
the modules must be individually addressed, the data rates are not
likely to be a problem.

In the preceding paragraphs we have tacitly assumed that the distortion sensing device is separate from the modules and feed. This would undoubtedly be the case for the direct and indirect error sensing methods described earlier in Sec. 3.3, but would not necessarily be the case of the RF sensing method. If RF distortion sensing were used, there could be some advantage in combining the distortion sensing and compensation circuits. Figure 3.35 shows two possibilities.

Figure 3.35a depicts a means of both sensing the errors and correcting within the feed. For the purposes of illustration, let us first assume that we are attempting to compensate for phase errors in some direction in which there happens to be an incident plane wave. (This requirement for an ideally-located plane wave will be removed later after the concepts have been described.) The "X" symbol denotes a reference element which must receive the incident reference signal. A phase detector in the feed is used to determine the phase difference between the signal arriving via the reference channel and that arriving via each of the feed ports. This phase difference is then removed by the indicated phase shifter. In the absence of phase shifter errors, the outputs of all feed ports would be made coherent in the direction of the reference signal.

In Fig. 3.35b, error detection and compensation is performed within the individual elements. With this scheme, the reference signal arriving on the target side of the array is received and relayed to the feed side for reradiation. Thus, the membrane and each array module will be simultaneously illuminated with a coherent signal on both sides of the array. If each module had a phase detector, the phase difference between the two signals could be measured. The measured phase difference would be determined by the location of the module and the path length differences between the reference signals arriving at the front and rear side of the array face. By measuring the phase difference for reference sources in four different directions, it would be possible for

(A)
SENSING & COMPENSATION
IN FEED
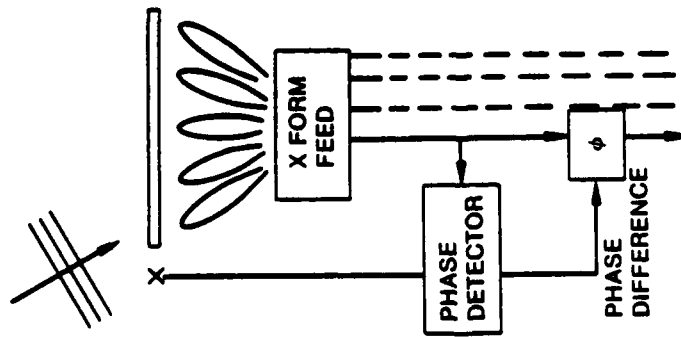
(B)
SENSING & COMPENSATION
IN EACH ELEMENT
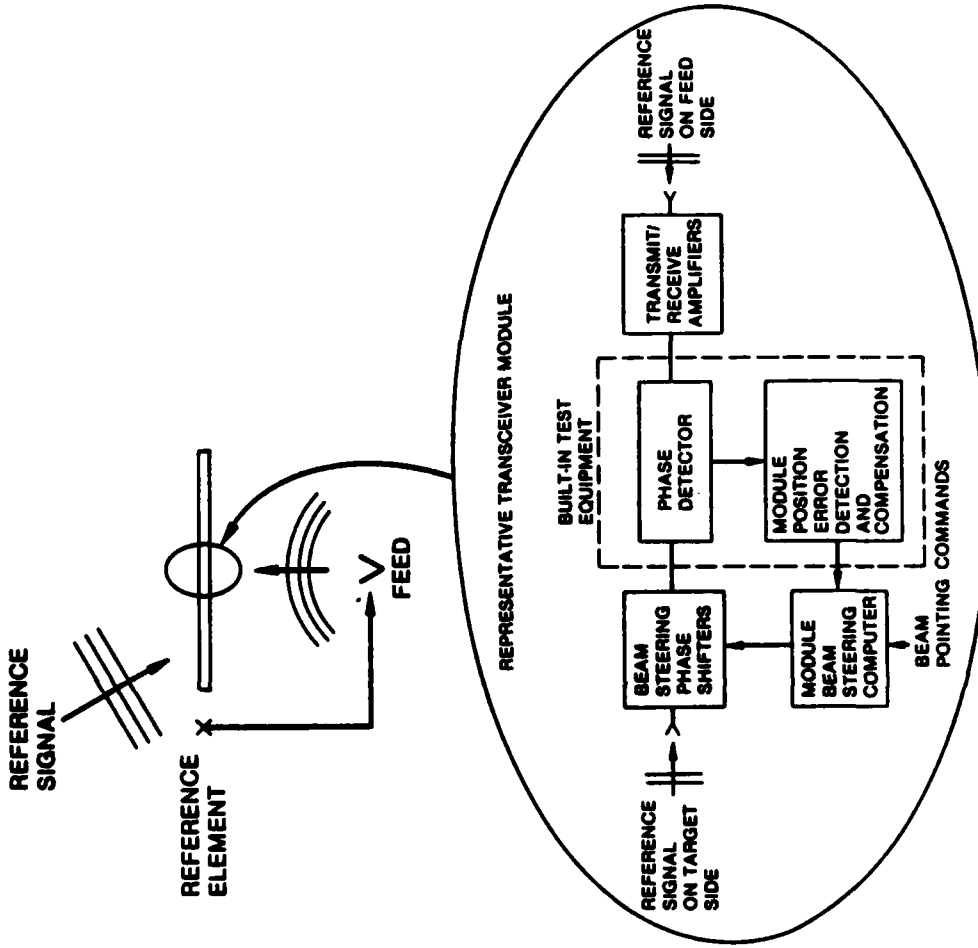
Figure 3.35. Integrated RF Phase Sensing and Compensation Methods

81

the module to determine its own position. This self-surveying capability could be independently done within each module to update its coordinates used in computing the proper phase shift for steering the beam in a specified direction.

The hardware and logic necessary to implement the displacement sensing and compensation with the array modules could probably be added to the module circuits fairly easily and would result in an exceedingly robust method of dealing with displacement errors. Figure 3.36 shows how the proposed Grumman/Raytheon transceiver module could be modified with the addition of a phase detector. A phase detector capable of making the necessary measurement has already been designed by General Electric.[1] Although General Electric was interested in monitoring transceiver performance, their design could as well be used to detect module displacement errors.

3.5 PERFORMANCE MONITORING

Table 3.4 lists the key performance parameters which could be monitored to verify that an orbiting SBR is in fact meeting the required specification. In the following subsections, we discuss each performance parameter and identify alternative methods of measuring the parameter.

The discussion focuses on "total system tests" which directly measure the performance of the fully integrated system. Although subsystem testing will be necessary to isolate the source of deficiencies, the higher level tests considered here are needed to measure the overall system performance.

3.5.1 Sensitivity

Table 3.5 lists a number of techniques which might be employed to measure system sensitivity.

---

[1] R.J. Naster et al., op. cit.
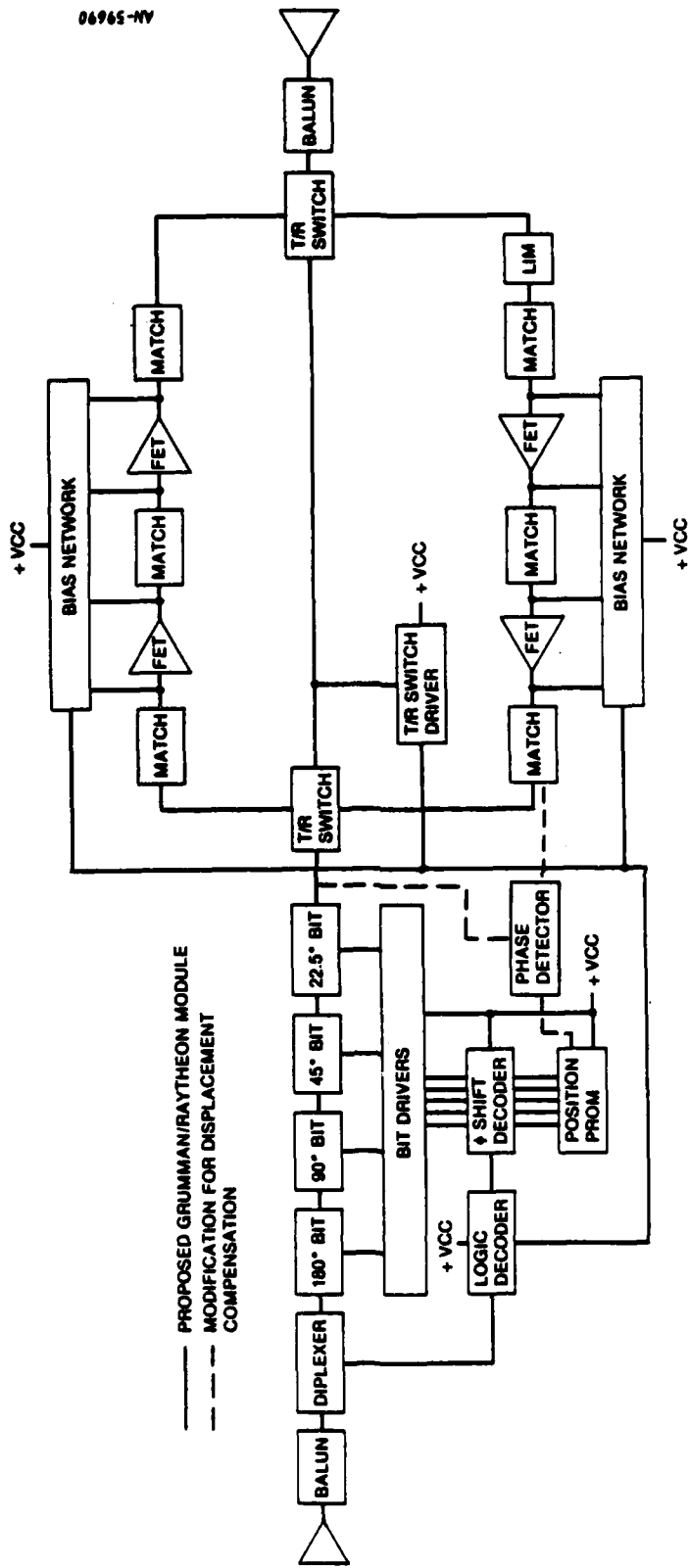
Figure 3.36. SBR Transceiver Module Functional Block Diagram

83

TABLE 3.4

KEY PERFORMANCE PARAMETERS

Sensitivity
Accuracy
Resolution
Sidelobe Levels
Clutter Rejection
Adaptive Nulling

Conventional targets of opportunity (aircraft and satellites) could be used to obtain a rough estimate of the system sensitivity. However, since the radar cross section (RCS) of these targets is generally uncalibrated and fluctuates wildly for small changes of aspect angle, these conventional targets would not lead to accurate measurements of sensitivity.

A radar's sensitivity is generally established with the aid of calibrated test targets of known RCS. Corner reflectors and spheres of large radius $(R \gg \lambda)$ are frequently used. They are generally located on boresight towers which are high enough to push any multipath effects into sidelobes. Balloons are useful for ship-based radars when boresight towers are not available.

Unfortunately, ground clutter precludes the use of conventional stationary calibrated targets. When the SBR directs its beam to a stationary target, the target return will be competing with a huge clutter return at the same Doppler offset as the target. Thus, if a ground- or airborne-calibrated target is to be used, it must be moving with a radial velocity above the minimum detectable velocity (MDV) of the radar.

84

TABLE 3.5

SENSITIVITY MEASUREMENT TECHNIQUES

Technique	Issues
Conventional Targets of Opportunity	
Aircraft/Satellite	Target calibration difficult
Calibrated Targets (Spheres/Corner Reflectors)	
Stationary	Ground clutter prevents detection (no Doppler)
Rotating/Moving	Multipath and $\ddot{R}$ may be a problem
Airborne	Requires low RCS vehicle
Orbital	Sphere ideal (~1 m diameter), some already in orbit, Doppler rates must be considered
Ground-Based Transponder	
Delayed Replay	Requires calibrated receiver and transmitter (may require SBR mods)
Frequency-Shifted Replay	Requires calibrated receiver and transmitter
Ground-Base Receiver and Transmitter	Requires calibrated receiver and transmitter (may require SBR mods)

Calibrated ground-based targets could in principle be rapidly moved in straight lines or rotated around a point in order to generate the required Doppler shift. However, both methods would be subject to multipath and a Doppler spreading of the signal as a result of radial accelerations (i.e., the rotating target would be constantly accelerating and decelerating along the radar line-of-sight; the target following a straight path would similarly have to accelerate and decelerate to remain within a line of practical length).

These problems could perhaps be alleviated by placing the calibrated target on an airborne platform, although one would then have to contend with the possible interfering effects of the support platform. In pursuing this approach, the following question would have to be addressed: How difficult would it be to make a support platform capable of supporting a calibration target, yet have negligible RCS compared with the calibration target?

One attractive method of solving both the clutter problem and the platform problem is to use calibration spheres in orbit. Conducting spheres with a diameter of about 1 m could simulate targets with an RCS of 1 m^2. Multipath would not be a problem with such spheres, nor would there be interference from a supporting platform. The Doppler frequencies for such orbital spheres might differ substantially from those for real targets; although designing the radar to cover these additional Doppler rates would not be a significant problem.

The only concern we can identify is the cost of placing the calibration spheres in orbit. However, with Shuttle coming on line, we doubt that orbiting the spheres would be much of a problem. Furthermore, some calibration spheres were orbited a number of years ago under a previous Lincoln Laboratory program. Some of these targets may in fact still be in orbit and could be used for SBR calibration.

Another possibility listed in Table 3.5 is to use a ground-based transponder. Under this approach, the SBR beam would be directed to transmit in the direction of a calibrated ground-based receiver. The received signal would then be re-radiated at a power level chosen to simulate a target of specified RCS. Measurement of the power received on the ground and the signal-to-noise level at the SBR receiver would permit an estimate to be made of the radar sensitivity.

Using a transponder, the ground clutter problem could be solved in two ways. First, the transponder's emission could be delayed so that it arrives at the radar at a different time than the mainbeam clutter return. (The radar would thus record a false range, but this range difference would be of little consequence.) Second, the transponder could shift the frequency of the return so that it falls outside of the clutter-blinded Doppler band. In this way the transponder could simulate moving targets of any desired velocity, RCS, and range.

As will be seen in later subsections, a transponder would be desirable for making a number of other calibration measurements as well. Thus, one might make a strong case for it on the basis of its versatility. The only concern we have identified about its use for sensitivity calibration, is that the transponder's receiver and transmitter must have a fairly accurate power calibration. (The orbital calibration spheres are of course free of such errors.)

Finally, it should be noted that a minor variation on the transponder idea would be to use an independent ground-based receiver and transmitter.

3.5.2 Accuracy

Table 3.6 lists various methods of measuring SBR range and angle measurement accuracy. If aircraft targets were used, the estimates of accuracy would be limited by the uncertainties in the target's true position at the time of the measurement. With the use of GPS or other tracking aids, the target position uncertainties could probably be made insignificant.

Ground-based devices, as listed in Table 3.6, could also be used, although these approaches must deal with the same clutter, multipath, and changing Doppler problems previously noted in measuring system sensitivity.

87

TABLE 3.6

RANGE AND ANGLE ACCURACY MEASUREMENT TECHNIQUES

Technique	Issues
Satellites of Opportunity	Doppler rates must be considered
Test Aircraft	Requires position/time correlation by on-board navigation, ground tracking, or GPS
Ground-Based Transponder	Return must be separable from clutter (frequency shift, time delay, high power)
Ground-Based Transmitter	Does not determine range measurement accuracy
Rotating Target	Multipath and R may be a problem
Ground Clutter Spread Measurement	Requires no additional targets or transmitters

Finally, it should be noted that it may be possible to measure the beam pointing accuracy by aiming the beam at the nadir and observing the Doppler of the clutter. Since the clutter Doppler can be related to the beam pointing angle, this approach can be used to detect beam pointing errors. This approach is investigated in Ref. 1. A principal advantage is that the measurements can be made autonomously by the radar without the aid of targets or transmitters at known locations.

3.5.3 Resolution

Table 3.7 identifies some possibilities for measuring the angle, range, and Doppler resolution of an SBR.

A straightforward method might be to simply track two aircraft which are flying in an ever tightening formation. If the targets are of

---

[1] Grumman Aerospace Corporation and Raytheon Company, private communication, January 1978.

TABLE 3.7

RESOLUTION MEASUREMENT TECHNIQUES

Technique	Issues
Aircraft Tracking	
Tight Formation (Range Resolution)	Unequal target RCS will affect resolution
	Aircraft separation/geometry must be known
Overtaking Flights (Doppler Resolution)	Unequal target RCS
	Aircraft separation/geometry must be known
Ground-Based Transponder (Range and Doppler Resolution)	Requires transponder(s) with adjustable delay and frequency shift
Ground-Based Receiver (Angle Resolution)	Measures transmit beam resolution
Ground-Based Transmitter (Angle Resolution)	Measures receive beam resolution

comparable RCS, the region in which the radar is unable to distinguish the two targets can be used to estimate the system's range resolution. The actual estimate of range resolution would require a computation of the geometry and the corresponding target separation in range when the targets became indistinguishable.

Analogously, a flight of two aircraft with one overtaking the other could be used to establish the Doppler resolution of the system. This test woulu require a favorable target/radar geometry.

Range and Doppler resolution could also be determined, and perhaps more easily, with the use of a ground transponder. Range resolution could be measured by having the transponder emit two signals, one

delayed from the first by a progressively increasing time delay. Alternatively, two signals with differing frequencies could be emitted to observe the Doppler resolution.

Angular resolution could be observed by scanning the beam across a fairly simple receiver which records the signal strength. The measured main beam pattern would establish the transmit beam resolution. The receive beam resolution could analogously be obtained with the use of a ground-based beacon.

3.5.4 Antenna Sidelobes

Table 3.8 lists some possibilities for measuring the antenna sidelobe levels.

Although the first two methods are possible, we do not believe they are as promising as the latter two. By measuring the signal-to-noise ratio of known targets in the sidelobes, it would be possible to estimate the sidelobe level. However, in order to do this, the signal would have to be sufficiently strong to overcome the 100 dB or more two-way antenna sidelobe suppression. Overcoming this much suppression would require either a target with very high RCS and/or very short range.

It has been suggested that by examining the Doppler spectrum of the return clutter, it might be possible to estimate the antenna sidelobe levels. This suggestion is motivated by the observation that the clutter frequency varies with position and hence might be linked with the off-boresight angle. We do not believe this is a very promising approach for the following two reasons: (1) the nominal variations in clutter power due to the differing backscattering coefficients of the earth's surface within the field-of-view will be large enough to obscure all but large variations in sidelobe levels, and (2) there is not a one-to-one correspondence between clutter Doppler and off-axis angle. The

TABLE 3.8

ANTENNA SIDELOBE MEASUREMENT TECHNIQUES

Technique	Issues
Calibrated Targets in Sidelobes	Requires excessively large or very close targets
Ground Clutter Measurement	Lack of one-to-one correspondence between clutter Doppler and off-axis angle, plus nominal clutter RCS variation, makes assessment difficult
Ground-Based Receiver	Measures transmit sidelobes
	Complete sidelobe pattern can be measured
	Measurements can be done on a non-interfering basis with normal operation
Ground-Based Transmitter	Analog of above to measure receive sidelobes

isodops of the return signal (lines of constant Doppler offset) are conic surfaces which pass through large areas of the antenna pattern. Thus, the return at any one Doppler offset represents the integrated power over a widely-spread portion of the antenna pattern. The return power cannot be measured and used to infer the sidelobe level in any particular region.

The last two methods listed in Table 3.8 appear to be more promising and fairly simple to implement. A ground-based receiver can be used to measure the radar signal either when the radar is scanning in some specified pattern or when the beam is fixed and the radar passes through the ground receiver's field-of-view. In either case, a complete sidelobe pattern can be obtained in time. If the radar is programmed to cooperate, the pattern can be obtained fairly rapidly; however, even if the radar continues on with its normal tasks, the sidelobe levels can be

obtained eventually on a non-interfering basis. The only key require-
ment on the ground-based receiver is that it have sufficient dynamic
range to measure the anticipated very low sidelobes.

The above procedures will be adequate for measuring the transmit
sidelobes. An analogous procedure with a ground-based transmitter could
be used to measure the receive sidelobes.

3.5.5 Clutter Rejection

An SBR's ability to detect low RCS and/or low velocity targets is
critically dependent on its clutter rejection capability. Previous
attempts to predict a radar's detection capability in a clutter environ-
ment have been frustrated for two principal reasons:

1. The magnitude and fluctuation statistics of earth-generated
     clutter are not known very accurately.

2. There is some uncertainty as to how much clutter attenuation
     is achievable by the available equipment.

Once the radar is in orbit, both of these uncertainties could be
resolved fairly rapidly by generating clutter maps. That is, the radar
could be systematically directed to aim the beam in selected regions and
measure the received power. Assuming that the radar is not noise
limited, and that the sample region is free of real targets, the clutter
power spectrum could be measured. This spectral data could then be com-
pared with target cross sections and Doppler frequencies to determine
under what situations a desired target could be detected.[1] In addition,
some target measurements should be made to verify that the target sig-
nals are not attenuated during processing. This could be done using
calibrated targets or calibrated transmitters as discussed earlier in
Sec. 3.5.1.

---

[1] Once such clutter maps have been generated for major portions of the
earth, the search regions might be shifted to regions of less clutter.

92
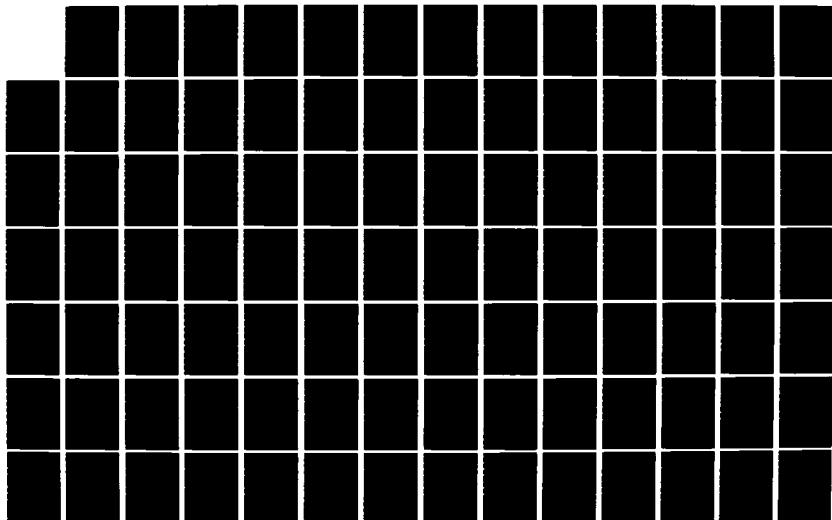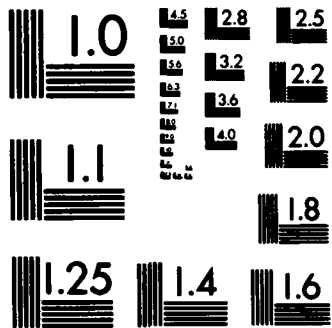
MICROCOPY RESOLUTION TEST CHART
NATIONAL BUREAU OF STANDARDS-1963-A

3.5.6 Adaptive Nulling

To verify that the SLC/Adaptive Nulling circuits are functioning according to specifications, the radar could be illuminated with a number of interfering signals. By varying the amplitude of these signals and observing the effect on the target signal, it would be possible to assess the performance of the nulling circuits.

In performing these tests, it is important to keep in mind that an adversary might be observing the tests for the purpose of finding countermeasures to use against the system. For this reason, it would be desirable to encrypt the communications links to prevent his listening in on such tests.

4   PASSIVE SPACE-FED LENS RADAR

The objective of the work reported here was to examine the trade-offs associated with a passive version of the space-fed lens array and to perform a first-level design of a passive space-fed lens which:

- Is sized to operate against penetrating aircraft in the presence of clutter and jamming

- Extrapolates from existing concepts for active phased-array lenses

- Employs reasonable characteristics for its passive modules

- Investigates both phased-array and traveling-wave tube (TWT) approaches

- Indicates new technical areas which need advancement

Figure 4.1 shows both an active and a passive space-fed lens array system in simplified block diagram form. In the active system, the main lens array modules include the power amplifiers, the low-noise amplifiers, and the phase shifters. In the passive system, the power amplifiers and low-noise amplifiers have been moved to the feed array, and only the phase shifters remain in the main array modules.

This relocation has three primary effects on the system. First, the number of amplifiers is reduced from 100,000-200,000 in the main array (131,000 in the baseline design) to something typically in the range of 1 to 200 in the feed array. This opens up the possibility of using amplifiers which are more complex but have better performance. Second, the weight of the main array modules is reduced. And third, the phase shifters now experience full RF power, and thus add an insertion loss to the passive system's loss budget.

The approach taken in this analysis is to first develop two sets of equations: the loss difference equations (search and track), and the system weight equations (passive and active). These are plotted on a coordinate system with power as the ordinate and aperture as the

94
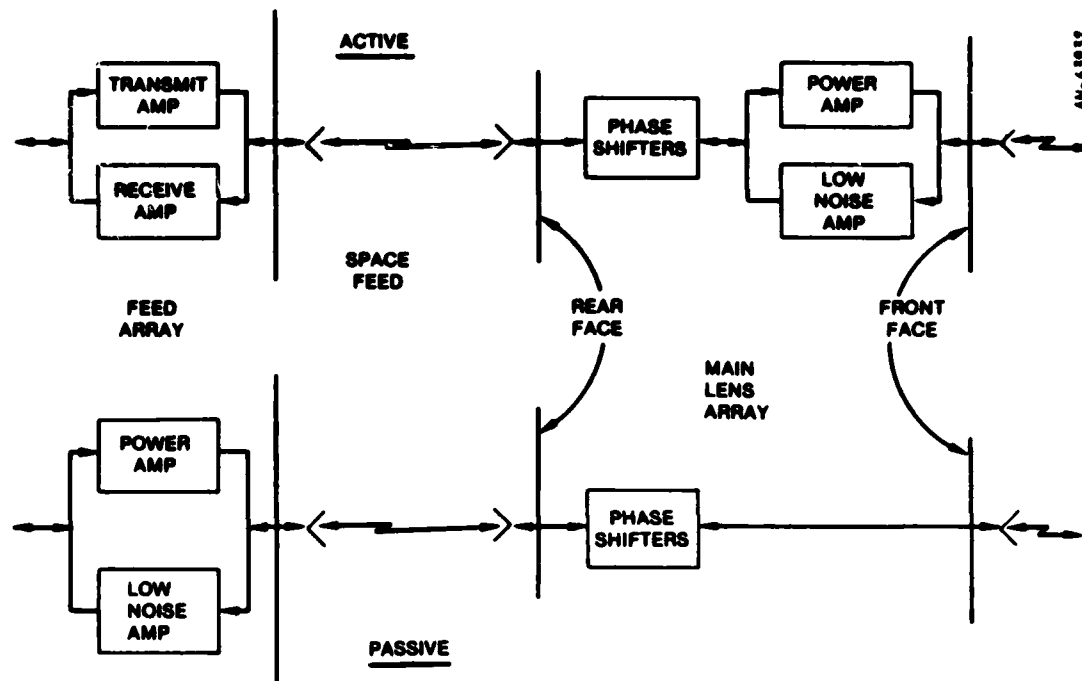
Figure 4.1. Space-Fed Lens Array Systems

abscissa. Then, procedures are examined for overcoming the passive system's insertion-loss penalty. These procedures include:

- Reducing the RF losses
- Improving the power amplifier efficiency
- Reducing DC bias loads
- Reducing power distribution weight
- Reducing passive module weight
- Changing the operating frequency

4.1 LOSS DIFFERENCE EQUATIONS

The loss difference equations are developed using numbers from a Grumman report.[1] The systems to which these numbers apply are termed the baseline systems in this analysis.

---

[1] Grumman Aerospace Corporation/Raytheon Company, private communication, December 1977.

95

These numbers, listed in Table 4.1, are divided into transmit and receive losses for both the active and passive systems. Those loss numbers which differ for the two systems have been extracted from Table 4.1 and listed in Table 4.2. To obtain the final loss difference, the transmit and receive columns in Table 4.2 have been summed, and the total active loss has been subtracted from the total passive loss, for a loss difference of 3.4 dB.

This is the loss which the passive system must overcome in order to be competitive with the active system. It should be noted that 2.4 dB of the 3.4 dB is contributed by the two-way phase shifter insertion loss. Using this loss difference, one may now write the two loss difference equations, one for search and one for track.

$$10 \log \frac{P_p}{6074} + 10 \log \frac{A_p}{\frac{\pi(71)^2}{4}} = 3.4 \qquad \text{(search)}$$

$$10 \log \frac{P_p}{6074} + 20 \log \frac{A_p}{\frac{\pi(71)^2}{4}} + 20 \log \frac{0.24}{\lambda} = 3.4 \qquad \text{(track)}$$

where the logarithms reference the power (P_p), aperture (A_p), and wavelength (λ) of the passive system to the corresponding parameters of the active system:

Power developed = 6074 W

$$\text{Aperture} = \frac{\pi(71)^2}{4} = 3959.2 \text{ m}^2$$

Wavelength = 0.24 m (1.25 GHz)

The first equation states that performance in search is proportional to the product of power and aperture (in logarithmic form) and

TABLE 4.1

BASELINE LOSS

	Transmit		Receive	
	Active Lens	Passive Lens	Active Lens	Passive Lens
Antenna Losses				
Aperture illumination	0.00	1.2 [**]	2.80	1.2 [**]
Spillover		0.3		0.3
Blockage, 4.7 m dia out of 71 m	0.00	0.00	0.00	0.00
Mechanical errors	0.04	0.04	0.04	0.04
Missing elements	0.08	0.08	0.08	0.08
VSWR: (1.5:1): front face	0.18	0.18	0.18	0.18
(1.35:1): back face	0.00	0.10	0.00	0.10
Theoretical prediction inaccuracies	0.40	0.40	0.40	0.40
	0.70	2.30	3.50	2.30
Phase Shifter Losses and Associated Hardware				
Cable and antenna element	0.20	0.20	0.20	0.20
Feed	0.00	0.20	0.00	0.20
Duplexer	0.30	0.30	0.30	0.30
Receiver protector			0.30	0.30
Phase shifter [*]		1.20		1.20
Miscellaneous	0.10	0.10	0.10	0.10
	0.60	2.00	0.90	2.30
Non ohmic	0.20 [†]	0.30 [††]	0.20	0.30
Additional Losses ($\theta = 35°$)				
Atmospheric	0.56	0.56		
Processing			3.40	3.40

---

[*] $f = 1.25$ GHz

[**] 17.3 dB edge taper for truncated Gaussian illumination, 34 dB peak sidelobe (first), n = 2.4

[†] 6.03° phase, 0.57 dB amplitude, 1.5% element failure

[††] 13.6° phase, 0.40 dB amplitude, 1.0% element failure

TABLE 4.2

BASELINE LOSS DIFFERENCE

	TRANSMIT		RECEIVE	
	ACTIVE LENS	PASSIVE LENS	ACTIVE LENS	PASSIVE LENS
APERTURE ILLUMINATION	0.0	1.2	2.8	1.2
SPILLOVER	—	0.3	—	0.3
VSWR (1.38:1) BACK FACE	0.0	0.1	0.0	0.1
FEED	0.0	0.2	0.0	0.2
PHASE SHIFTERS	—	1.2	—	1.2
NON OHMIC	0.2	0.3	0.2	0.3
	0.2	3.3	3.0	3.3

LOSS DIFFERENCE BETWEEN
BASELINE SYSTEMS
3.4 db

that 3.4 dB must be added to the passive system's performance, in terms
of these two parameters, to obtain performance equivalent to the active
system. The second equation makes a similar statement for the track
mode, where performance is proportional to the product of power and
aperture squared divided by the square of the wavelength.

These two equations are plotted in Fig. 4.2. A passive system
operating at a point located on one of the curves would have performance
equivalent to the active system's performance in the same mode (search
or track). Where the two curves cross, performance in both modes is
equivalent. An operating point above the curves indicates better per-
formance for the passive system, and below the curves worse, than for
the active system.

From the loss difference equations, it can be seen that only the
track curve changes as the operating frequency is changed; the search
curve remains fixed. As the operating frequency is changed, the track
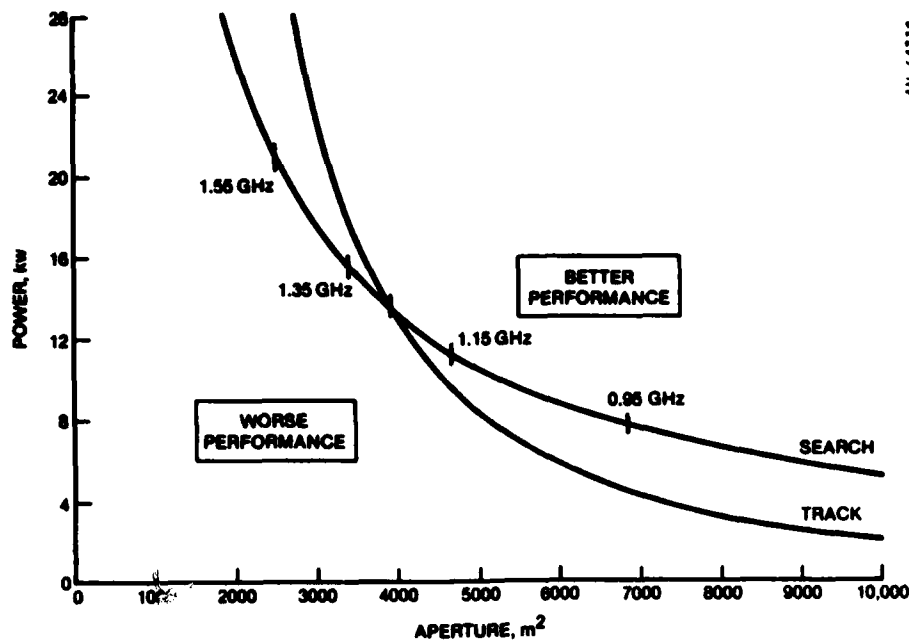
Figure 4.2. Loss Difference Equations (1.25 GHz)

curve shifts toward or away from the origin and crosses the search curve
at new points. Several of these crossover points are shown in Fig. 4.2
along with the corresponding operating frequency. Thus, the primary
effect of changing the operating frequency is to trade power and aper-
ture (if performance is to be equal to that of the active system in both
modes).

Although the search curve remains fixed (based upon the loss
difference equations) as operating frequency is varied, it is possible
that components which are less lossy might be selected at a new opera-
ting frequency, and thus the curve pair (track and search) might move
downward. This was examined as part of this study, but did not turn out
to be the case.

Figure 4.3 shows the movement of the search curve as a function of
modifying the loss difference. As the search curve (and the correspond-
ing track curve) moves up or down with changes in loss difference, the
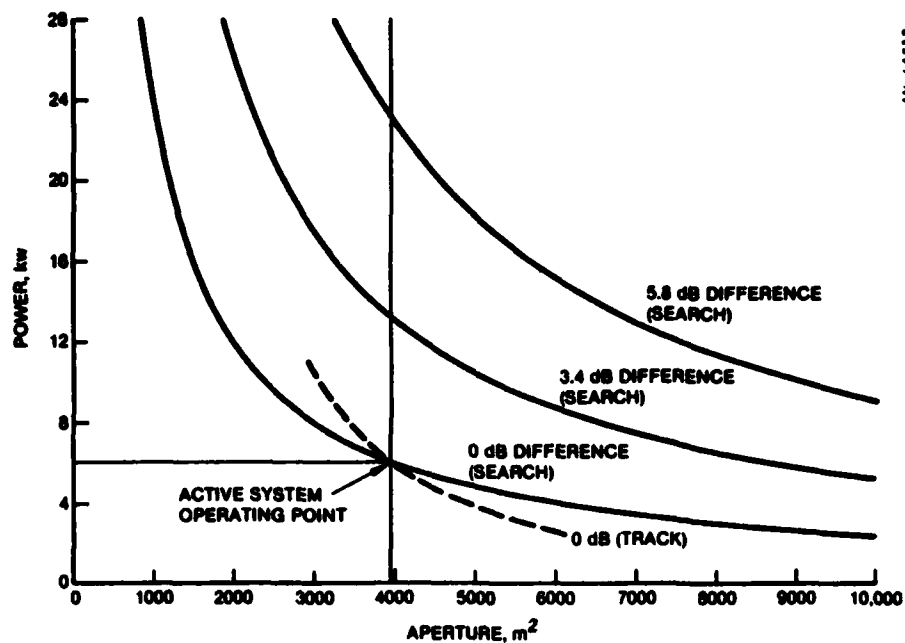
Figure 4.3. Search Curves as a Function of Loss Difference (1.25 GHz)

---

crossover point remains pegged at the same aperture value. The bottom
curve (0 dB), with the track curve shown dashed, is for a system with
the same loss budget as the active system. The active system operating
point is at crossover. The upper search curve (5.8 dB) is the perfor-
mance curve for a system in which the phase shifter insertion loss has
been doubled (from 2.4 dB to 4.8 dB).

4.2 WEIGHT EQUATIONS

In order to compare various system configurations, it is necessary
to develop weight equations which reflect the penalty, in terms of
weight, for adding additional power or aperture. Grumman weight esti-
mates, shown in Table 4.3, have been used for this purpose. From these,
we have derived the specific weights (per watt of power and per square
meter of aperture) shown in Table 4.4. Using these specific weights,
the weight equations can be written as follows:

TABLE 4.3
BASELINE WEIGHTS

Component	Unit Weight (lb)	Total Weight (lb)
Spacecraft Structure		
Lower Systems Package	570	
Upper Systems Package	250	
Mast Cannister	95	
Mast	250	1,165
Phased Array Antenna		
Structure	1,300	
*Modules (130,000 at 0.03 lb each)	3,900	5,200
Electrical Power System		2,150
Radar Electronics (Upper Systems Package)		120
Communications and TT&C		315
Attitude and Velocity Control		250
Redundancy and Miscellaneous		300
		9,500

*Use 0.02 for passive system modules.

$$W = 2150 + 0.354P_A + 1.31A_A \qquad \text{(active system)}$$

$$W = 2150 + 0.354P_P + 0.985A_P \qquad \text{(passive system)}$$

where P_P and A_P are passive system power and aperture, P_A and A_A are active system power and aperture, and 2150 is the additional fixed weight.

TABLE 4.4
SPECIFIC WEIGHTS

Weight of Electrical Power System (EPS)	2,150 lb
RF Power Developed (Active System Operating Point)	6,074 W
Specific Weight of EPS = 2,150/6,074 =	0.354 lb/W_{RF}
Weight of Antenna (Active, Modules = 0.03 lb each)	5,200 lb
Weight of Antenna (Passive, Modules = 0.02 lb each)	3,900 lb
Area of Antenna	3,959 m^2
Specific Weight of Antenna (Active) = 5,200/3,959 =	1.31 lb/m^2
Specific Weight of Antenna (Passive) = 3,900/3,959 =	0.985 lb/m^2
Additional Fixed Weight	2,150 lb

These two equations are plotted in Fig. 4.4 for a baseline weight of 9500 lb. Also plotted on the same graph is that portion of the search and track curves, from Fig. 4.2, which governs performance. For any point on that curve, the passive system's performance is equal to or better than active system performance in both search and track. At point a, the crossover point, performance is "equal to" in both modes.

A natural first question to ask is: What is the minimum-weight passive system, which will perform equal to or better than the active system, that can be achieved by modifying only the power and the aperture? This can be solved as a constrained optimization problem, and the answer is a passive system weight of 10,716 lb, with the weight allocated to power and aperture as indicated by the corresponding weight line in Fig. 4.4.

A second alternative is to find procedures for reducing some of the passive RF losses and thus moving the track-search curve downward. If 1.35 dB of loss can be recovered, the crossover point will intersect

102
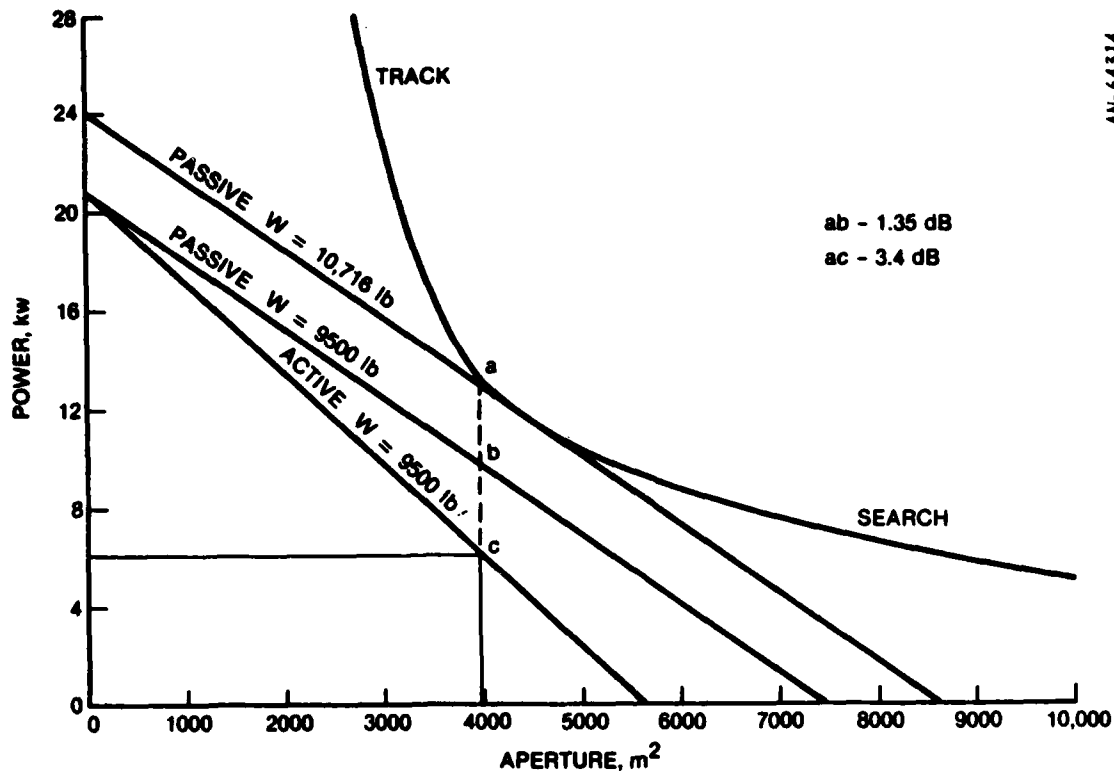
Figure 4.4. Alternative System Designs

the 9,500 lb passive weight line at point b. If 3.4 dB can be recov-
ered, the intersection will occur at point c. Systems with these RF
loss reductions will have the active system equivalences shown in Table
4.5.

The possibility also exists of modifying the coefficients in the
passive weight equation to cause the 9,500 lb weight line to swing
upward and contact the performance curves. This is illustrated in Fig.
4.5 along with the coefficient changes needed to accomplish this swing.
Table 4.6 summarizes the system characteristics for systems which are
achieved in this fashion.

TABLE 4.5

PASSIVE SYSTEM EQUIVALENCES FOR RECOVERED RF LOSSES

Loss Improvement	System Equivalence
1.35 dB	Performance
	Weight
	Size
	(Higher Power)
3.4 dB	Performance
	Power
	Size
	(Lighter Weight)
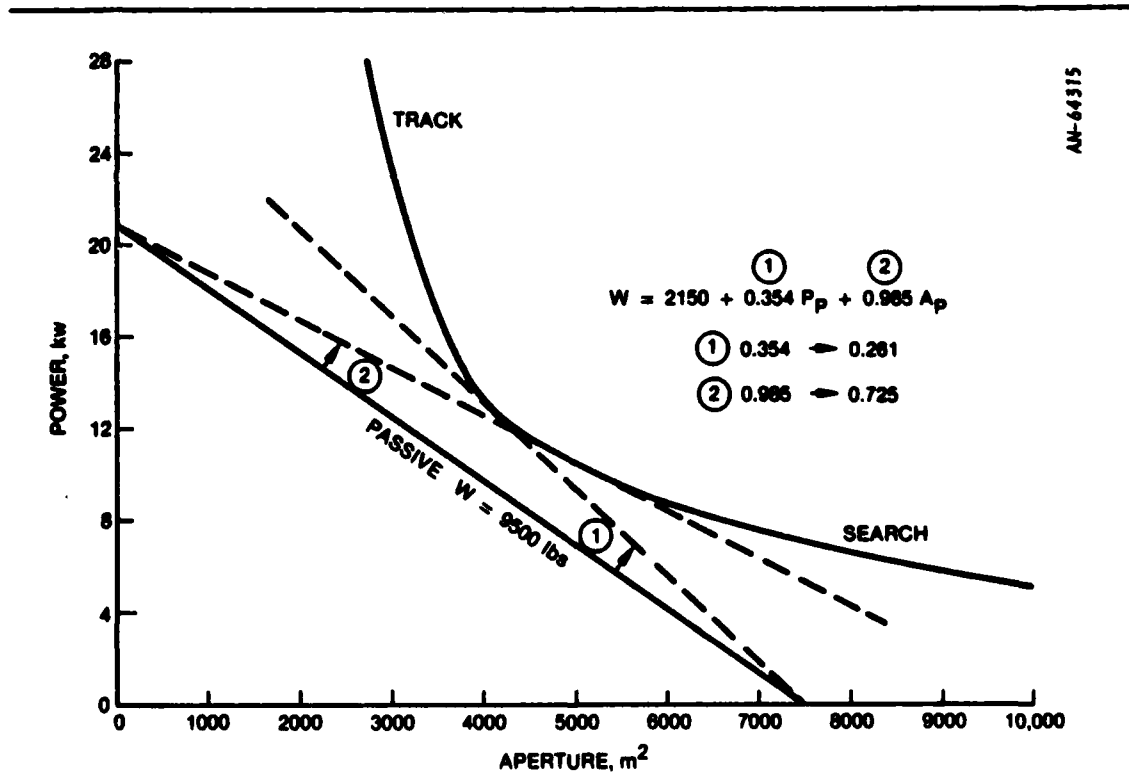
Figure 4.5. Requirements for Reaching Weight Parity With the Active System

104

TABLE 4.6

PASSIVE SYSTEM EQUIVALENCES FOR INDICATED COEFFICIENT CHANGES

Coefficient	System Equivalence
0.354 → 0.261	Performance
	Weight
	Size (Approximate)[*]
	(Higher Power)
0.985 → 0.725	Performance
	Weight
	(Higher Power)
	(Larger Size)

[*] Slight adjustment in frequency would be needed to reposition crossover point.

The remainder of this section examines methods by which these system modifications can be achieved.

4.3 REDUCTION OF RF LOSSES

Two components which contribute directly to the passive system's loss chain are the phase shifters and the low-noise amplifiers. As mentioned earlier, phase shifters contribute loss because they follow the power amplifiers in the passive system design. The low-noise amplifiers have been assumed to contribute loss equally to the active and passive baseline systems; however, moving these amplifiers to the feed array in the passive system makes possible an improved design because of the reduced number required.

Since any reduction in phase shifter insertion loss is a direct improvement in the passive system (all other characteristics remaining

fixed), phase shifter technology was examined in some detail. A summary
of this examination is shown in Table 4.7. In this table, each of the
phase shifter types, considered as alternatives to the MMIC shifters, is
shown to have inherent disadvantages. Thus, the conclusion to be drawn
from this examination is that, if the weight and loss estimates are
roughly accurate, and if the shifters can be made to draw negligible
bias current, then monolithic microwave integrated circuit (MMIC)
shifters are unquestionably the best choice for this application.

TABLE 4.7
PHASE SHIFTER TECHNOLOGY

MMIC IGFET Shifters

    Provided loss estimate for this analysis (passive) (2.2 dB)

    Assumed to draw negligible bias current (active and passive)

    Provided weight estimate for this analysis (0.02 lb)

Pin Diode Shifters

    No RF loss improvement

    Excessive bias currents

Ferrite Shifters

    Better loss performance

    Not applicable at 1.25 GHz

    Excessive weight at higher frequencies

Line Length Shifting (TEM Lens)

    Higher RF losses

    Severe feed design problem

Variable Dielectric Shifting (Waveguide Lens)

    Excessive weight

    Severe feed design problem

Conclusions for the low-noise amplifiers are not so well defined. The noise figure estimate for these amplifiers, based upon the use of FETs, was 2.0 dB for both the active and passive systems. This estimate seems high, considering what is now available. [See, for example, the NE700 and 720 GaAs FETs manufactured by Nippon Electric Company, Ltd (NEC).]

In addition, both the gain and noise figure of these amplifiers improve with cooling. Keeping the temperature of the amplifiers low and stable is a major problem if they are spread out over a 71 m aperture. But if there are several orders of magnitude fewer of them and they are concentrated in the feed array, as in the passive system, it may be possible to cool them to improve the gain and noise figure.

However, there is little motivation for improving noise performance if system noise is not predominant. If clutter or jamming dictate the noise floor, as will sometimes be the case for the SBR mission, then system performance will not be enhanced by reducing the noise figure.

4.4   POWER AMPLIFIER EFFICIENCY

In Sec. 4.2, procedures were examined for rotating the 9500 lb passive weight line upward toward the equivalent performance curve (Fig. 4.5). One procedure for accomplishing this is to reduce the power system specific weight: at a specific weight of 0.261 W/lb the weight line will be tangent to the equivalent performance curve. If all of the power system inefficiency is assumed to be associated with the power amplifiers, then this can be accomplished by increasing the power amplifier efficiency from 35% to 47.5%. As shown in Table 4.6 and Fig. 4.6, this yields a passive system with equivalent performance, weight, and size, but radiating a higher level of RF power.

Power amplification for the active system is assumed to take place in solid-state amplifiers located throughout the main array. In the

107
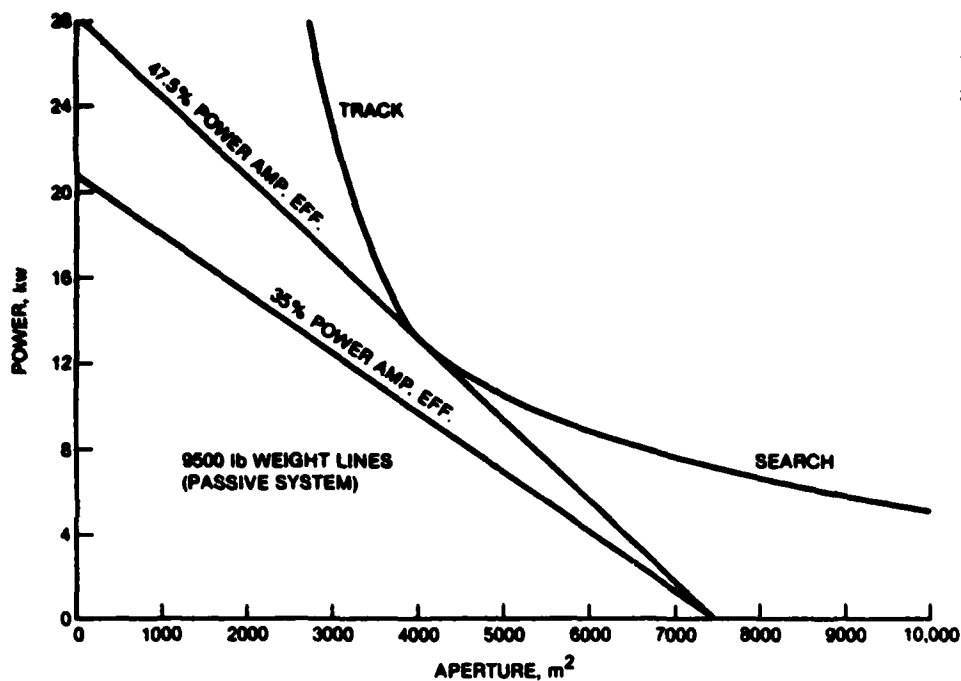
Figure 4.6. Effect of Improved Power Amplifier Efficiency

---

passive system, these amplifiers are located in the feed array, and consequently a much smaller number are required. This again allows the use of alternative devices for amplification. One attractive possibility is the traveling wave tube (TWT) amplifier.

The two most outstanding attributes of TWTs are high power amplification, up to 60 dB in a single device, and wide bandwidth, as much as an octave or more. For space applications, TWT designs are predicated on periodic permanent-magnet (PPM) beam focusing structures, which limit the average power handling capability. (Increasing this limit is an active area of research. Designs for tubes handling up to 260 W have been published in the open literature.) Most of the recent TWT designs for use in space have efficiencies in the range of 45% to 55%, are relatively light in weight, and have life expectancies approaching ten years.

These tubes are more commonly used at operating frequencies higher
than L band, although one L band design has flown on the MARISAT satel-
lite. This does not necessarily imply that TWTs at L band are impracti-
cal: new tube types are generally developed where there is an immediate
application to fund that development, and L band is an uncommon fre-
quency band for communication satellites.

In applying TWTs to the passive design, the major parameters of
interest are the weight of the tubes, the power handling capability of
the tubes, and the conversion efficiency. To express this, the 9500 lb
passive weight line equation was written as

$$9500 = (2150 - 120) + W_{TWT} + \frac{12.9}{(\% \text{ eff})_{TWT}} P_P + 0.985 A_P$$

where   9500 = total system weight

                120 = active feed weight

                W_{TWT} = total weight of the traveling wave tubes

                $(\%)_{TWT}$ = efficiency of the tubes

and P_P and A_P are as before.

In Fig. 4.7, the efficiency and weight per tube are plotted for
division of approximately 13 kW average power between various numbers of
tubes. If 55% is taken as the maximum achievable efficiency, and if
tube weight can be held to something between 8 and 16 lb (reasonable
numbers for lightweight TWTs), then the power per tube which must be
attained is between 200 and 350 W average. If this level of performance
can be achieved, then all of the difference in performance between the
passive and active system can be made up by going to TWTs as the power
amplification device.
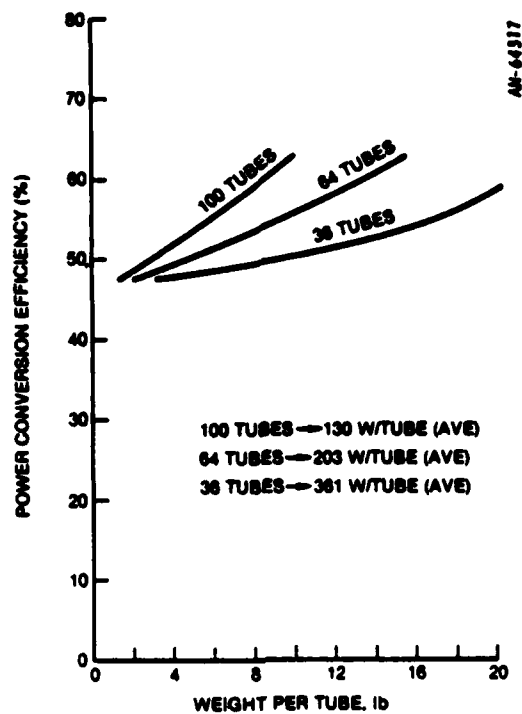
Figure 4.7. Traveling Wave Tube Weight Versus Efficiency for a Passive System Which Matches the Active System in Size, Weight, and Performance

---

4.5 FIXED DC LOADS

In the preceding section it was assumed that all of the DC power was utilized by the power amplifiers, and that the DC requirements of other circuits were negligible by comparison. In this section we lift that restriction.

From the data available, in Ref. 1, it was impossible to determine whether bias currents to circuits other than the power amplifiers were considered in the determination of the battery weight. For this reason two cases are considered: one in which an additional fixed DC load is part of the 2,150 lb battery weight, and one in which fixed loads are in addition to those supplied by the 2,150 lb of batteries.

---

[1] Grumman Aerospace Corporation/Raytheon Company, private communication, December 1977.

110

Further, it is reasonable to assume that this additional fixed
load supplies the low-noise amplifiers in the active system and, because
of moving these amplifiers to the feed array in the passive system, this
load becomes negligible. Where it is appropriate to distribute this
fixed active load to obtain numbers on a per-module basis, this is done
at the active system operating point with 130,000 modules assumed.

The computations for each of the two cases are summarized in
Tables 4.8 and 4.9. The corresponding weight lines are shown in Figs.
4.8 and 4.9 for the two cases. Since bias power on the order of 0.1 W
per low-noise amplifier would be expected to be dissipated, movement of
these amplifiers to the fixed array, alone, might be sufficient to favor
the passive design.

4.6 POWER DISTRIBUTION WEIGHT

In the preceding section, it was assumed that the power system
weight was reduced by eliminating that portion of the batteries sup-
plying power to the low-noise amplifiers. Moving these amplifiers and
the power amplifiers to the feed array should also reduce the weight of
the power distribution system.

From Fig. 4.5, the amount of weight which must be taken out of
power distribution before the passive system's weight and performance
are equivalent to those of the active system (assuming power distribu-
tion weight is charged to the EPS) is an amount sufficient to reduce the
power system specific weight from 0.354 to 0.261. This weight was cal-
culated to be 559 lb or 17.5 lb per gore. This would yield the passive
weight line that was labeled (1) in Fig. 4.5.

Now, assume the second case (Sec. 4.5)—batteries for fixed load
included in the 2,150 lb—and assume that power distribution weight is
also removed. Then the equation for the EPS specific weight coefficient
for the passive system becomes

111

TABLE 4.8

CASE 1

- 2150 lb battery weight supplies only RF load

- Output power is 6074 W average. Efficiency is 35%.

- Required DC power is $6074/0.35 = 17,354$ W

- Specific weight for DC power is $2150/17,354 = 0.124$ lb/W and is the penalty in terms of weight for adding additional DC loads

- To match the 10,716 lb passive system weight line on Fig. 4.4

$$\frac{10,716 - 9500}{0.124} = 9806 \text{ W}$$

of fixed load power can be supplied by the active system.

- Thus, if $9806/130,000 = 0.075$ W is supplied to each low noise amplifier in the active system, the two systems are automaticallly equivalent in performance and weight.

$$Y \times \frac{(2150 - x)}{6074} = 0.261$$

where

$x =$ amount of weight removed from the power distribution system

$(2150 - x) =$ remaining power system weight

$Y =$ that part of the weight charged to the RF power in the active system

TABLE 4.9

CASE 2

- 2150 lb battery weight includes additional fixed DC loads
  (supplied to the low noise amplifiers)

- Y% of the battery weight supplies the RF portion of the load, and
  the specific weight for RF power is

$$\frac{0.Y \times 2150}{6074} = (\text{specific weight})_{RF}$$

- At 35% efficiency, 17,354 W of DC power are still required for the
  RF load and the specific weight for DC load is

$$\frac{0.Y \times 2150}{17,354} = (\text{specific weight})_{DC}$$

- From Fig. 4.5, the passive weight line achieves equivalent
  performance when the power system specific weight is 0.261. This
  occurs when $Y = 0.261/0.354 = 0.74$.

- Thus, an active system in which $(1.0 - 0.74) \times 2150 = 559$ lb is
  devoted to fixed loads is equivalent to a passive system with
  these loads removed.

- On a per module basis this is

$$\frac{P_{DC}}{130,000} = \frac{559}{0.74 \times 0.124 \times 130,000} = 0.047 \text{ W/module}$$

113
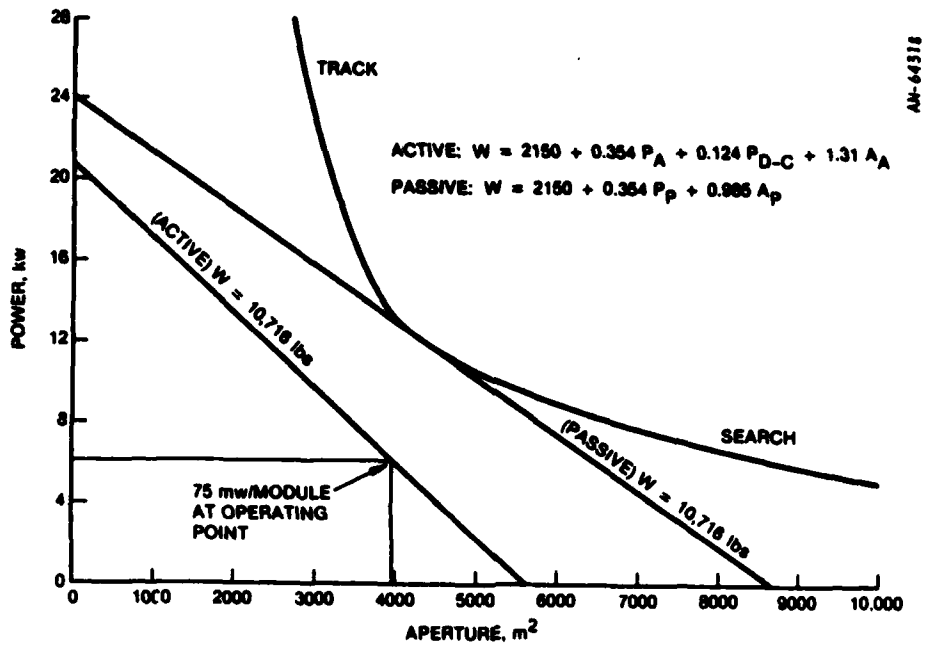
Figure 4.8. Case 1: Batteries for Fixed Load Added to 2150 lb Power System Weight
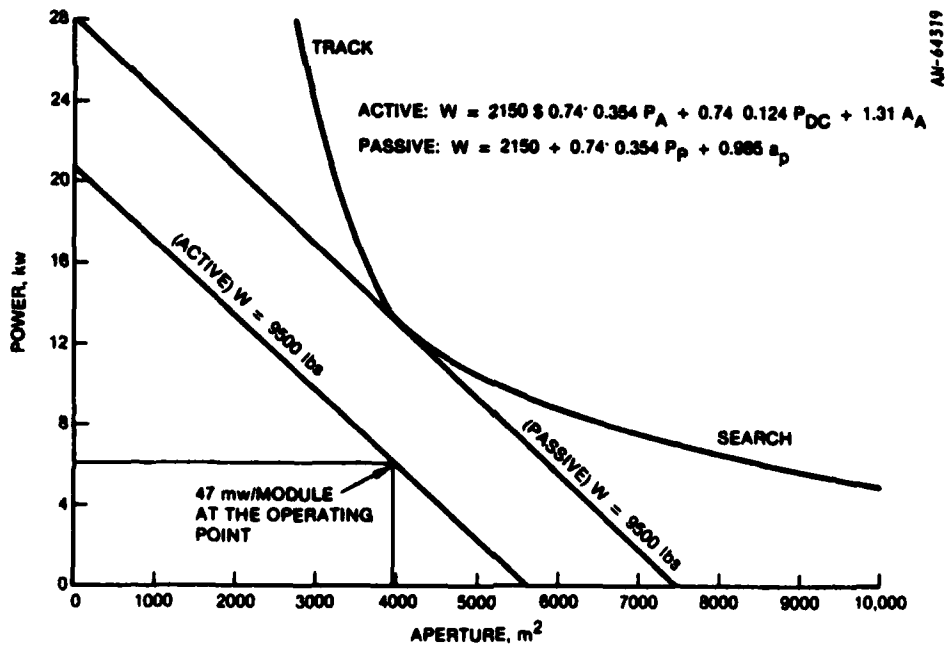
Figure 4.9. Case 2: Batteries for Fixed Load Part of 2150 lb Power System; 74% of Weight Allocated to RF, 26% of Weight Allocated to Fixed Load

114

If we let u equal the watts per module at the active-system
operating point and v equal the weight removed on a per-gore basis,
the preceding equation, after some algebra, may be written as

$$4240u + 11.33v = 200$$

This equation is plotted in Fig. 4.10. Any combined savings on or
above this line will yield a passive system with equal or better perfor-
mance. Note also that the intercepts on either axis correspond to the
points previously computed on an independent basis for each of those
variables. Thus, for example, a saving of 10 lb per gore and 10 mW per
module would make the passive system equivalent in weight and perfor-
mance (and very close to the same size).

To further explore the potential for equivalence, phase shifter
insertion loss was assumed to double, increasing the loss difference to
5.8 dB, and a new line was plotted on the power per module versus weight
per gore axes. This plot shows that a combination of 100 mW/module and
17 lb/gore saving would give weight, performance, and size equivalence.

4.7   MODULE WEIGHT

One final consideration is the weight estimates for the active and
passive system modules (0.03 lb per module for the active system and
0.02 lb per module for the passive system, both based upon MMIC techno-
logy). If the weight of the passive system module can be reduced from
0.02 lb to 0.012 lb, the 9500 lb passive system weight line will swing
upward (Fig. 4.11) to contact the equivalent performance curve as shown.
Also, if the active system module weight has been underestimated and
turns out to be 0.039 lb, the active system weight becomes 10,716 lb,
and the corresponding passive system weight line contacts the equal
performance curve (Fig. 4.12). This not only shows a procedure for
reducing the differential between the two systems, but also demonstrates

115
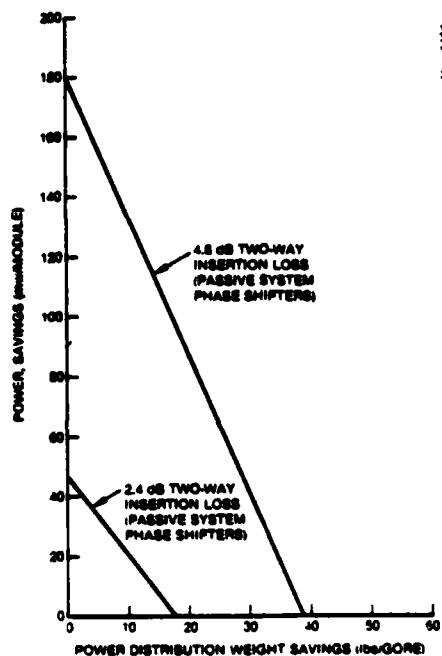
Figure 4.10. Loci of Weight and Power Savings Which Provide Equivalent Passive System Performance for Two Values of Phase Shifter Loss

the sensitivity of the system designs to the estimates used in the computations.

4.8 SUMMARY AND CONCLUSIONS

In this analysis each portion of the system that would be modified by changing from an active to a passive design was examined in independent fashion. The degree of change required, in each case, to yield equivalent performance was determined. In some cases (e.g., fixed DC loads) it appeared that a single variable might be capable of swinging the balance in favor of a passive design. Certainly, when all variables are taken in concert, a passive design could be developed which would be superior to the active design. This passive design would feature the following subsystems:

- Temperature stabilized (and possibly cooled) FET low-noise amplifiers in the feed array

116
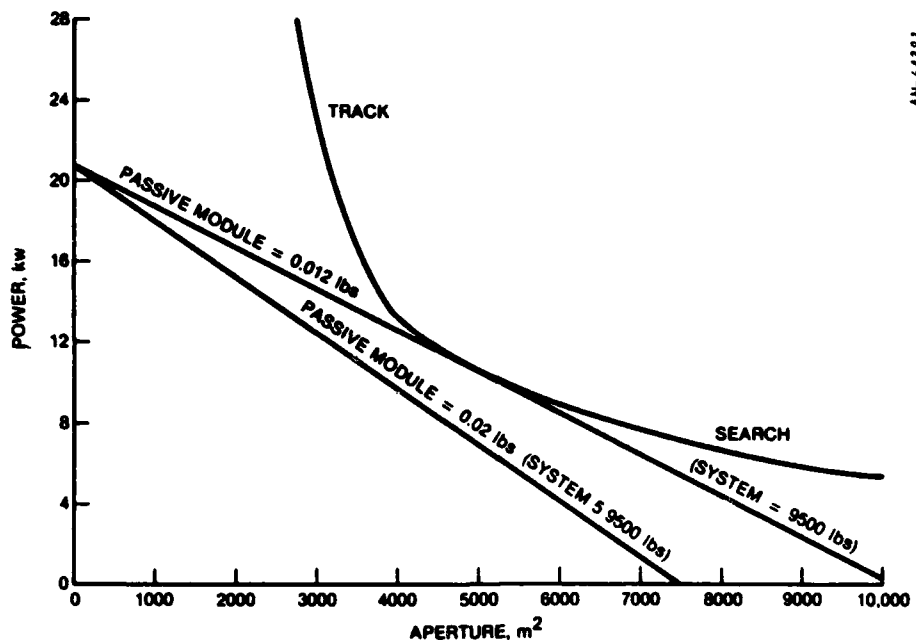
Figure 4.11. Decreased Passive Module Weight
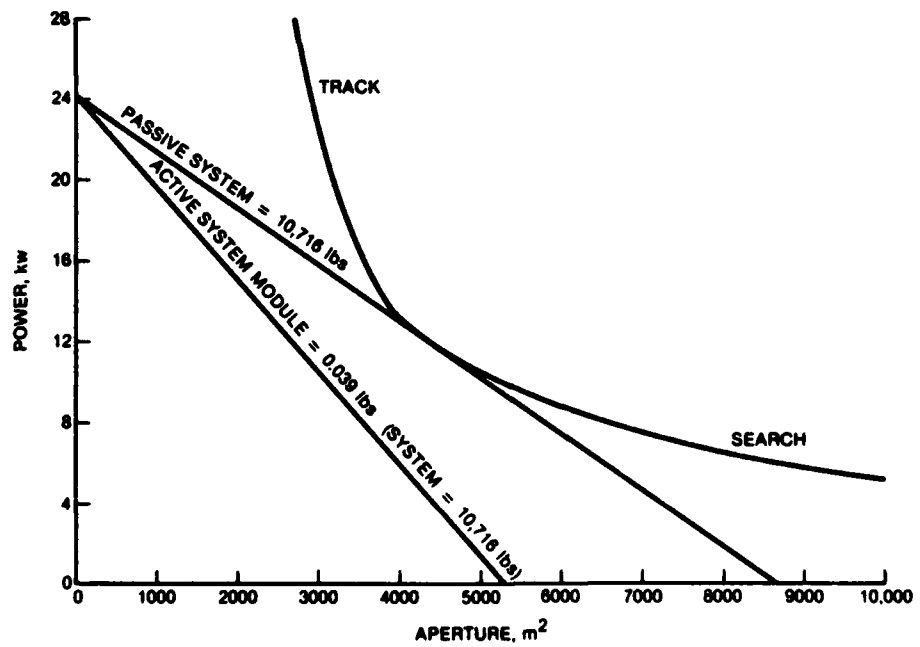
Figure 4.12. Increased Active Module Weight

117

- Multiple TWT amplifiers in the feed array, developed specifically for space-based radar

- Phase shifters in the main array with a maximum one-way insertion loss of 2.4 dB

One note of caution should be injected in these conclusions. While the passive system looks extremely promising, the results of this study are highly dependent upon the validity of the assumed numbers. As better numbers become available, these should be factored back into this analysis to see if these conclusions remain in place.

5   ENVIRONMENTAL SURVIVABILITY

The objective of this task is to assess the problems that SBRs may encounter because of particle radiation in space, both natural and caused by nuclear detonations.

All satellites must be designed to operate for a reasonable lifetime in the natural space environment (and some systems in a specified nuclear environment). Several characteristics of space-based radars, however, make them more susceptible to radiation problems. First, SBRs would operate in mid-altitude orbits (e.g., 900 n mi or 5,600 n mi circular) to optimize surveillance coverage. Operation in these orbits results in an exposure to a high level of particle radiation from the earth's Van Allen belts. Second, some subsystems (particularly the antenna RF modules) may have very little weight budget to spare for shielding, and therefore must inherently tolerate a higher total dose. A third increase in total dose exposure comes from the desire for increased satellite operational life. Because SBRs are large expensive systems, they will probably be designed for a mission life of at least five years.

The two important effects on SBRs in the space environment that we examine are: (1) degraded performance of electronic circuits that results from the total dose of trapped particle radiation and (2) soft errors (changes in bit state) in logic and memory components resulting from energetic trapped protons and cosmic rays. The approach is first to characterize the space particle radiation environment; then to determine the total dose hardness levels achievable with continued development of circuit hardening technology; and finally, to estimate satellite lifetime in the natural and nuclear environment.

Our conclusions may be briefly stated as follows.

119

Current technology in integrated circuit hardening should produce a total dose hardness of approximately 5×10^5 rads (Si) for devices suitable for the RF modules. This hardness is adequate for SBR deployments in any of the four candidate orbits analyzed, with a mission life in the natural environment of a couple of years. A hardness of 5×10^6 rads , which appears achievable with future technology (1985-90 timeframe), is required for a five-year mission life in any of the candidate orbits. Survival of a saturated nuclear environment requires a hardness of $1-5 \times 10^7$ rads (Si), depending on the specific orbit. The development and consistent fabrication of devices as hard as this is more uncertain. For the onboard processor, current technology (5×10^5 rads) is adequate in both natural and nuclear environments, with appropriate shielding.

Logic and memory components in RF modules and data processors should not have a major problem with bit errors caused by cosmic rays or high-energy trapped protons if the component sensitivity is similar to that of CMOS/SOS (CMOS silicon-on-sapphire) devices.

5.1 PARTICLE RADIATION IN SPACE

5.1.1 Candidate SBR Orbits

The first step in assessing the effects of particle radiation on SBRs is to characterize the trapped radiation environment. This was done for four different orbits which represent those of a number of SBR concepts:

1. 450 n mi, circular, 90° inclination
2. 900 n mi, circular, 90° inclination
3. 5,600 n mi, circular, 90° inclination (6-hour period)
4. 350 × 6,500, elliptical, 63° inclination (4-hour period)

These orbits have been considered for operational SBR systems in a number of recent studies.[1,2] In these studies surveillance coverage has been evaluated for SBRs in circular orbits with inclinations from 45° to 90°. While the radiation dose will be greater for lower inclinations, the difference should be less than a factor of two over the range 90° to 45°. Since a specific orbital configuration has not been defined (by optimizing coverage for selected missions) we have chosen 90° inclination for consistency in the comparison. The elliptical orbit can provide increased length of coverage for the northern hemisphere (with the proper orbit orientation). The inclination is 63° so that the orbit does not precess in its plane and the apogee recurs at latitude 63°N.

5.1.2 Natural Radiation Environment

Particle fluxes encountered by satellites in the four orbits were determined by using space radiation models, developed by the National Space Science Data Center (NSSDC), listed in Table 5.1. The models specify trapped-particle energy spectra (flux versus energy) for various regions of space; thus, the particle flux at any particular point in an orbit can be determined or an average flux can be determined by averaging over a number of points in an orbit and a number of orbits. Averaging over a number of orbits is required because the trapped particles are contained by the Earth's magnetic field, which is not azimuthally symmetric. The solar proton model characterizes the exposure to solar-flare protons based on the statistical occurrence of flares, their intensity, and the amount of shielding provided by the Earth's magnetic field for a given satellite orbit.

A number of models are used to describe the trapped particle environment because they summarize data obtained by various instruments

---

[1] A.D. Stathacopoulos et al., Internal Document, April 1982.

[2] J.A. Norby et al., Internal Document, January 1981.

TABLE 5.1

SPACE RADIATION ENVIRONMENT MODELS

Region/Radiation Type	Model (Epoch)[*]
Inner-Zone Electrons	AE5 Solar Minimum (1975) AE6 Solar Maximum (1980)
Outer-Zone Electrons	AEI7-HI (1980)
Protons	AP8-MIN (1964) AP8-MAX (1970)
Solar Protons	SOLPRO

[*] Year which model best represents.

on different spacecraft, in different orbits, and at times of different solar activity. The models serve to consolidate the data into consistent sets for each type of particle and level of solar activity. For outer-zone electrons, two models are in current use, AEI7-HI and AEI7-LO, appropriate for solar maximum and solar minimum times.[1] The AEI7-HI model was used in this analysis, since it specifies somewhat higher fluxes of electrons at energies above 1 MeV. Although there is some uncertainty in the validity of electron models for this region, AEI7-HI represents the best conservative estimate currently.[2,3]

[1] Outer-zone electrons are trapped on geomagnetic field lines with L > 2.8 . L-values are specified in units of earth radii and relate to the radial distance measured in the equatorial plane for a particular field line.

[2] A.L. Vampola et al., "A New Study of the Outer Zone Electron Environment: A Hazard to CMOS," AIAA 15th Aerospace Sciences Meeting, January 1977 (UNCLASSIFIED).

[3] A.L. Vampola et al., "A New Study of the Magnetospheric Electron Environment," Journal of Spacecraft and Rockets, Vol. 14, 1977 (UNCLASSIFIED).

Average fluxes of electrons and trapped protons for the four orbits are shown in Figs. 5.1 and 5.2. For trapped protons and inner-zone electrons the AP8-MIN and AE6 models were used since they represent higher flux levels than the AP8-MAX and AE5 models, respectively. Figure 5.3 shows the average flux of solar protons, calculated from the expected 12-month fluence computed by the SOLPRO model, for comparison with the trapped proton flux. Only for the 450 n mi orbit is the solar proton flux comparable significant; for the other three orbits the trapped-proton fluxes are much greater.

It is apparent from Figs. 5.1 and 5.2 that the trapped-particle environment is considerably different for the four orbits in terms of both flux and energy. The next step is to calculate the radiation dose resulting from these environments as a function of shielding thickness. The dose calculations were made initially using an analytical technique developed by Burrell et al.[1] This technique considers isotropic incidence for the particles and slab geometry which is appropriate for assessing radiation dose on such SBR components as RF modules. The dose-depth calculations were checked with computations using an alternative method performed by the Air Force Geophysics Laboratory.[2] For thin shielding (<0.5 g/cm^2 Al or about 75 mils thickness) the main contribution to the total dose is from electrons. The five-year total dose as a function of shielding thickness for each orbit is shown in Fig. 5.4. To estimate the required radiation hardness for electronics it is necessary to determine (1) the amount of shielding that may be afforded by the satellite structure or other components, and (2) the amount of shielding that may be added to a subsystem or component within some constraint (e.g., weight). For SBRs, the most critical components both in terms of available shielding and constraints on additional shielding are

---

[1] M.O. Burrell et al., "The Calculation of Electron and Bremsstrahlung Dose Rates," in Protection Against Space Radiation, NASA SP-169, 1968 (UNCLASSIFIED).

[2] P.L. Rothwell, private communication.
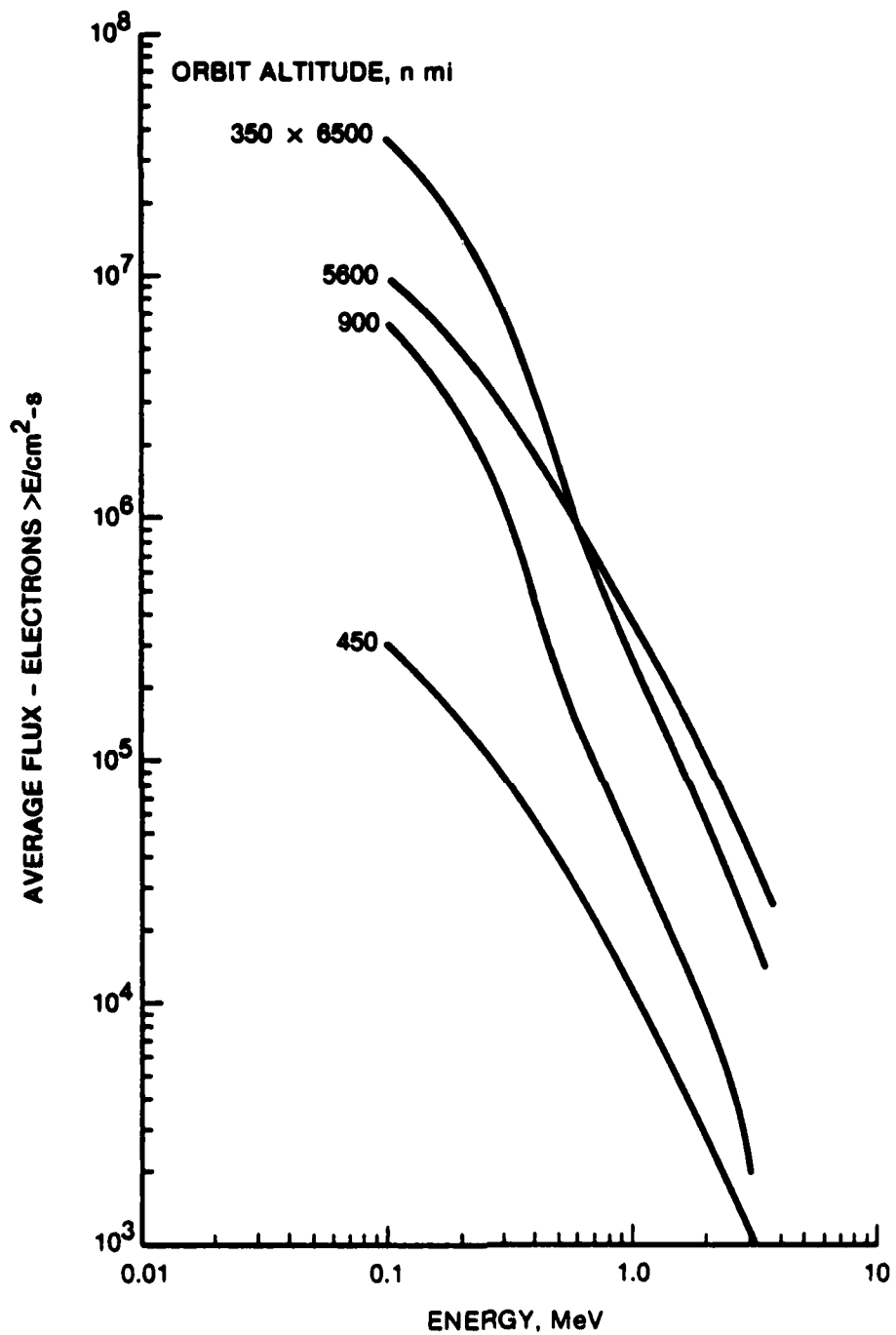
Figure 5.1. Trapped Electron Environment
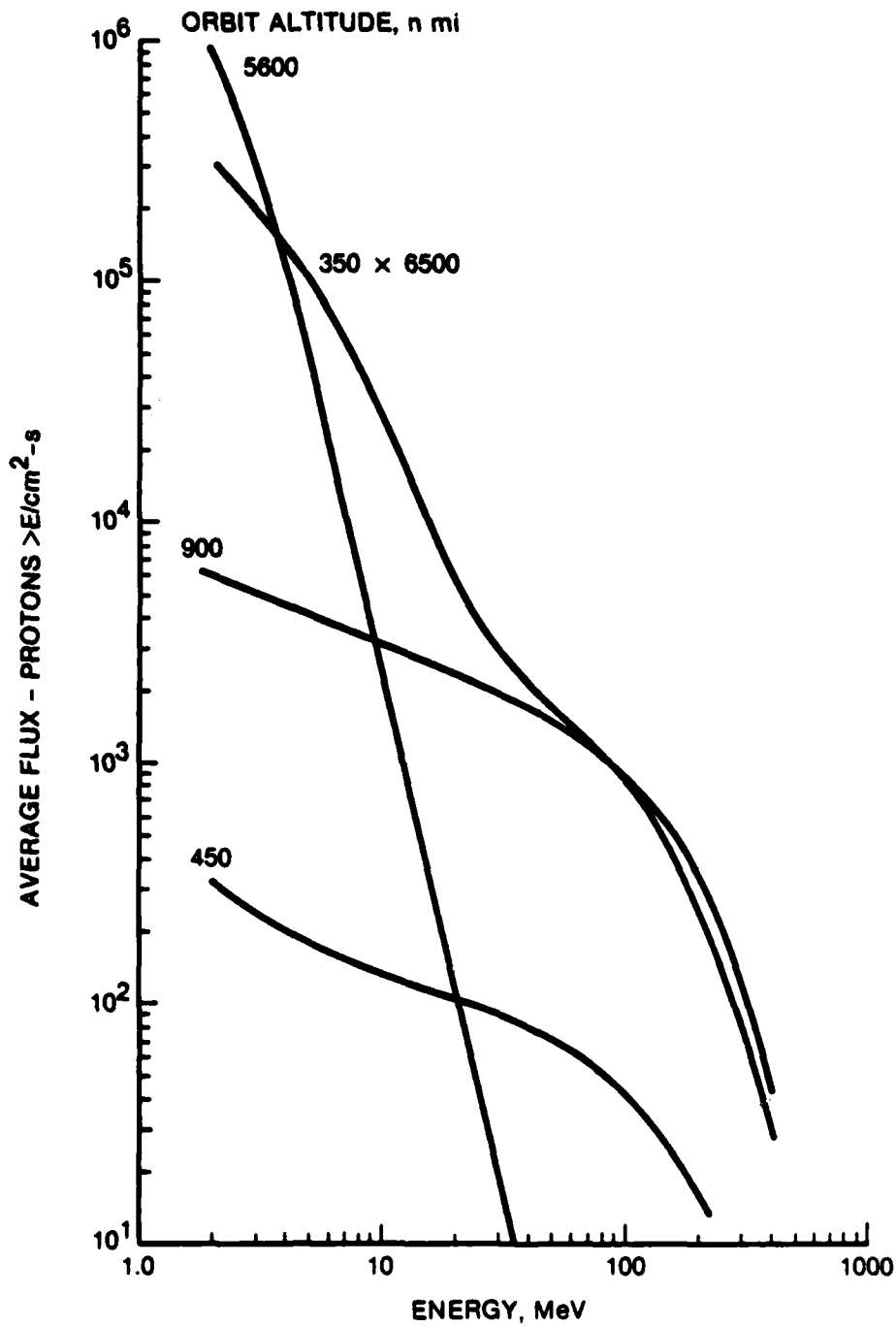
Figure 5.2. Trapped Proton Environment
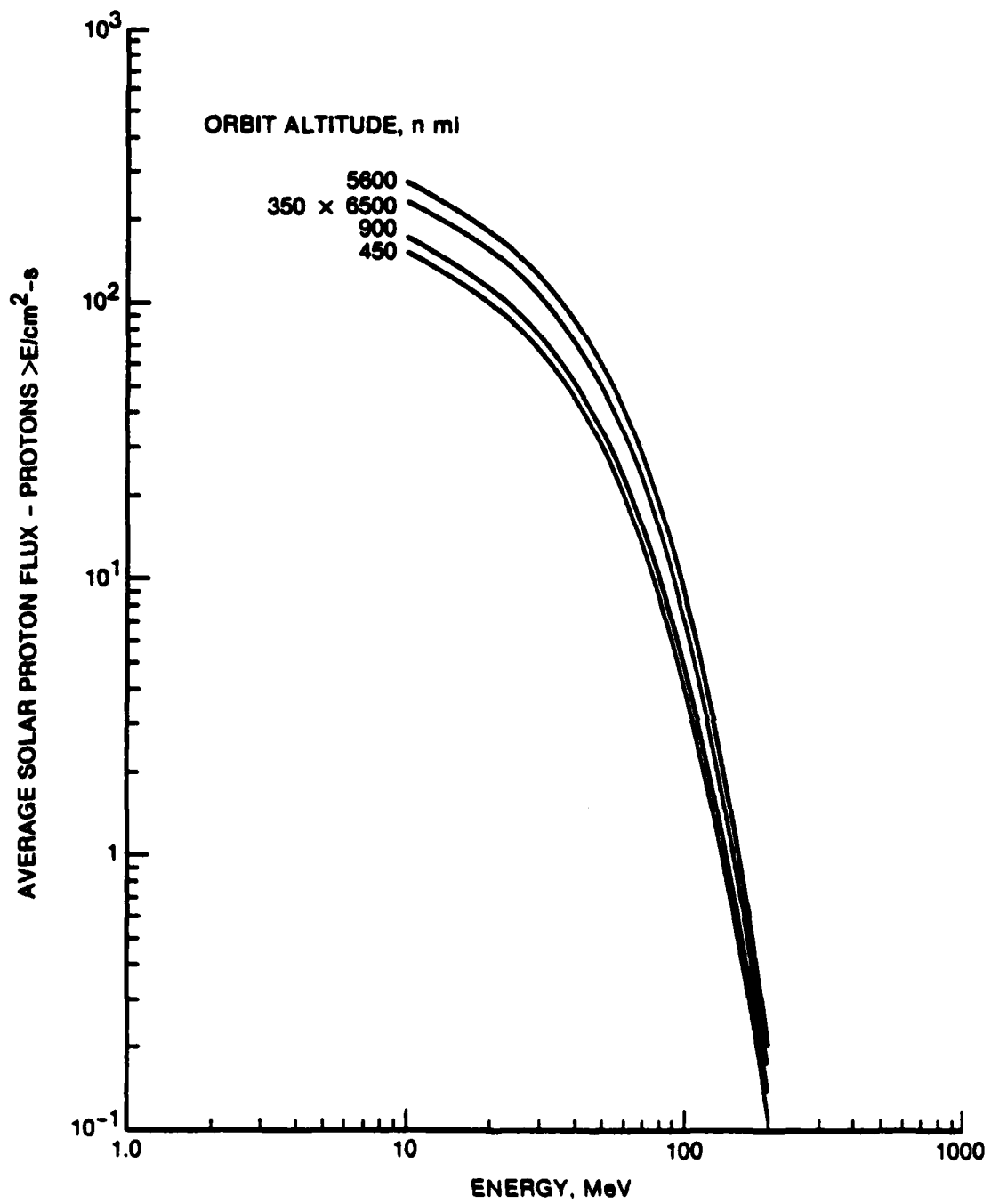
Figure 5.3. Average Expected Exposure to Solar Protons
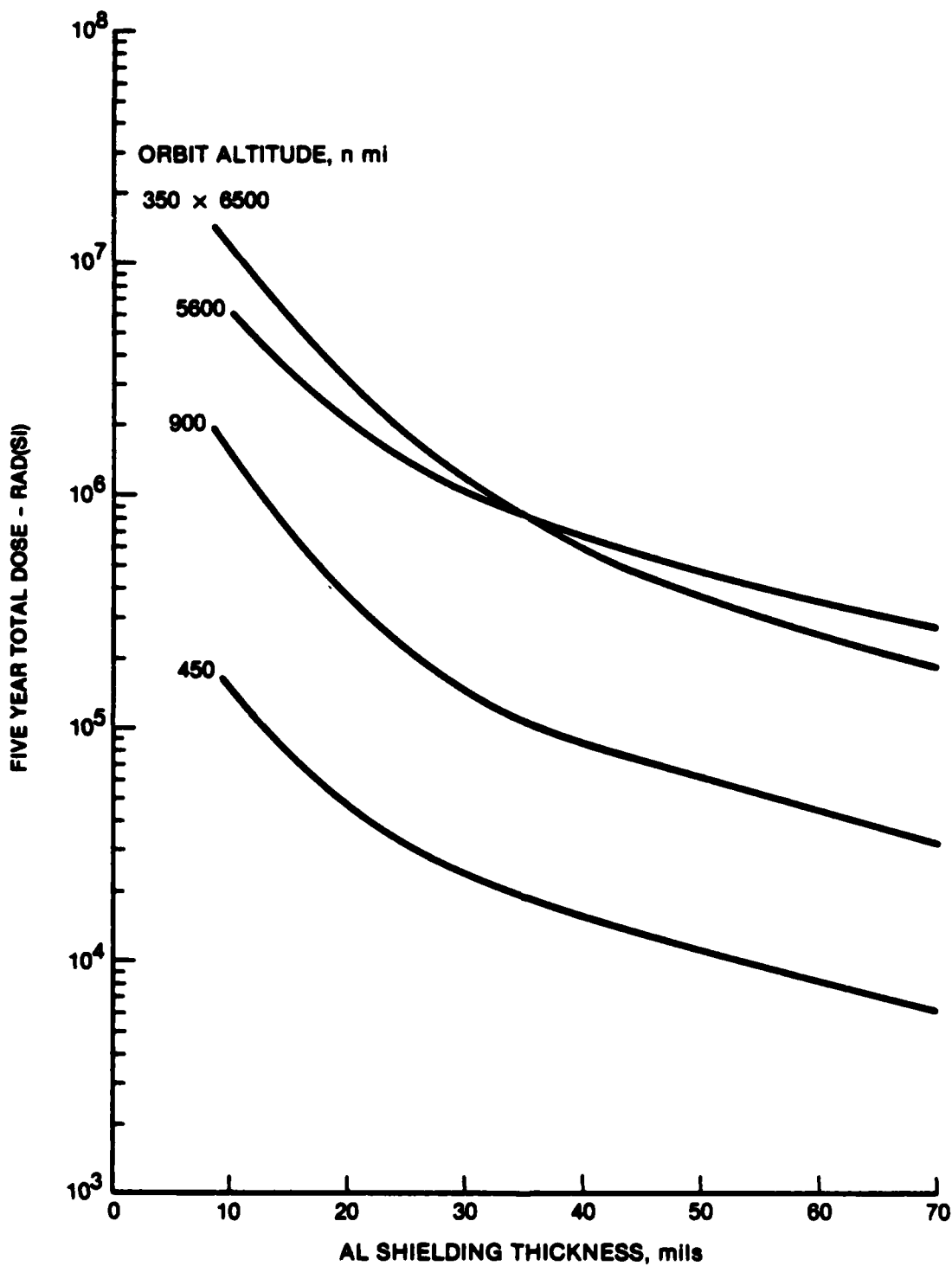
Figure 5.4. Total Dose Versus Shielding Thickness

127

the RF modules and power regulators which must be located on the antenna
aperture. Because of the large number of RF modules, they contribute a
large fraction of the total spacecraft weight and it is very important
that the weight of each module be as small as possible. Weight is not
as important for the power regulators since they will be fewer in number
(perhaps 1 regulator to 36 RF modules);[1] however, both regulators and
modules may be constrained to a thickness of approximately 0.125-0.140
in so that large aperture antennas can be packed efficiently for launch
and deployment. This constraint, as much as the weight, could limit the
shielding thickness.

There are several designs for the RF transmit/receive modules.
The module consists of integrated circuit components or, ideally, a
single, monolithic chip containing (1) a microwave phase shifter, (2)
amplifier (for active arrays), and (3) logic and memory devices for
phase-shifter control. The circuit or components are mounted within a
small aluminum package. Generally, the module's area ranges from about
0.5 to 1.0 in^2 and the circuit components or single chip weighs 0.5 to
1.0 g.[2,3] Within these ranges we can estimate the available shielding
as a function of total module weight as shown in Fig. 5.5.

A reasonable goal for total module weight is about 2 g considering
the chip weight and minimum packaging requirements. At this weight the
shielding thickness would be about 15 to 25 mil for a module area of 1
to 0.5 in^2. For these two values of module area, doubling the shielding
thickness increases the total weight by about 50%. For a module of 0.5
in^2, weighing 3 gm, the shielding thickness would be about 50 mils (on
both the top and bottom of the package). This thickness would be nearly
the maximum possible with a module thickness constraint of 0.125-0.140

---

[1]E.E. Miller, private communication, March 1981.

[2]Raytheon Company, private communication, November 1980.

[3]General Electric Company, private communication, September 1980.
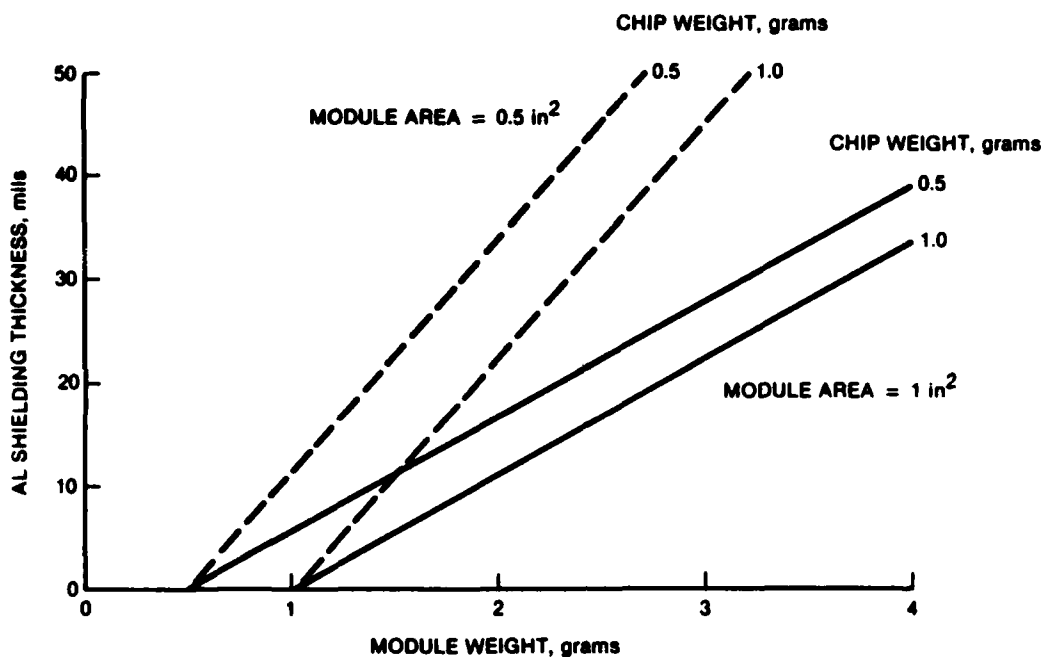
Figure 5.5.   Shielding Thickness Versus Module Weight

in including room for the chip itself. As a result we conclude that there are three shielding thicknesses applicable to RF modules: (1) 15 mils, probably the minimum that can be provided, (2) 25 mils, a reasonable shielding thickness without a large increase in module weight, and (3) 50 mils, the maximum thickness with a module thickness constraint. The five-year total dose hardness requirements for these three shielding thicknesses and the four candidate orbits are shown in Table 5.2. Here we have doubled the total dose values from Fig. 5.4 to account for particle radiation penetrating both sides of the module package and ignored the shielding that may be provided by the chip substrate for radiation coming from one side of the package.

TABLE 5.2

SPACE RADIATION ENVIRONMENT SUMMARY

SBR Orbit	5-Year Total Dose, rads (Si) Al Shielding Thickness		
	15 mils	25 mils	50 mils
450 n mi	2×10^5	6×10^4	2×10^4
900 n mi	2×10^6	4×10^5	2×10^5
5,600 n mi	6×10^6	4×10^6	10^6
35 × 6,500, 63° (4-hr elliptical)	10^7	4×10^6	10^6

The on-board signal processor is another subsystem on SBRs which will contain VLSI memory and logic components. Some performance estimates with 1983-84 technology for an advanced on-board signal processor (AOSP) with the processing capability required for SBRs are described in Table 5.3.[1] If the components can achieve a total dose hardness level of 10^6 rads, then the shielding requirements and weight are minimal. For example, 50 mils of aluminum shielding for a 2.5 ft^3 volume would weigh about 6 lb—the 50 mils shielding thickness would be adequate for 5-year life in any of the candidate orbits. Even if the shielding were increased to as much as 3 g/cm^2 (approximately 450 mils) the required weight would be about 60 lb. This level of shielding would be required for the higher-altitude orbits if the devices were hard to only 1×10^5 rads.[2] If the components of the AOSP can achieve a hardness level $>10^5$ rads then it appears that the required shielding will not have any

---

[1] Raytheon, private communication, March 1982.

[2] Space Electronics Planning Briefing, USAF Space Division, May 1981 (UNCLASSIFIED).

TABLE 5.3

AOSP PERFORMANCE ESTIMATES--1983-84 TECHNOLOGY

	Memory	Logic
Technology	STL	Bipolar-STL
Volume, ft^3	0.3	<2
Power, W	150	900
Weight, lb	16	<100
Total Dose Hardness, rads (Si)	1×10^6	1×10^6

significant impact on spacecraft design; if 10^6 rad hardness can be achieved, normal electronic packaging will provide adequate total-dose shielding for the natural environment.

5.1.3 Nuclear Radiation Environment

Satellites can be damaged by exoatmospheric nuclear bursts. Damaging effects are caused by exposure both to prompt gamma and x-ray radiation and to an enhanced level of trapped radiation. Damage by prompt effects can occur only when the satellite is within line-of-sight of the exoatmospheric nuclear detonation; however, depending on the sensitivity of a particular satellite to this prompt radiation pulse, the range at which damage occurs can be thousands of miles or more. The damage mechanism is primarily transient currents resulting either from radiation-induced ionization within electronic components or from a system-generated electroamgnetic pulse (SGEMP) produced when X rays are absorbed by the satellite skin, cable shields, or other components. For the most part these effects are sufficiently well understood for hardened systems to be designed with high confidence.[1] Because of this and

---

[1] W.F. Rich and T.A. Stringer, "System-Generated Electromagnetic Pulse and Spacecraft Charging Effects: A Review of the Technology as Applied to System Hardening Problems," IEEE Trans. Nuclear Science, Vol. NS-27, No. 6, December 1980.

the fact that system sensitivity depends on specific satellite design features, the emphasis here is on delayed effects--the radiation dose from enhanced radiation belts. Even when hardened to survive prompt effects, a satellite will still be exposed to a higher total dose from trapped particles.

The enhanced trapped radiation results from beta-decay of weapon fission fragments and from the initial ionization of the weapon casing and the surrounding atmosphere. Exoatmospheric nuclear detonations are likely in a nuclear war even if satellites are not attacked directly. High-altitude detonations to produce EMP (electromagnetic pulse) effects over large areas on the ground and ABM (anti-ballistic missile) detonations could occur at altitudes between 100 and 400 km, which is the appropriate region for radiation belt enhancement.

Generally, the maximum level of enhanced radiation is considered to be the saturation condition defined by Schulz.[1] This level decays after the weapon detonations with a time constant (for decay to one-half the value) which is estimated to be between 10 and 20 days. To simplify estimates of satellite survivability, a constant 10-day fluence of fission electrons is defined (as a function of orbit inclination and altitude) to represent the maximum enhanced nuclear environment. Satellites hardened to withstand this level will probably survive for relatively long times in a nuclear environment; satellites which do not achieve the level can only be expected to survive at most a few days in an enhanced environment.

Even though a saturated condition is defined, the electron fluence for a given satellite orbit can be considerably lower if the exoatmospheric detonations occur only at higher latitudes. If this is the case there are regions of the radiation belts that are not enhanced because

---

[1] M. Schulz, Application of a Limit of Stably Trapped Electron Flux, Aerospace Corporation SAMSO TR-71-265, September 1971 (UNCLASSIFIED).

the motion of the injected electrons and ions is restricted in certain directions by the earth's magnetic field. This effect is illustrated schematically in Fig. 5.6. In this figure the shaded region represents enhanced trapped particle radiation resulting from a number of weapons detonated at mid-latitudes. Above a certain latitude the magnetic field lines are open to interplanetary space and no trapping occurs; the inner boundary is defined by the magnetic field and the lowest-latitude detonation. Satellites with orbits that cross this region will be exposed to a lower fluence than they would if the entire trapping region were enhanced. For orbits above a certain altitude, however, there will be no latitude effect since the portion of their orbit within the trapping region will always see the enhanced fluence.

The 10-day fission electron fluence (for saturated belts) is shown in Fig. 5.7 for circular orbits with 90° inclination. The curves are

SPATIAL DISTRIBUTION OF RADIATION
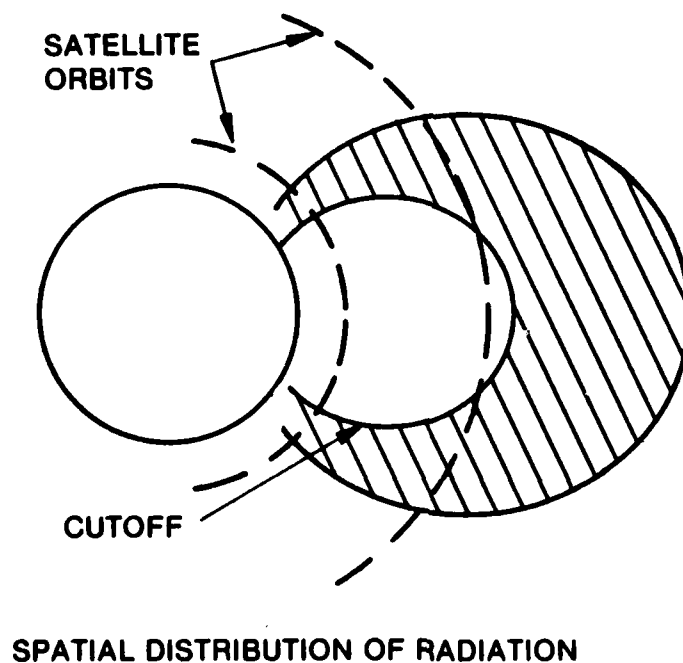
Figure 5.6. Spatial Distribution of Enhanced Radiation
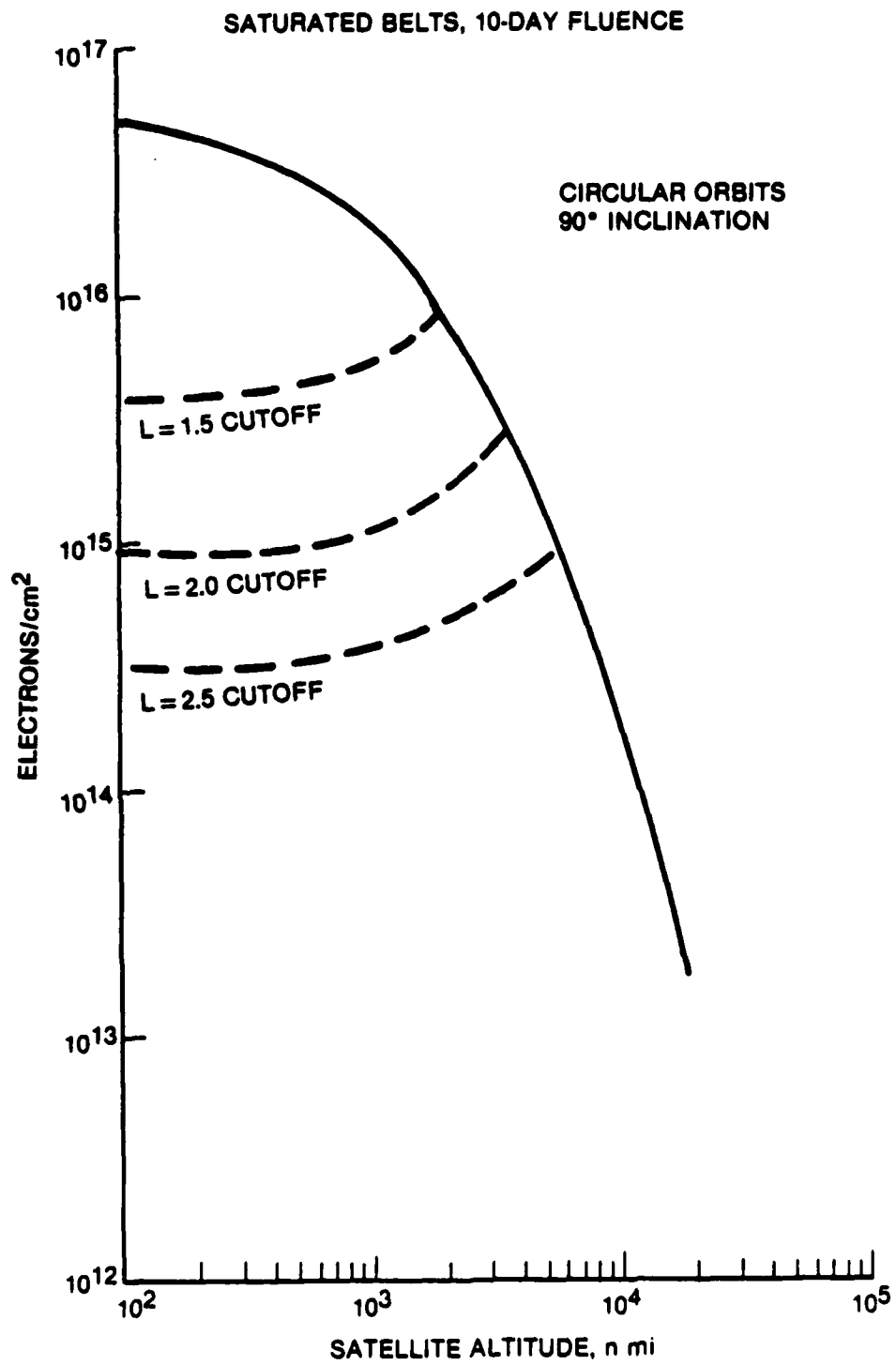
Figure 5.7. Nuclear Enhanced Environment

134

applicable to any orbits inclined at more than about 60°. The solid
curve represents saturation of the entire trapping region and the dashed
curves represent the fluence levels for three inner boundaries. The
parameter used to specify the boundary is the L-value of the magnetic
field line, where L equals the equatorial crossing distance, in earth
radii, of a particular field line. L = 2.5 corresponds approximately
to the northern latitude of CONUS and the Soviet Union and L = 2.0 and
1.5 correspond to the mid and southern latitudes of CONUS and the Soviet
Union, respectively. This latitude cutoff is very important for lower-
altitude satellites (below a few thousand nautical miles) since their
level of exposure can vary by more than an order of magnitude depending
on the assumed cutoff.

Because the fission electrons in the enhanced radiation belts have
more energy than the natural electron environment, an increase in the
shielding thickness for components has a lesser effect in reducing total
dose. The total dose for a 10-day fluence in saturated belts versus
shielding thickness is shown in Fig. 5.8 for the four candidate orbits.
The two sets of curves illustrate the sensitivity to the assumed cutoff
latitude. By comparison with Fig. 5.4 it is apparent that, regardless
of orbit, module components must be much harder to survive in nuclear-
enhanced environment than in the natural environment. For the more
conservative assumption of an L = 1.5 cutoff, the required hardness is
well above 10^7 rads for all the orbits except 5,600 n mi. This high-
altitude orbit is not sensitive to various cutoff values in the range
L = 1.5 to 2.5 . For this reason the dose shown for a 5,600 n mi orbit
is the highest that could be expected regardless of the location of the
exoatmospheric bursts.

Since more shielding can be provided for the onboard processor,
its component hardness requirements are less than those for module
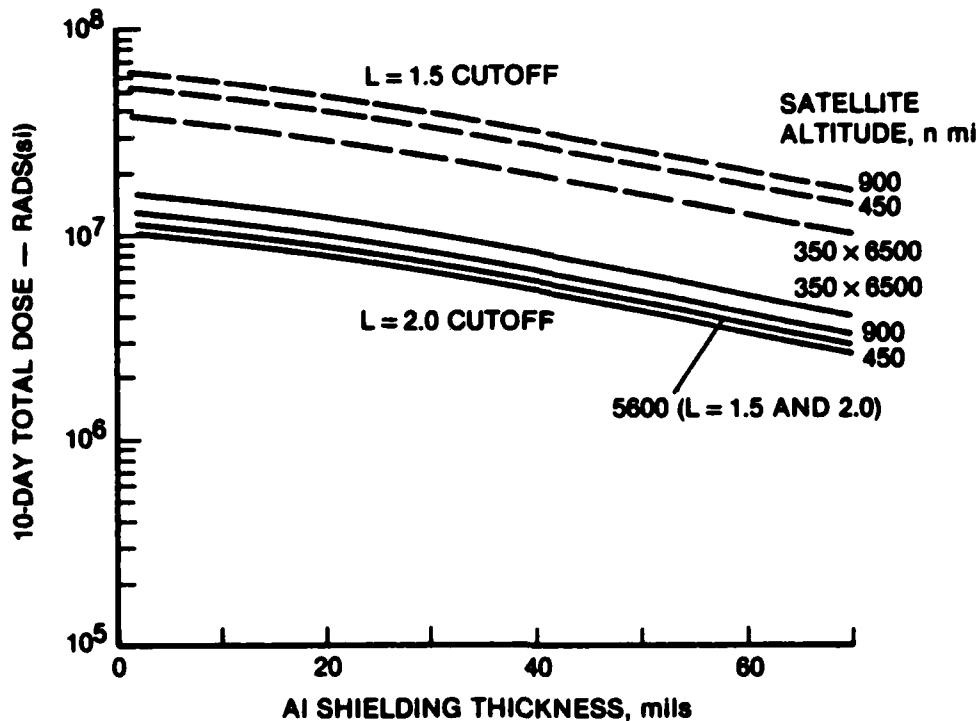
Figure 5.8. Total Dose for a Saturated Nuclear Environment

components. Shielding to the bremsstrahlung level[1] would require a component total dose hardness of 10^5 rads. With this hardness the processor could survive the 10-day saturated belt fluence _after_ five years in orbit, for any of the candidate orbits. For a processor with a volume of two cubic feet the shielding weight would be about 160 lb.

5.2 RF MODULE COMPONENT TECHNOLOGY AND RADIATION HARDNESS

5.2.1 Radiation Damage to Semiconductors

The electrical behavior of semiconductor devices can be changed by exposure to radiation because of two effects produced within the

---

[1]The level where the penetrating fission electron dose is equivalent to the bremsstrahlung dose resulting from electron energy loss in the shield material. For aluminum this shield thickness is approximately 450 mils or 3 g/cm^2.

semiconductor—displacement and ionization. Displacement is the removal of an atom from its normal position in the crystal lattice and ionization is the formation of ionized atoms and free electrons within the material. These two effects account for the three major types of radiation damage in semiconductor devices: (1) transient damage, (2) surface damage, and (3) displacement damage.

Both transient and surface damage result from ionization. Typically, the transient effect is a current within the device as a result of a radiation pulse (X rays from a nuclear weapon for example). For sufficiently large currents, circuit latchup or breakdown may result. One protection feature would be to remove the power and shut off the circuits when a radiation pulse is detected.

Surface damage, also the result of ionization, refers to effects near the surface of devices or in the insulating layers near the surface. Charge collection in these regions changes the electrical properties of devices, particularly the required threshold voltages for MOSFETs. Charge deposited in the SiO_2 layer beneath the gate acts as an additional gate voltage. Displacement damage occurs in the bulk semiconductor material and changes the electrical properties because the displacement sites act as recombination centers for the charge carriers and, in effect, reduce the carrier lifetime.

These effects can be produced by more than one type of radiation and a particular radiation can produce more than one effect. The combinations of radiation type and damage effect are summarized in Table 5.4 for both the natural environment and a nuclear weapon environment.

In a nuclear environment both neutrons and X rays (or gamma rays) can cause comparable ionization effects. Displacement effects are produced by neutrons. After the initial transient ionization, which can affect all semiconductors, the dominant damage is either surface or

137

TABLE 5.4

SUMMARY OF RADIATION DAMAGE EFFECTS

Radiation Source	Damage Effect	Radiation
Natural Environment	Ionization	
	Transient (single particle upset)	p and cosmic rays
	Surface	e and p
	Displacement	e and p
Nuclear Weapons	Ionization	
	Transient	n and x-rays
	Surface	n and x-rays
	Displacement	n

displacement. For MOSFET devices, which are not particularly suscept-
ible to displacement effects, the dominant damage is from surface ioni-
zation. For bipolar devices (including solar cells) the dominant
effects will be from displacement since these devices generally are not
sensitive to surface ionization effects.

In the Van Allen belts, both electrons and protons can cause ioni-
zation and displacement damage; however, the magnitude of displacement
damage is so low that only solar cells are affected since they are the
most sensitive devices to displacement effects. Transient ionization
effects in the natural space environment are generally not a problem
although high-energy protons and cosmic rays can produce upsets or bit
errors in LSI memories and false signals in particularly sensitive
detectors such as star or horizon sensors. Proton-induced bit errors
are discussed in Sec. 5.2.5. Since there is no significant displacement
damage to electronic components, natural space radiation effects are
caused primarily by surface ionization damage.

5.2.2 Functional Components of RF Modules

A desirable goal of the RF module technology development program is to fabricate all the electronic components on a single monolithic chip. If this cannot be achieved then it is desirable to have two chips—one with the microwave components (phase shifter and amplifier) and one with the logic and memory components. The function of the RF module is to receive and transmit the radar waveform with a specific phase shift determined by the desired beam direction and the module location within the array. For an active array, the signal would be amplified within the module before being transmitted. Information on the desired beam direction is transmitted to the modules with the radar waveform. The information is decoded and the appropriate phase shift is calculated by the logic elements in the module.

At the present time functional modules with discrete components are being developed for design and test purposes. Table 5.5 lists the specific components.

5.2.3 Integrated Circuit Hardening Technology

Within the last few years there has been rapid progress in various integrated circuit technologies, and many efforts directed toward improving radiation hardness. These efforts include improving the hardness of existing technologies (bipolar and MOS) as well as developing new technologies which promise higher levels of radiation tolerance. CMOS/SOS (CMOS silicon-on-sapphire) and GaAs (gallium arsenide) are the most promising of these new technologies. In this section we will briefly describe the radiation hardness of current IC devices and the improvements that are expected with new device technologies. It should be mentioned that the hardness levels for a device type generally must be expressed as a range since specific device hardness can depend on details in design and manufacturing. The attempt here is to characterize the hardness of various devices and note the differences.

TABLE 5.5
RF MODULE COMPONENTS

Type	Device	Technology
Microprocessor	RCA 1802A	CMOS/SOS
RAM	RCA MWS5114	CMOS/SOS
EEPROM	HNVM 3708	CMOS
Comparator	LM 193	

Radiation hardness generally is characterized by three measures which relate to the three basic types of damage: (1) total dose (rads), which measures tolerance to accumulated charge within the device; (2) dose rate (rads/s), a measure of sensitivity to transient ionization; and (3) neutron fluence (1 MeV neutrons/cm^2), a measure of hardness to displacement damage. All devices are sensitive to some level of radiation as characterized by these three measures; however, a given technology generally is relatively more sensitive in one or two areas and hardening improvements are directed toward these areas.

Table 5.6 lists the hardness goals for electronic circuits for USAF Space Division systems and for the DoD VHSIC (Very High Speed Integrated Circuit) Program.[1,2] The total dose hardness levels are far below those required for SBR RF modules. Although the VHSIC goals will likely be increased to the levels required for strategic and space systems, the current VHSIC program does not include GaAs technology, which is very promising for RF module applications.

---

[1] Space Electronics Planning Briefing, USAF Space Division, May 1981 (UNCLASSIFIED).

[2] VHSIC Specifications Handbook, Preliminary, Office of Undersecretary of Defense, Research and Engineering, January 1982 (UNCLASSIFIED).

TABLE 5.6

COMPARISON OF HARDNESS GOALS

	Space Division System Requirements[*] (Minimum, Near-Term)	VHSIC Requirements (Minimum)
Total Dose, rads	5×10^4	1×10^4
Prompt Dose Rate, rads/s		
Survival	1×10^{10}	1×10^8
Upset (Non-Volatile Elements)	1×10^9	No requirement
Upset (Other Elements)	2×10^8	1×10^7
Pulse Length	10 ns[†]	10 µs
Neutron Hardness, n/cm^2 (1 MeV)	JCS maximum	1×10^{11}
Single Event Upset	1×10^{-4} errors/ bit/day[§]	No requirement

---

[*]Assumes shielding equivalent to 3 g/cm^2 Al.

[†]Assumes prompt transient suppression.

[§]Without error detection and correction.

Bipolar devices are most sensitive to displacement damage and transient upset as compared to total dose hardness (generally $>10^6$ rads). These characteristics would seem to indicate that bipolar devices would be appropriate for space applications where only the natural environment and total radiation dose are of concern (i.e., a nuclear weapon environment is not considered in the system design). However, bipolar devices require more power than NMOS and bulk CMOS devices which utilize FETs (field-effect transistors). While NMOS and CMOS devices have the advantage of lower power consumption for space

applications, they are much less hard to total dose, and their applications to space systems may be restricted for this reason since the natural environment is a fundamental design consideration.

There are three bipolar technologies for logic and memory devices which are the most common for application to radiation hardened systems. These are TTL (transistor-transistor logic), ECL (emitter-coupled logic) and I^2L (integrated injection logic). ECL is the bipolar technology hardest to displacement damage, with a damage threshold that is greater than 10^{15} n/cm^2. I^2L neutron hardness is in the range of 5×10^{13} - 5×10^{14} n/cm^2 ; however, a category of I^2L termed integrated Schottky logic (ISL) is hard to approximately 10^{15} n/cm^2. TTL neutron hardness is in the range of 10^{14} - 10^{15} n/cm^2 , with hardened TTL and advanced Schottky devices (a type of TTL) at the upper end of the range. These three bipolar technologies are susceptible to transient upset over the range 10^7 - 10^9 rads/s and operate satisfactorily with total dose exposure of more than 10^6 rads except for I^2L which can fail at 10^5 - 5×10^5 rads.

MOS technologies are much harder to displacement damage, typically with damage thresholds greater than 10^{15} n/cm^2. Their susceptibility to transient upset is on the same order as bipolar devices, 10^7 - 10^9 rads/s except for CMOS/SOS which is the hardest technology for this type of damage. CMOS/SOS devices can withstand short radiation pulse levels above 10^{10} rads/s.

Unhardened MOS devices (NMOS and CMOS), however, are sensitive to a radiation total dose of 10^3 - 5×10^4 rads with NMOS being the most sensitive. Hardened CMOS and CMOS/SOS devices have exhibited total dose hardness from 10^5 to better than 10^6 rads. An advantage of CMOS/SOS compared with bulk CMOS devices, as mentioned above, is a much higher threshold for transient upset and insensitivity to latchup because of the sapphire isolation. A disadvantage, however, is the difficulty in

implementing input protection circuitry on the sapphire substrate.
Without this protection CMOS/SOS devices are sensitive to electromag-
netic pulse (EMP) environments in which energy can enter the circuit
through input, power, or output leads.

GaAs is a developing technology which is particularly attractive
for many microwave applications when compared to silicon devices. They
offer the potential for significantly faster logic circuits (speed in-
crease by a factor of 10) with operating power requirements equal to or
less than CMOS devices. Although further research on radiation effects
is needed, the available data indicate that GaAs FETs are as hard as or
harder than comparable silicon devices.[1] This is especially the case
for total-dose hardness, where GaAs devices have demonstrated hardness
levels greater than 10^7 rads. At the present time only transient charge
trapping at low dose rates has been found to be a problem for some GaAs
devices.[2] GaAs devices, similarly to CMOS/SOS, should not be suscept-
.ible to latchup.

A very important advantage of GaAs devices is that radiation hard-
ness is inherent and does not require special hardening processes or
procedures. For this reason, as well as their speed and low power
advantages, GaAs is the most promising technology for electronics
required to operate in severe nuclear radiation environments.

The radiation hardness characteristics of various IC technologies
are summarized in Table 5.7. The data was compiled by reviewing the
goals and published results on progress in a number of laboratory
programs on hardening technology.

---

[1] P.H. Phillips, "Space Hardened Microelectronics," Military Electronics/
Countermeasures, August 1982 (UNCLASSIFIED).

[2] M. Simons and E.E. King, "Long-Term Radiation Transients in GaAs FETs,"
IEEE Trans. Nuclear Science, Vol. NS-26, No. 6, December 1979.

TABLE 5.7

RADIATION HARDNESS OF INTEGRATED CIRCUITS

	Neutron Hardness n/cm^2	Dose Rate Hardness rads (S1)/s	Total Dose Hardness rads (s1)
Current Technology			
Bipolar			
TTL (hardened)	$10^{14}-10^{15}$ (10^{15})	10^7-10^9	$> 10^6$
I^2L (ISL)	$5 \times 10^{13}-5 \times 10^{14}$ $(>10^{15})$	10^8-10^9	$10^5-5 \times 10^5$
ECL	$> 10^{15}$	10^8-10^9	$> 10^6$
NMOS (hardened)	$> 10^{15}$	10^8-10^9	10^3-10^4 (10^4-10^5)
CMOS	$> 10^{15}$	$5 \times 10^7-10^9$	$10^4-5 \times 10^4$
Hardened CMOS	$> 10^{15}$	$5 \times 10^8-10^9$	10^5-10^6
CMOS/SOS	$> 10^{15}$	10^{10}	$5 \times 10^5->10^6$
Future Technology (1985-90)			
CMOS/SOS	$> 10^{15}$	$10^{10}-10^{11}$	$> 10^6$
GaAs	$> 10^{15}$	$> 10^{10}$	$> 10^7$

144

5.2.4 Applications to SBRs

Considering the total-dose hardness requirements described in Secs. 5.1.2 and 5.1.3 for RF module circuits and the necessity for low power consumption, it appears that hardened CMOS and CMOS/SOS are the most appropriate current technologies for module development. By the late 1980s when SBRs first could be deployed, GaAs technology will be much advanced and GaAs LSI digital ICs will have been developed for a number of applications. Since GaAs is appropriate for microwave amplifiers and the phase shifter circuitry in the RF modules, it is the most promising technology for module fabrication on a single, monolithic chip. GaAs devices promise total-dose hardness levels that exceed those required for all candidate SBR orbits even with minimal shielding.

CMOS/SOS technology also promises to provide total dose hardness to the level required for RF modules. Since this technology is more advanced than GaAs, it offers an alternative perhaps with less risk for the logic and memory components of the modules. Both CMOS/SOS and GaAs offer good performance for transient upset and neutron hardness, which is required for a nuclear weapon environment. However, there are two possible drawbacks to CMOS/SOS: (1) although devices have been built with hardness in excess of 10^6 rads, a process which is both reliable and hard has not yet been clearly demonstrated, and (2) there are difficulties in fabricating high power input protection to increase the damage threshold to pulse injection.[1]

From the technology assessment described above it appears that current technology generally could provide devices with a total dose hardness of 5×10^5 rads . Progress in device hardening technology in the next few years will likely increase this level in the 1985 timeframe to $10^6 - 5 \times 10^6$ rads and even up to 10^7 rads if large-scale GaAs devices are realized.

---

[1] D.M. Long, "Hardness of MOS and Bipolar Integrated Circuits," IEEE Trans. Nuclear Science, Vol. NS-27, No. 6, December 1980.

5.2.5 Single Particle Upsets

It has been known for some time that cosmic rays could produce logic upsets or errors (also called soft errors) in semiconductor memories.[1] These upsets can be produced by single particles in either bipolar or MOS memories but there is a wide range of susceptibility. Dynamic NMOS memories appear to be very susceptible and it has been found that single particles can produce latchup in CMOS memories.[2,3]

The upsets are the result of the intense ionization produced within the device either (1) by ionization energy loss along the path of the primary particle or (2) by a nuclear interaction between the primary particle and a nucleus in the device medium. The primary particles can originate from cosmic rays, neutron (nuclear weapon) environments, radioactive impurities in the IC packaging materials (with alpha particles emitted in the radioactive decay), and the Earth's radiation belts. This last source is of particular importance for SBRs because SBRs in the candidate orbits will be exposed to fluxes of high-energy protons and typical shielding thicknesses will not be effective in reducing the flux.

We can make a rough estimate of the magnitude of the problem by calculating the error rate using cross sections determined by recent experiments with dynamic and static RAMs.[3,4,5] The predicted error

---

[1] D. Binder et al., "Satellite Anomalies from Galactic Cosmic Rays," IEEE Trans. Nuclear Science, NS-22, No. 6, 1975.

[2] W.A. Kolasinski et al., "Simulation of Cosmic Ray Induced Soft Errors and Latchup in IC Computer Memories," IEEE Trans. Nuclear Science, NS-26, No. 6, 1979.

[3] P.J. McNulty et al., Proton Upsets in LSI Memories in Space, Space Systems and Their Interactions with Earth's Space Environment, AIAA, New York, 1980.

[4] P.J. McNulty et al., "Upset Phenomena Induced by Energetic Protons and Electrons," IEEE Trans. Nuclear Science, Vol. NS-27, No. 6, December 1980.

[5] G.J. Brucker et al., "Simulation of Cosmic Ray Induced Soft Errors in CMOS/SOS Memories," IEEE Trans. Nuclear Science, Vol. NS-27, No. 6, December 1980.

rates for the candidate orbits are shown in Table 5.8. For NMOS and CMOS devices the results are based on cross sections for protons with energy greater than 40 MeV. The proton environment described in Sec. 5.1.2 was used to determine integral proton fluxes.

There have been some simulated cosmic ray tests on specially designed CMOS/SOS memories with results suggesting that this technology is not very sensitive to single particle upsets because of the very small junctions in these devices. The error rate listed in Table 5.8 for these devices is that resulting from cosmic ray interactions. Upsets from radiation belt protons would occur at an even lower rate. This result is promising; however, more experimental data is needed.

It is important to mention that the experimental data for different types of memory devices is sparse, that there are wide variations in susceptibility between devices, and that theoretical models of the interactions and effects are not sufficiently developed so that confident predictions can be made. For RF module development, it is important to establish the susceptibility of logic and memory devices to this effect as the IC technology is being developed. Error detection and

---

TABLE 5.8

SOFT ERROR RATE IN LOGIC DEVICES

	Soft Error Rate, errors/bit/day		
SBR Orbit	NMOS	CMOS	CMOS/SOS
450 n mi	2×10^{-5}	2×10^{-6}	$<2 \times 10^{-9}$
900 n mi	10^{-4}	10^{-5}	$<2 \times 10^{-9}$
5,600 n mi	2×10^{-5}	2×10^{-6}	$<2 \times 10^{-9}$
350 × 6,500 n mi (4-hr, elliptical)	10^{-4}	10^{-5}	$<2 \times 10^{-9}$

correction capability could be implemented at the chip level, or at the system level with the memory of each module updated periodically.[1]

5.3 CONCLUSIONS

Total dose hardness requirements for RF module and onboard processor components were described in Secs. 5.1.2 and 5.1.3. These requirements were based on a five-year mission life in the natural environment and survival of a saturated nuclear enhanced environment. Alternatively we can consider specific component hardness levels and estimate the satellite lifetime. Table 5.9 lists satellite lifetimes (limited by the life of the RF module) in the natural environment for the candidate orbits and three shielding thicknesses. Component total dose hardness is assumed to be at least 5×10^5 rads--the level assessed to be available with current technology methods for design and fabrication. For this hardness level reasonable mission life can be assured for the lower-altitude orbits (450 and 900 n mi) with 25 mils of shielding, but 50 mils of shielding is required to achieve a life of a few years in the higher orbits.

A similar lifetime calculation for an enhanced nuclear environment can be made. Table 5.10 lists the lifetime in days in a saturated environment. These estimates are made assuming a component total dose hardness of 10^7 rads, which is considered to be the level of future technology. Only the 5,600 n mi orbit with 50 mils of shielding survives the saturated 10-day fluence with a component hardness of 10^7 rads. Survival in the other orbits would require the same shielding and a component total dose hardness of at least $4-5 \times 10^7$ rads.

Table 5.11 summarizes the conclusions from this assessment of satellite lifetimes. Current technology (at the level of 5×10^5 rads)

---

[1] J.P. Retzler, "Fault Tolerant Memories for Single Particle Radiation Effects," IEEE Trans. Nuclear Science, Vol. NS-28, No. 6, December 1981.

TABLE 5.9

SBR LIFETIME IN NATURAL ENVIRONMENT

	Lifetime in Natural Environment,[*] yr		
	Al Shielding Thickness		
SBR Orbit	15 mils	25 mils	50 mils
450 n mi	>10	>10	>10
900 n mi	1.25	6.25	>10
5,600 n mi	0.4	0.6	2.5
350 × 6,500	0.25	0.6	2.5

[*]Current technology 5×10^5 rads.

TABLE 5.10

SBR LIFETIME IN NUCLEAR ENVIRONMENT

	Lifetime in Nuclear Environment,[*] days		
	Al Shielding Thickness		
SBR Orbit	15 mils	25 mils	50 mils
450 n mi	1	2	3
900 n mi	1	1	2
5,600 n mi	6	8	>10
350 × 6,500 n mi	2	2	3

[*]Saturated belts, L = 1.5 cutoff; future technology 10^7 rads.

149

TABLE 5.11

CONCLUSIONS

Natural Environment

- Current technology (5×10^5 rads) will support SBR deployment at:

    - 450 and 900 n mi for five-year life (25 mil shielding)

    - 5,600 and 350 × 6,500 n mi for 2.5-year life (50 mils shielding)

- Current technology adequate for onboard signal processor (all candidate orbits)

- Future technology (5×10^6 rads) required for 5,600 and 350 × 6,500 n mi orbits for five-year life (25 mils shielding)

Nuclear Environment

- Future technology required for survival (50 mils shielding)

    - 10^7 rads for 5,600 n mi orbit
    - 5×10^7 rads for other candidate orbits

- Current technology adequate for onboard signal processor with appropriate shielding (3.0 gm/cm^2)

Single Particle Upset

- Bit error rate not a major problem if component sensitivity similar to CMOS/SOS

150

will support SBR deployments in any of the candidate orbits with a mission life of a few years; the higher orbits require 50 mils of shielding for the RF modules to achieve this. This hardness level is adequate for the onboard processor in any of the candidate orbits with a modest amount of shielding. For module components a total-dose hardness of 5×10^6 rads , which appears easily achievable with future technology, is required to achieve a five-year mission life in any candidate orbit (although at this level only 25 mils of shielding is required).

Survival of a nuclear-enhanced environment requires 50 mils of shielding and a hardness of 10^7 rads in the 5,600 n mi orbit (5×10^7 rads in the other orbits). Current technology hardness levels are adequate for the onboard processor with appropriate shielding (to the bremsstrahlung level). For a processor with a volume of two cubic feet this amount of aluminum shielding would weigh about 160 lb.

Bit errors in RF module logic and memory components caused by cosmic rays or high energy trapped protons should not be a major problem if the component sensitivity is similar to CMOS/SOS devices.

6 GROUND-BASED EXPERIMENTS

6.1 INTRODUCTION

Testing of a large space-based radar (SBR) presents unusual difficulties for two reasons. First, because of the system's size, and its design for a zero-gravity environment, ground testing of the actual fully deployed system is difficult. Second, the stringent performance requirements make measurement and analysis very difficult. For example, two particularly stressing requirements are to maintain far-out sidelobes 70 dB below the mainbeam peak (14 dB below isotropic) and to adaptively create 110 dB nulls at specific angles. This requires very precise phase control of the array elements. Furthermore, the performance is very sensitive to a number of error sources including structural deformations, deployment errors, array module malfunctions, and feed subsystem errors. When these exacting measurement requirements are combined with a large deployable structure designed for zero gravity, direct ground-based measurement is virtually ruled out.

In view of the above problems, it is clear that it is necessary to find alternate methods of evaluating SBR performance. The approach taken here is to analyze a number of candidate test methods. In each case the advantages, disadvantages, and potential for making pertinent measurements are evaluated. Emphasis has been focused on large-scale tests which are unique to the SBR.

Ultimate ground-based determinations of SBR performance will necessarily require a combination of tests most likely augmented by computer simulation. For example, RF test data might be obtained on array segments measured in an anechoic chamber using near-field techniques. The test results would then be input to the computer simulation to predict the overall system performance. The simulation could also compensate for gravity effects on the measurements, and add in anticipated effects due to the space environment (e.g., thermal distortions).

The possible antenna systems which have been considered[1] include:

- Active space-fed lens
- Passive space-fed lens
- Corporate-fed array
- Reflect-array

There are three types of antenna tests required during the three stages of a development program. These types are:

1. Proof-of-design
2. Flight model acceptance
3. Pre-launch

The purpose of the proof-of-design tests is to verify that the design meets the electrical specifications. These tests can be made using models which may mechanically deviate substantially from flight models, for example by having a much stronger structure. The models may also differ electrically if the effect on performance measures is negligible or is known and can be compensated for.

Flight model acceptance tests must insure that the particular hardware under test meets all electrical and mechanical requirements. Gravity compensation is a major consideration and may be attempted mechanically, electrically, or analytically. These tests involve a combination of electrical and mechanical subsystem tests, tests of membrane and structural segments, analysis, and simulation.

Pre-launch tests must insure that the flight model still meets the specifications, after transportation, packaging, and other processing after acceptance testing. This may involve built-in-test capability, visual inspection, subsystem tests (e.g., transmitter stability), and/or special test equipment.

---

[1] See CR-2-1048, Vol. I, Sec. 2.1.

Testing for proof-of-design is emphasized in this report.

Section 6.2 of this report summarizes the potential test methods
which have been considered. This section also contains a subsection
entitled "matrix of antenna test techniques." This matrix consists of a
series of evaluations of the salient characteristics of the selected
test methods. The salient characteristics include a technique descrip-
tion, summaries of the advantages and disadvantages, and a discussion of
the pertinent issues associated with each of the key measurements. Two
test methods show considerable promise and have been investigated in
considerable detail. In particular, Sec. 6.3 discusses intermediate-
range (field) tests. Section 6.4 covers near-field tests. Section 6.5
presents a summary of study conclusions.

6.2   TEST METHODS

Potential tests include tests of the full-sized antenna, a fre-
quency-size scale model, and antenna sections. In all cases, the
methods for testing the antenna may be categorized according to the dis-
tance from the antenna at which measurements are made: far-field,
intermediate-field, or near-field.

6.2.1   Far-Field Range

An ideal far-field range is one with an extremely long range and
no reflections either from the ground or nearby obstacles. In practice,
far-field test ranges usually have a minimum length of $2D^2/\lambda$ where D
is the antenna diameter and λ is the wavelength. For a 35 m antenna
operating at L-Band, this minimum range is 10 km. A suitable test range
of this length is difficult to find. Furthermore, even this $2D^2/\lambda$
criterion is inadequate for some aspects of antenna testing. In partic-
ular, at this range, when the wavefront reaches the antenna under test,
it is not plane but has a spherical wavefront curvature with a maximum
deviation of 22.5 degrees of spherical phase over the aperture. This
causes errors in the measured pattern as discussed in the section on
intermediate range testing.

154

6.2.2 Intermediate Range

Intermediate ranges are those beyond the near field (i.e., a few to several wavelengths) but less than the Rayleigh distance $(2D^2/\lambda)$. Typically, an intermediate range would be D^2/λ or less.

Two intermediate-range measurement techniques have been considered. The techniques are: (1) intermediate-range with analytic correction, and (2) intermediate-range with aperture focus.

6.2.2.1 Intermediate Range With Analytic Correction

At all ranges short of infinity, the phase front is curved. As mentioned earlier, even at the Rayleigh distance of $2D^2/\lambda$, the phase curvature results in a deviation of 22.5 degrees across the aperture of the antenna under test. This is shown in Sec. 6.3 to have a significant impact on measured sidelobes. However, it is also shown that predictable corrections can be made to the measurements such that the residual error is negligible. Furthermore, these corrections are also applicable at ranges much shorter than $2D^2/\lambda$.

6.2.2.2 Intermediate Range With Aperture Focus

A well known technique for removing the major part of the quadratic phase error inherent in a finite range is to focus the antenna at a finite range rather than at infinity. This permits measurement of all antenna parameters with the possible exception of the adaptive null depth. This technique has the advantage that no assumptions about the aperture illumination or inherent errors are required. On the other hand, a phase shift must be included in the hardware. This could present some major difficulties and introduce new errors. Nevertheless, this technique is included in the matrix of test techniques.

6.2.3 Near-Field Testing

There are two near-field measurement techniques which have been considered--compact range and planar scan.

6.2.3.1 Compact Range

In this technique, a quasi-plane wave is generated at a short range by use of a collimating lens or reflector placed near the antenna under test. A major difficulty is that the lens or reflector must be larger than the antenna under test. For the large SBR such a collimating device would present difficulties. For this reason, the compact range technique was not considered in great detail. This technique is included, however, in the matrix of test techniques.

6.2.3.2 Planar Scan

In near-field scanning, the field is measured with a probe in the vicinity of the antenna under test. From the measured data, the far-field parameters are computed. Because these measurements are usually made at a distance of only a few wavelengths from the antenna under test, the test can be performed in an enclosed, controlled environment. In addition, the short range signal-to-noise ratios are high, a large dynamic range can be obtained, shielding from outside disturbances is possible, and measurements can be used as a diagnostic tool to determine antenna faults and provide otherwise unobtainable information on antenna behavior. Once the basic set of measurements is made, the entire antenna pattern can be computed.

A major disadvantage of the near-field technique is that a large number of data are required. For many probe locations the signal has to be measured in phase and amplitude. This data along with the probe position must be digitized and recorded, then processed by a special computer program. For high-gain antennas the computation becomes extensive. Another problem is that since the probe is near the antenna, care must be taken to minimize reflections. Also, precise phase measurements could present difficulties at high frequencies.

A common measurement technique is to mount the probe on a precisely calibrated two-axis transporter in front of the antenna. This is

called planar near-field scanning. Other methods are to rotate the axis of the antenna in one or two angles while the probe is moved in the orthogonal direction or held stationary, respectively. These methods are, respectively, the cylindrical and spherical scanning modes.

Near-field measurements are discussed in Sec. 6.4.

Two other techniques have been briefly considered. They are frequency-size scale modeling and test sections. These are included in the matrix of test techniques.

6.2.4 Matrix of Antenna Test Techniques

The following is a summary, in a matrix form, of several potential techniques for testing a large SBR. The techniques which have been considered include:

- Far-field
- Intermediate range—with analytic correction
- Intermediate range—with aperture focus
- Near-field—compact range
- Near-field—planar (or other) scan
- Frequency-size scale
- Test sections

For each of these techniques the summary matrix includes:

- A description of the technique.

- A summary of the principal advantages of the technique.

- A summary of the significant disadvantages of the technique.

- A short discussion of the pertinent issues associated with each of the five key measurements. The measurements are main beam gain, beamwidth, sidelobes, cross polarization and nulls.

Table 6.1 is a brief summary of the applicability of the measurement techniques. This is expanded upon below.

6.2.4.1 Far-Field

Description--Measure antenna pattern at a test range. By convention the test range length must be at least $2D^2/\lambda$. A standard gain horn or reflector is used as a probe. The antenna under test is conventionally rotated to exhibit the off boresight pattern. Alternatively, the probe could be moved, for example, by using an aircraft or satellite to fly the probe over the antenna under test. This approach has received relatively little attention, but one case has been reported where a transmitter on the moon was used to measure the antenna pattern of the 64 m NASA/JPL advanced antenna system (AAS) at Goldstone.[1] The Surveyor spacecraft transmitter was switched to a narrowband mode, and the Goldstone antenna was open-loop pointed with the standard computer-assisted command system. The far-field distance of the AAS at 2,295 MHz is 63 km, somewhat larger even than the SBR case. At the lunar range of 380,000 km the range is over six thousand times the $2D^2/\lambda$ distance. The phase error at the aperture edge due to phase front curvature in this case is 0.004 degrees. Figure 6.1 shows an example of how the Goldstone antenna was tested. Those test results are shown in Fig. 6.2. Figure 6.3 shows the typical antenna instrumentation required.

Advantages--The complete antenna is tested. The pattern is determined from direct measurements with no data transformations involved. The measurement time is relatively short if only limited information is required, such as a principal plane cut. It is good for comparison measurements such as gain or polarization.

Disadvantages--At $2D^2/\lambda$, a 22.5 degree phase error occurs at the edges of the array. This results in measurement errors, especially for

[1] G. Levy et al., "Lunar Range Radiation Patterns of a 210-Foot Antenna at S-Band," IEEE Transactions on Antennas and Propagation, Vol. AP-15, No. 2, March 1967, pp. 311-313.

TABLE 6.1

APPLICABILITY OF MEASUREMENT TECHNIQUES

Measurement Technique	Gain	Beam Pointing	Antenna Parameter Beamwidth	Sidelobe Level	Cross-Polarization Pattern	Adaptive Null Depth
Far-Field						
Conventional Test	X	X^1	X^1	X^1	X^1	X
Intermediate Range						
Analytic Correction	X	X^1	X^1	X^1	X^1	X
Aperture Focus	X	X^1	X^1	$?^1$	X^1	?
Near-Field						
Compact Range	X	X^2	X^2	X^2	$?^2$	?
Planar Scan	X	X	X	X	X	No
Other[3]						
Frequency Scale	?	?	X	?	?	X
Test Sections	?	?	?	?	?	No

Notes:

1. Rotating the antenna under test is a major potential problem; alternatively, the probe could be moved.

2. Rotating the antenna under test is a major potential problem, and a new collimation technique may be required.

3. Finding or constructing a suitable range is a major potential problem for all techniques except these.

159
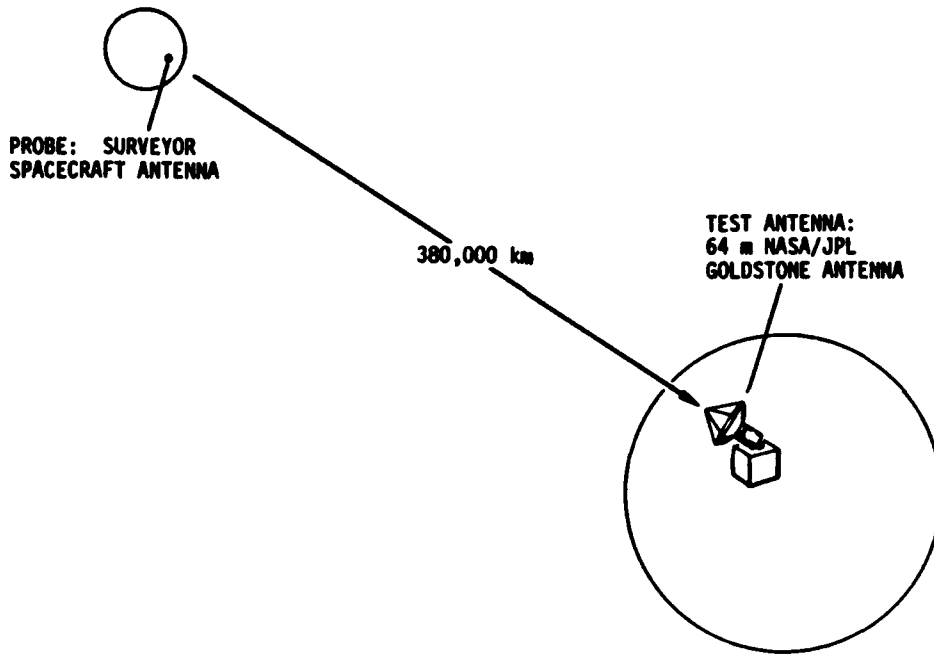
Figure 6.1. Lunar Range Antenna Pattern Measurements
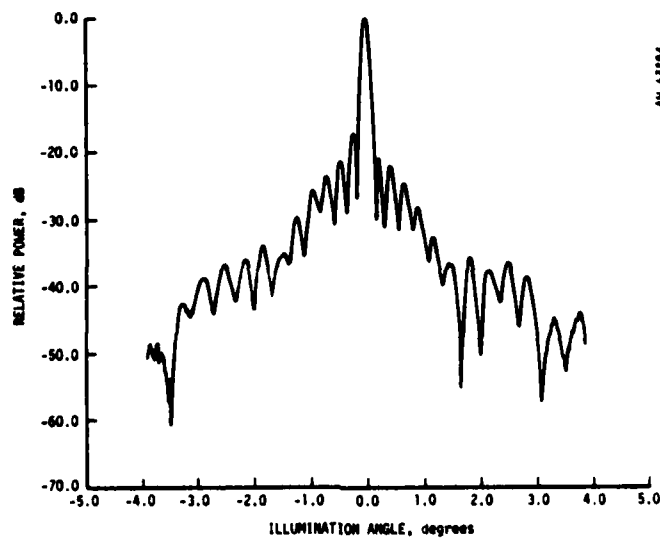
"G LEVY et al "LUNAR RANGE RADIATION PATTERNS OF A 210-FOOT ANTENNA AT S-BAND" IEEE TAP, MARCH 1967

Figure 6.2. Antenna Patterns Measured Using the Surveyor Spacecraft on the Moon as a Probe
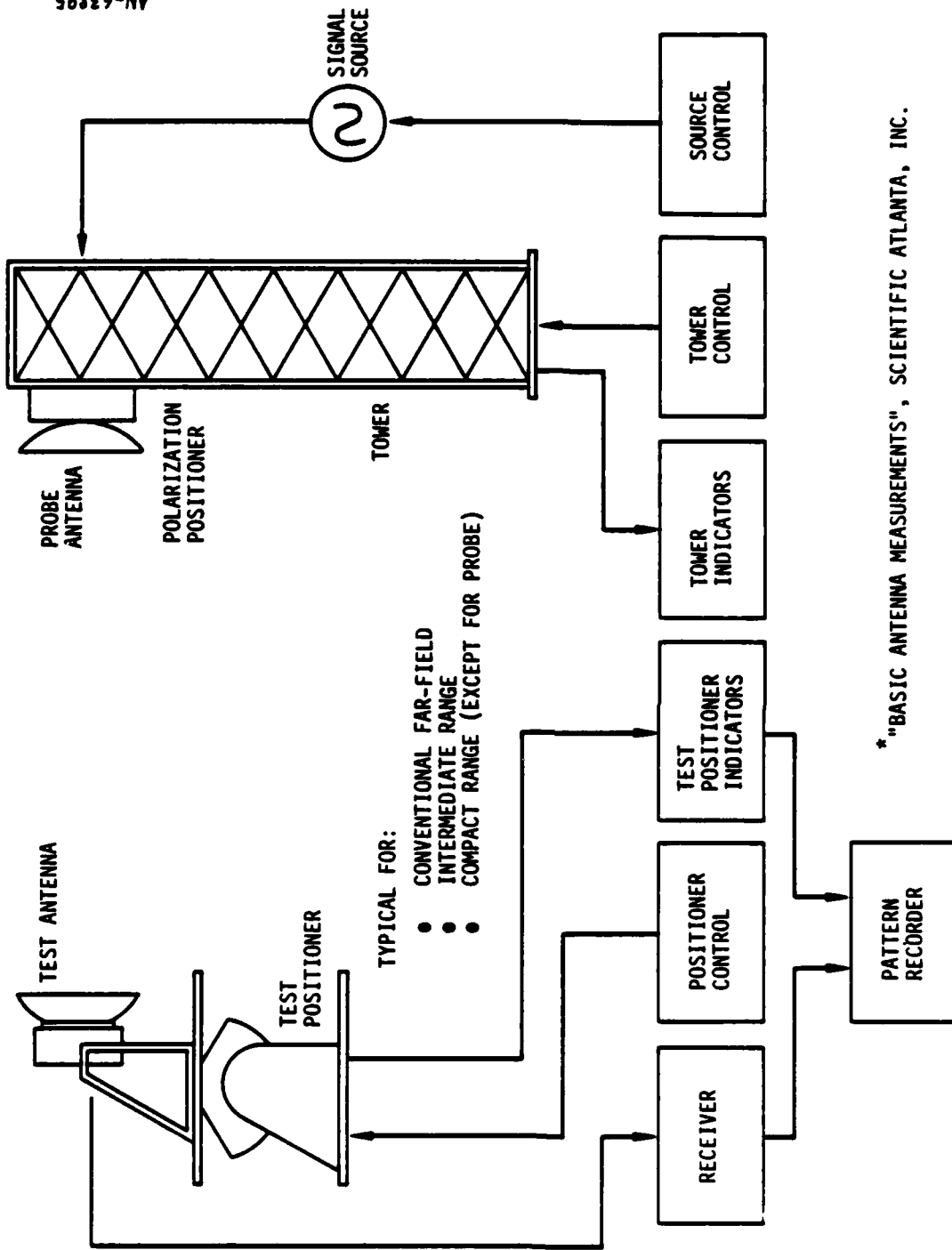
Figure 6.3. Antenna Instrumentation

the first sidelobe. A large range is required (e.g., for $\lambda = 0.24$ m and $D = 35$ m, $2D^2/\lambda = 10.2$ km). Multipath could be a problem if a suitable range cannot be found. Weather could be a problem. Two-axis rotation of the antenna under test or a distant moving probe is required. A distant moving probe presents special considerations. In particular, it might be difficult to route the probe through the precisely desired path or to exactly repeat a particular path. However, this may not be necessary. The antenna may be tested simply by making measurements along the known trajectory and then checking to see if they agree with the predicted measurements. If they do, then it is reasonable to assume that the antenna is performing as predicted at the other locations as well. Furthermore, the antenna can be electronically scanned during the test so that measurements can be made for several main beam scan states during each pass.

Potential Measurements

Main Beam Gain--This is a relatively simple measurement for this method using comparison with a gain standard. Multipath is the chief source of concern, and range calibration is essential.

Beamwidth--This could be measured with a distant moving probe. In the case of ground-based measurements this requires a precise calibration of the relative angle between the probe and the antenna under test along with calibrated relative gain measurements. Deformation of the antenna during rotation could introduce significant errors. This could be a major problem for a large antenna designed to operate in a zero gravity environment.

Sidelobes--These could be measured with a distant moving probe as discussed above or by rotating the antenna under test (AUT). In this case, deformation of the antenna test surface during rotation could introduce significant errors. This could be a major problem for a large antenna designed to operate in a zero gravity environment.

162

<u>Cross Polarization</u>--No unique problem for this technique.

<u>Nulls</u>--This is a relatively simple measurement for this method. Jammers can be positioned on the antenna range along with the probe, and signal-to-interference directly compared with and without adaptive nulling. For measurement of deep nulls, low levels of multipath are a necessity.

6.2.4.2 <u>Intermediate Range (With Correction)</u>

<u>Description</u>--Measure antenna pattern on a short test range. A typical range length would be D^2/λ , half the Rayleigh distance. A simple mathematical correction is used to account for the resulting sidelobes. A standard gain horn or reflector is used as a probe and the antenna under test is rotated to exhibit the off-boresight pattern, or a moving probe is used. Figures 6.4 and 6.5 illustrate these concepts.

<u>Advantages</u>--Range is reduced. Complete antenna is tested. No modifications to the hardware are required. Only simple corrections to the data are required.

<u>Disadvantages</u>--Range is still long for large antennas (the range for a 35 m antenna with a 0.24 m wavelength is 5.1 km). Weather could be a problem. Multipath could be a problem if a suitable range cannot be found. Two axis rotation of the test antenna or a moving probe is required.

<u>Potential Measurements</u>

<u>Main Beam Gain</u>--Measured in a straightforward manner using comparison with a gain standard and a computed correction term is added. Multipath is the chief source of concern, and range calibration is essential.
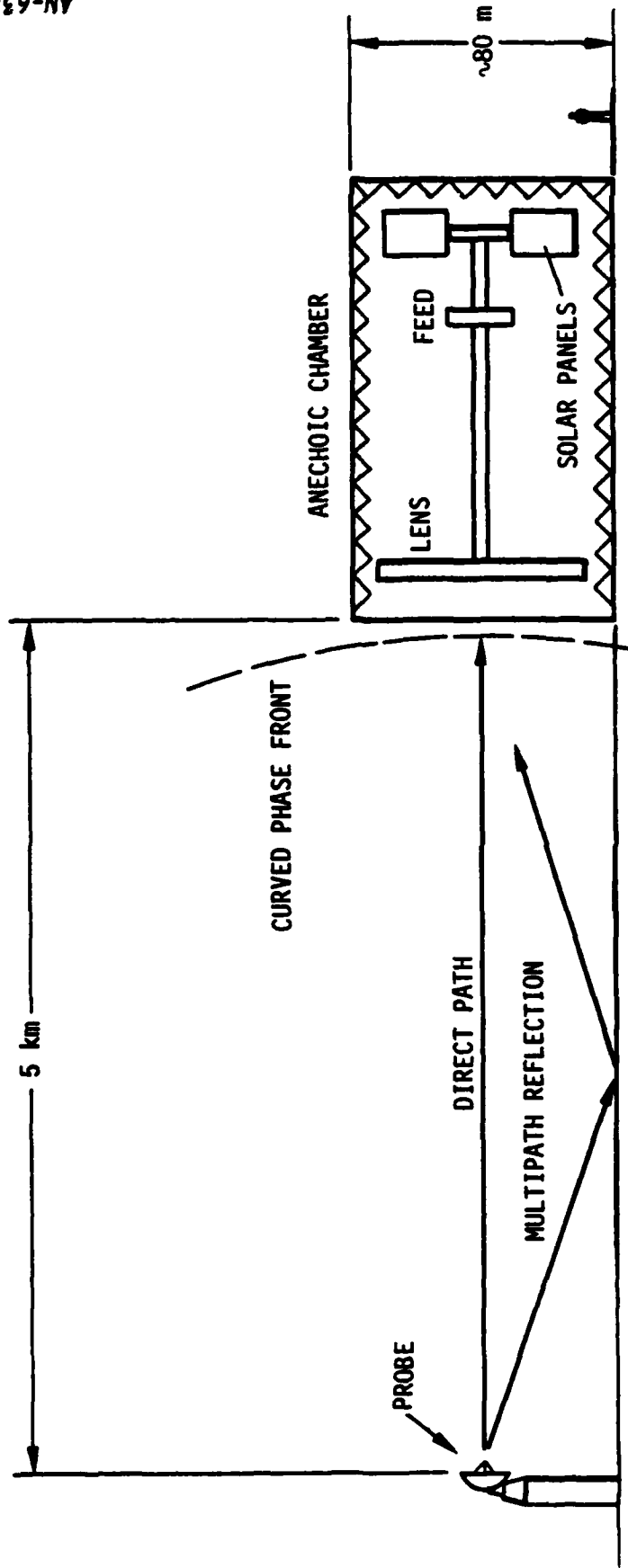
Figure 6.4. Range for Intermediate Range Testing
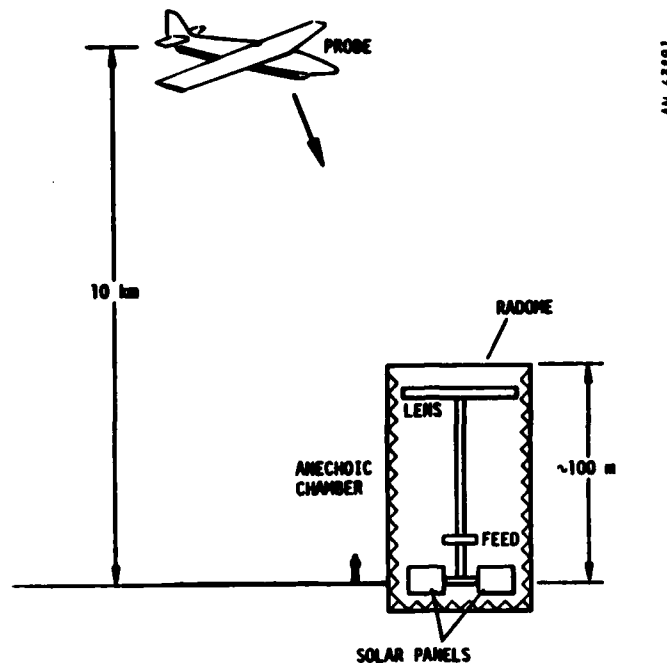
Figure 6.5. Full Scale Test Airborne or Satellite Probe

Beamwidth—One possibility is to use a moving probe. Care must be taken to prevent multipath. Another possibility is to rotate the antenna. This requires a precise calibration of the relative angle between the probe and the antenna under test along with calibrated relative gain measurements. Deformation of the antenna during rotation could introduce significant errors. This could be a major problem for a large antenna designed to operate in a zero gravity environment. A computed correction term is added to the measurements.

Sidelobes—For a fixed probe, deformation of the antenna test surface during rotation could introduce significant errors. This could be a major problem for a large antenna designed to operate in a zero gravity environment. A moving probe could solve this problem.

Cross Polarization—No unique problem for this technique.

165

<u>Nulls</u>--Similar to far-field case. This is a relatively simple measurement for this method, <u>assuming</u> that the adaptive circuits are not influenced by the larger quadratic phase error over the aperture compared to the "far-field" range. This must be verified by simulation.

6.2.4.3 Intermediate Range (With Aperture Focus)

<u>Description</u>--Insert a quadratic phase shift across the array elements to compensate for the spherical phase front. This is accomplished by using the feed and checking with the simulation. Focus is exact for beam peak only.

<u>Advantages</u>--Reduces the range. Tests the complete antenna. No analysis or transformations of measured data are required.

<u>Disadvantages</u>--Range is still long for big antennas. Inserting the phase shift could be difficult and could introduce uncertanties. Hardware modifications and/or phase bit switching could change the mutual coupling effects, module reflection coefficients, and element excitations. Multipath could be a problem. Weather could be a problem. Two axis rotation of the antenna is required, or a moving probe.

<u>Potential Measurements</u>

<u>Main Beam Gain</u>--Measured directly as in far field technique, but <u>assumes</u> that required phase shifts have no significant effects other than the desired quadratic phase compensation.

<u>Beamwidth</u>--This requires a precise calibration of the relative angle between the probe and the antenna under test along with calibrated relative gain measurements. For a fixed probe, deformation of the antenna during rotation could introduce significant errors. This could be a major problem for a large antenna designed to operate in a zero gravity environment. A movable probe could be used.

166

Sidelobes—The focus off axis is inexact. It is conceivable that we could refocus as we scan, but this would be complicated. Deformation of the antenna during rotation could introduce significant errors. This could be a major problem for a large antenna designed to operate in a zero gravity environment.

Cross Polarization—Measured directly.

Nulls—Similar to far-field case. This is a relatively simple measurement for this method assuming that the adaptive circuits are not influenced by the inserted phase shifts. This must be verified by simulation.

6.2.4.4 Near-Field, Compact Range

Description—Use a large reflector or lens to collimate the probe beam, thus obtaining a plane wave illumination on a short range as shown in Fig. 6.6. Either the antenna under test must be rotated, or the angle of the plane wave illumination must be changed. No existing systems are capable of changing the angle of the plane wave.

Advantages—The test range is much shorter. Multipath problems are reduced. Direct measurements with no analysis or data modification. No weather problems. Can be made secure.

Disadvantages—Requires a reflector or lens larger than the test antenna. Subject to errors in the lens or reflector. Distorted by diffraction from the edges of the collimating lens or reflector.

Potential Measurements

Main Beam Gain—Measured directly using comparison with a gain standard.
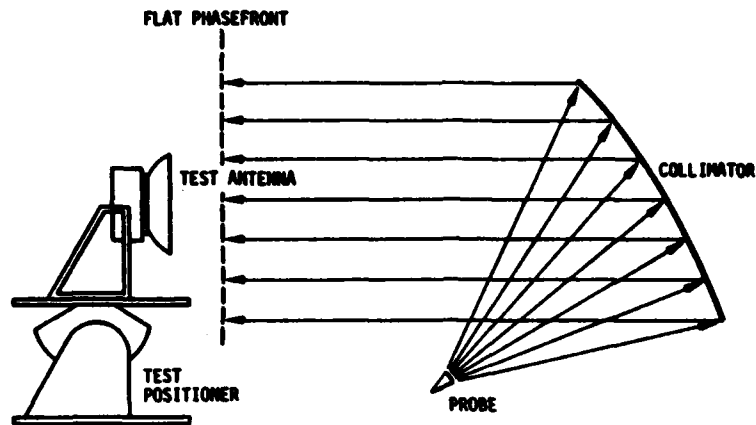
Figure 6.6. Compact Range Method

Beamwidth—Same as far-field (or intermediate range) except that a moving probe cannot be used, so the antenna under test must be rotated or a new technique developed. Rotating the lens rather than the antenna is not a reasonable solution, since the lens is even larger than the antenna.

Sidelobes—These could be measured by rotating the antenna under test. A new collimation technique may be required.

Cross Polarization—Sensitive to cross-polarization of collimating system.

Nulls—Introduction of jammers requires multiple feeds for collimating lens or reflectors, which would be defocused, and in general not appear to be point sources. This requires study and development as a new technique.

168

6.2.4.5 Near-Field Measurements, Planar (or Other) Scan

Description—Sample the amplitude and phase on a precisely known surface (usually a plane, cylinder, or sphere) then compute the far-field pattern by using a mathematical transformation (Fourier for plane wave). This method was used for testing the AEGIS antenna, as shown in Figs. 6.7 and 6.8.

Advantages—Very compact test facility. No weather problems. Can be made secure. Multipath problems are reduced. Good accuracy. Complete 3-D pattern obtained, including polarization, for any range. Near-field antenna interactions are treatable. Antenna errors can be localized quickly. Can measure wide-angle sidelobes or widely scanned beams when non-planar scanning is used.

Disadvantages—Must collect lots of data. Precise adjustment of test equipment is required. Measurements are very demanding. Must do lots of number crunching. Automated and sophisticated data taking system is required. Time lag between measurement and results is a potential problem during design development. Probe multipath effects are uncertain.

Potential Measurements

Main Beam Gain—Can be computed with minimal residual error.

Beamwidth—Determined from the computed pattern.

Sidelobes—Computed just as the main beam. No additional data is required.

Cross Polarization—Can be computed.

Nulls—It appears to be impossible to introduce jammers to allow adaptive nulling, and even if this problem were solved, the capability of accurately computing 110 dB nulls is at best questionable.

169

AN-63897

AN/SPY 1A ANTENNA
- S-BAND PLANAR ARRAY
- 12 FEET DIAMETER

PROBE CARRIAGE

WAVEGUIDE PROBE

ANTENNA LIFT ASSEMBLY

GUIDE RAILS

AN/SPY 1A ANTENNA

RF ABSORBER
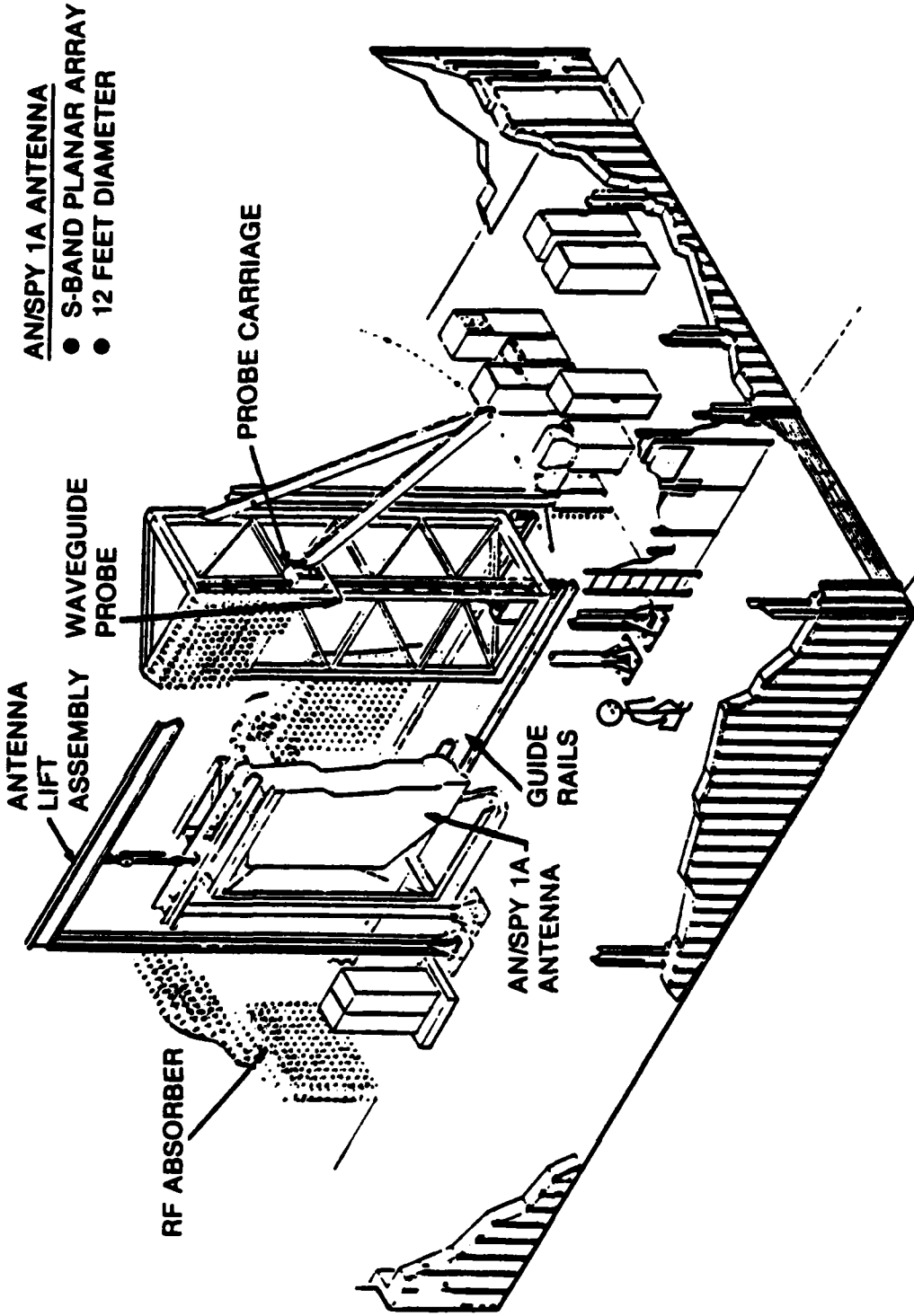
"NAVAL OCEAN SYSTEMS CENTER TR 499, JUNE 1980

Figure 6.7. AEGIS Planar Scan Near-Field Antenna Test System

170
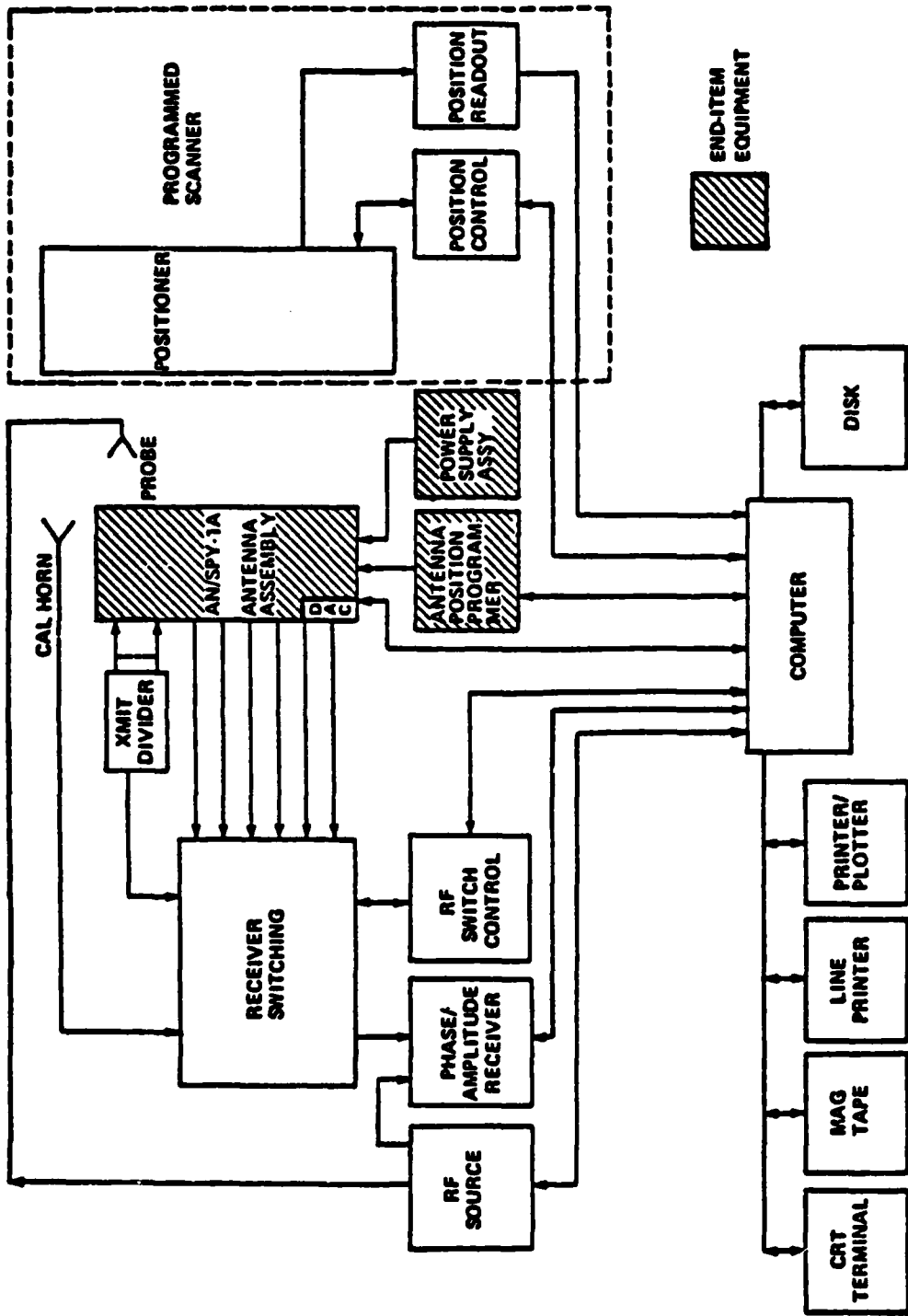
Figure 6.3. Block Design—AEGIS Near-Field Antenna Test System

6.2.4.6 Frequency-Size Scale

Description—Construct a smaller version of the antenna which replicates in scale the feed and any obstructions, and use a frequency scaled in the same ratio. Possibly use only the feed and use a fixed phase shift in place of the modules.

Advantages—Range is short. Can test a complete antenna. Can test adaptive nulling. Test procedures are simple.

Disadvantages—Requires construction of a whole new (but smaller) antenna. A scaling uncertanty is involved. Weather and multipath could be a problem.

Potential Measurements

Main Beam Gain—Measured directly similar to far-field technique, but assumes accuracy of scale model.

Beamwidth—Measured directly similar to far-field technique but assumes accuracy of scale modoel.

Sidelobes—Very sensitive to accuracy of scale model.

Cross Polarization—Sensitive to accuracy of scale model.

Nulls—Testing the adaptive nulling would be the major advantage of this technique, since the key feed effects and multipath time delay should be modeled accurately.

6.2.4.7 Test Sections

Description—Test only sections of the antenna; then compute the full antenna performance using the simulation.

Advantages—The range is shorter. If indoors, weather and inter-
ference problems are eliminated. Multipath is reduced. Measurements
are simplified. Technique is fast if only limited information is
required.

Disadvantages—Does not test true antenna. Subject to errors in
assumptions about how the sections interact. Cannot test adaptive
nulling.

Potential Measurements

Main Beam Gain—Determined by measurement and computation.

Beamwidth—Determined by measurement and computation.

Sidelobes—Determined by measurement and computation; sensitive to
accuracy of the simulation.

Cross Polarization—Determined by measurement and computation;
sensitive to accuracy of the simulation.

Nulls—Nulling capability with a single section could be obtained,
but extrapolating this to the full system relies more on the model
employed in the simulation than on the measured data.

6.2.4.8 Review of Techniques Matrix

A review of the potential measurement techniques and desired
parameters indicates that, with the exception of adaptive null measure-
ments, most of the techniques are capable of providing the desired data
if (1) a suitable range were available, and (2) the required movement of
the antenna under test and/or the probe could be achieved. Therefore,
these two practical conditions emerge as the key issues for all measure-
ments excepting adaptive nulling, which is discussed separately below.
Rotating a very large structure appears to be difficult at best, and the

issues involved would require study far beyond the scope of the present contract.

Moving the probe—e.g., by flying over the antenna under test in an aircraft or satellite—is a possible alternative. The aircraft/satellite approach has the virtue of eliminating the specular ground reflection which is the major source of multipath as discussed in Sec. 6.3. The primary disadvantages involve cost and the logistics of insuring that the satellite or aircraft is in the right place at the right time—which is mitigated by the fact that the array beam can be steered at will. This technique certainly deserves further study.

The most attractive alternative to a distant moving probe is a near-field scan technique involving a very close moving probe. These two alternatives are selected as the most attractive means for providing all antenna measurements excepting nulling. Since the near-field technique involves issues of test design very similar in nature to other tasks in this study, it is selected for more detailed consideration in Sec. 6.4. The distant moving probe technique is left for future study of the logistic and cost issues which are key to that technique.

For adaptive null depth measurements, the applicable techniques are Far-field and Intermediate-range measurements, and frequency scale tests. The key issue in scaling is the fidelity of the scale model. Relatively little can be done to resolve this issue without definitely specifying the design of the antenna under test, and it is felt that this is best left until the design is more firmly established. Far-field testing has been extensively studied, whereas the intermediate-range technique has only been recently proposed; therefore, this technique is also selected for further study in Sec. 6.3. Although the initial motivation for selecting this technique involved the nulling measurement, it is also applicable to the other antenna parameters, and indeed is applicable as a refinement of the conventional far-field

174

technique; therefore, rather than restricting attention to nulling, it is studied in the broad context of the overall measurement problem.

6.3 INTERMEDIATE RANGE MEASUREMENTS

Antenna pattern measurements are frequently made at a range of $2D^2/\lambda$ from the antenna, where D is the antenna diameter and λ is the wavelength. This is called the Rayleigh distance. For most antennas this gives a good approximation to the antenna pattern at all longer ranges. In particular, for the mainlobe the measured gain is approximately 99% of the true gain. Sidelobe measurements are also quite good for all sidelobes beyond the first two. However, for large antennas operating at high frequencies, the Rayleigh distance is quite large. For example, the Rayleigh distance for a 35 m diameter antenna operating at a 0.24 m wavelength is greater than 10 km. Furthermore, even at the Rayleigh distance, the error in the first two sidelobes is usually noticeable and becomes quite large for antennas specifically designed to have low near-in sidelobes. This error is due to the phase curvature or sphericity of the wavefront at the antenna when it is used as a receiver.

There appears to be a potential solution to the problem. The effect of the phase curvature on the antenna pattern can be calculated exactly for a known aperture distribution. Thus, the appropriate correction can be determined exactly for this specific case. It seems reasonable that if the actual antenna aperture distribution is close to the assumed distribution one would expect the correction terms for measurement at the Rayleigh distance would also be close to the ideal case. Furthermore, the same argument should be true for measurements made at ranges shorter than the Rayleigh range (intermediate range).

To test this hypothesis, an investigation into the potential usefulness of determining the far-field pattern by appropriately correcting intermediate-range measurements was begun. Two intermediate ranges were

175

considered (Rayleigh and 1/2 Rayleigh) in order to examine the sensitivity to range.

The specific procedure was to use the SARF simulation to first calculate the antenna pattern at the three ranges R, R/2 , and ∞ (where R is the Rayleigh distance) using the ideal (-40 dB Taylor) antenna weighting. The differences between the pattern gain at the shorter (R and R/2) distances and at infinity determine the noise-free antenna pattern correction terms. Next, the amplitude and phase of each antenna element is perturbed by amplitude and phase deviations similar to those expected in an actual antenna. (These are obtained as samples from Gaussian distributions with one sigma values of 2 degrees in phase and 0.25 dB in amplitude.) The SARF simulation is then used again to compute the antenna pattern for the sample perturbed antenna. The computed patterns at R and R/2 represent the patterns which would be measured for a test antenna having the specified phase and amplitude perturbations; the pattern computed at R = ∞ represents the desired far-field pattern for the perturbed array. The patterns at R and R/2 are then "corrected" by adding the noise-free antenna pattern correction terms computed earlier. The resulting patterns are then compared with the computed far-field pattern. The difference represents the residual error after the correction scheme has been applied. This procedure is then repeated with a new set of noise samples.

An example of the results is shown in Table 6.2 and illustrated in Fig. 6.9 for a 35 m diameter L-band array with a 40 dB Taylor weighting. The results shown have an accuracy of 0.1 dB. Therefore, if measurement noise of 2 degrees phase and 0.25 dB amplitude is accepted as reasonable, it may be concluded that intermediate-range measurement with correction is a promising technique for the case of uncorrelated noise.

However, it must be mentioned that correlated noise is a possibility. Such cases were not evaluated in this study. The reason is that

TABLE 6.2

ERROR IN INTERMEDIATE-RANGE MEASUREMENTS WITH CORRECTION

(All Values in dB)

	Peak	First SL[*]	Second SL[*]	Third SL[*]
True Value at ∞	51.0	40.6	41.0	41.7
Rayleigh Distance				
Correction	0.1	1.1	0.2	0.2
Residual Error	[†]	$\pm$0.1	$\pm$0.1	$\pm$0.1
Half-Rayleigh Distance				
Correction	0.7	5.9	1.0	0.6
Residual Error	[†]	$\pm$0.2	$\pm$0.2	$\pm$0.3

Assumptions

    Diameter = 35 m

Wavelength = 0.24 m

Weighting = 40 dB Taylor

    Noise = Gaussian Phase ($\sigma = 2°$)

        Gaussian Amplitude ($\sigma = 0.25$ dB)

---

[*] Sidelobe values are specified as dB below peak gain.

[†] Residual error is much less than $\pm$0.1 dB.

---

it is expected that the results would depend on the specific models for the correlation. Selection of an appropriate model is beyond the scope of this study. It is recommended that further studies in this area should address the issue of representing correlated noise models.

The above analysis was based on a perfect test range. In practice, the test environment cannot be ignored. The most significant feature of an actual test range is the presence of multipath. In the
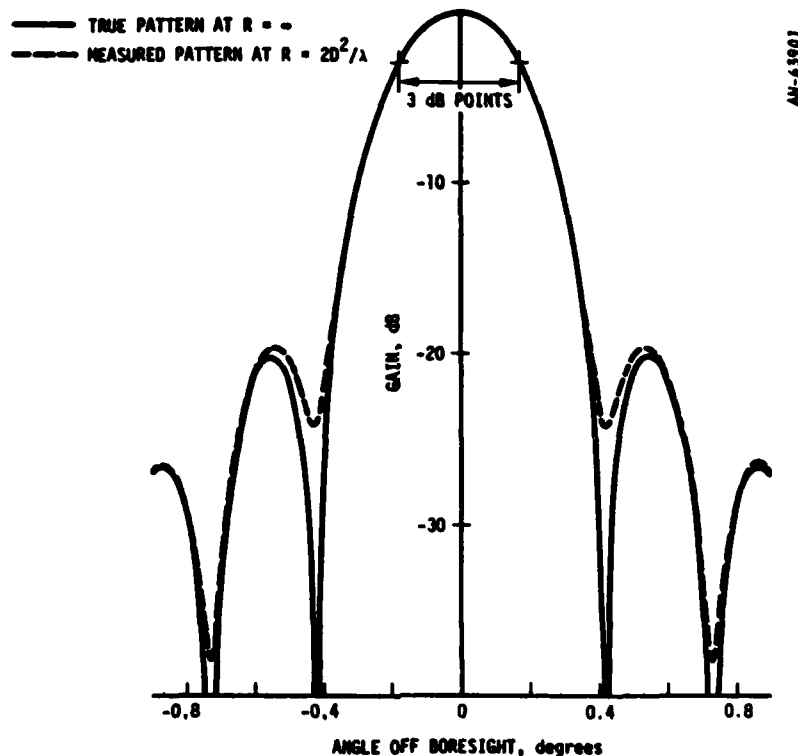
Figure 6.9. Curved Phase Front Effect--"Far-Field" Range

following paragraphs we consider the effect of test range multipath on antenna pattern measurements made in the intermediate range of D^2/λ.

For the 35 m diameter antenna operating at a 0.24 m wavelength, the intermediate range (D^2/λ) is 5.1 km. A conceptual range model[1] for testing this antenna is shown in Fig. 6.10. We assume three specular reflections near the midpoint of the range and three reflections close-in to the probe antenna. We also assume the worst case of unity reflection coefficients. This is because a summation over high frequency terms is more likely to approximate zero. For a high gain probe antenna with a 2° beamwidth, the amplitude taper across the 35 m antenna is less

[1] J. Appel-Hansen, F. Jensen, and A. Ludwig, SAR Antenna Test Techniques, Final Report, TICRA APS Engineering Consultants, Copenhagen, Denmark, January 1980.

178
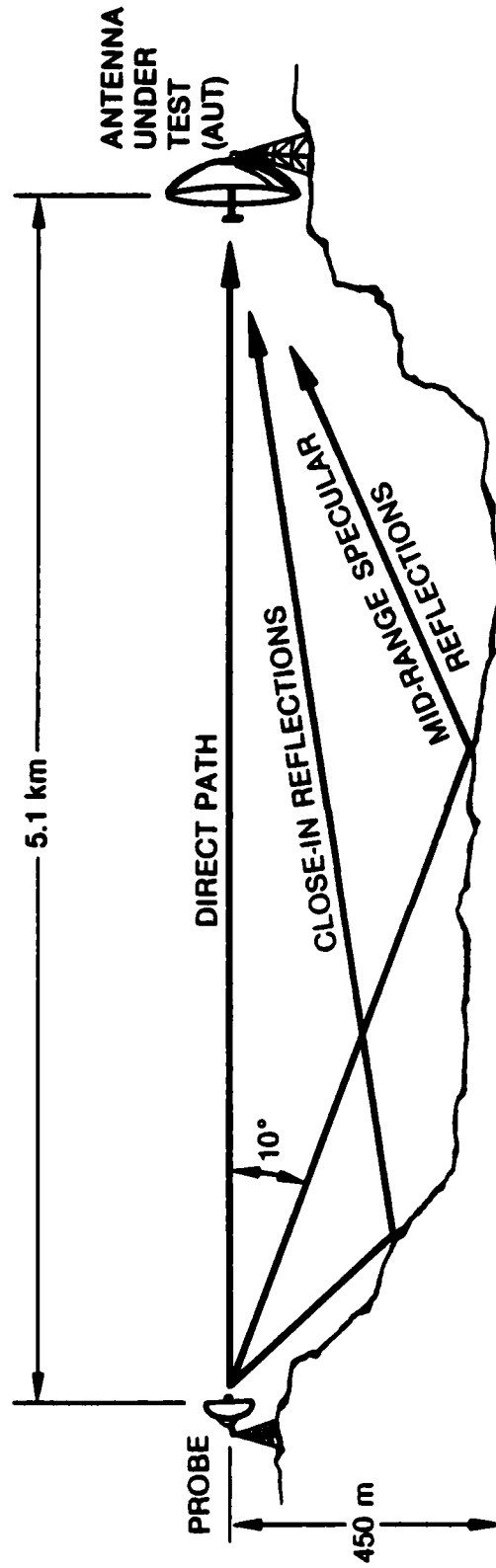
Figure 6.10. Conceptual Test Range for Intermediate Range (D^2/λ) Testing

than 0.12 dB. For any reasonable probe antenna sidelobe pattern the
reflections at angles of greater than 10° should be down by at least 30
dB relative to the direct path.

Consider first the measurement of the relative mainlobe gain as a
function of scan angle or frequency. The reflection levels are shown in
Table 6.3. When making the measurements, the main beam of the antenna
under test (AUT) is pointing directly at the probe antenna and the
effective reflection level is reduced by the antenna pattern of the AUT.
In particular, the midpoint reflections are reduced by the -40 dB side-
lobe level. The resulting root sum square (RSS) effective reflection
level is -32.5 dB. This is equivalent to a normalized voltage error of
0.0237. This could cause a maximum amplitude or phase deviation of ± 0.2
dB or ± 1.4 degrees, respectively. It was shown in the cited reference

TABLE 6.3

EFFECT OF MULTIPATH ON A HALF-RAYLEIGH TEST RANGE

Reflection Point Relative to Probe Antenna[†]		Reflected Signal[*] Strength, dB	View Angle From AUT, deg	Effective Reflection Level for AUT Main Beam, dB
Height, m	Range, m			
450	2,550	-30	10.0	-70
380	2,600	-32	8.0	-72
350	2,500	-32	8.0	-72
4	0	-37	0.04	-37
6	2	-37	0.07	-37.2
12	4	-37	0.13	-37.7
RSS		-25.4		-32.5

[*] Specular reflection coefficients conservatively assumed equal to unity.

[†] Arbitrarily chosen for illustrative purposes.

that these results are a good approximation to the values which would be
obtained by using a more rigorous analysis.

In measuring the absolute mainlobe gain, one must also consider
the error at the gain standard horn (probe). The major consideration is
that the gain standard horn will respond approximately like the peak
error in the incident field. This can be accounted for by measuring the
response of the gain standard horn as the frequency is swept across the
band and then subtracting out the best linear fit. The residual will
provide an excellent measure of the actual range multipath and can be
used as a correction factor for the multipath effect at each frequency.
It is estimated that with this procedure the resulting error in the gain
standard horn response will be negligible with respect to the relative
errors.

In making sidelobe measurements, it is assumed that the main beam
never points at a reflection point. This can be ensured by always
orienting the antenna so that the main beam points above the horizon.
In this case, a reasonable assumption is that the direct path and
reflections couple equally into the test antenna. Therefore, the RSS
reflection level of -25.4 dB is used as a relative interference level to
estimate the error.

Table 6.4 summarizes the effect of reflections on the measurement
of mainlobe and sidelobe gain. These results are based on a straight-
forward derivation using the postulated model. In a recent study by
Appel-Hansen, et al.,[1] a similar analysis was performed. They then
undertook a simulation of the effect of reflections and compared the
results. Their conclusion was that the results were similar and there-
fore the model is a valid tool. This leads us to believe that our
results are also representative of the true expected errors.

---

[1] J. Appel-Hansen, et al., op. cit.

TABLE 6.4

SUMMARY OF EFFECT OF REFLECTIONS ON TEST ANTENNA

	Mainlobe Error		Sidelobe Error[*]	
	Amplitude, dB	Phase, deg	Amplitude, dB	Phase, deg
One—30 dB Reflection	±0.003	±0.02	±0.03	±1.8
Multiple Reflections (RSS = -25.4 dB)	±0.2	±1.4	±0.5	±3.1

[*] This is for RSS sidelobes, it does not apply to the nulls.

The conclusion is that reflections are probably not severe enough to rule out intermediate-range measurements of mainlobe and major sidelobes. They do, however, present a significant potential for error. Reflections will cause errors in measuring nulls.

The usefulness of the technique of intermediate-range measurement with correction may be summarized as follows. In the absence of correlated noise in the aperture distribution, the mainlobe and sidelobe gain can be measured with good accuracy. Care must be taken in test range selection so that reflections are minimized. The effect of correlated noise is unknown and requires a selection of models of correlation before the effect can be analyzed.

6.4 NEAR-FIELD MEASUREMENTS

The principle of the near-field technique is to measure the radiated field in the vicinity of the antenna, and then using the measured amplitude and phase compute the far-field pattern. The measurement locations must be within 1/2 wavelength of each other and may be situated on an arbitrary but known surface. The usual surfaces are planar, cylindrical, or spherical. Planar measurements are the easiest to

implement for a large antenna and also lead to the simplest computation of the far field. Furthermore, a planar near-field scan could possibly help to identify specific antenna errors. A primary concern is the relationship between constraints on the measurements and the accuracy of the computed far-field pattern.

There are five major classes of potential sources for error in the computed far-field pattern. They are:

1. Limited measurement plane (finite scan)
2. In-plane probe position errors (x,y position)
3. Out-of-plane probe position errors (z position)
4. Amplitude and phase measurement errors
5. Multiple reflections

With the aid of a modest digital computer and using a Fast Fourier transform, the computational errors can easily be made negligible relative to the combined errors in the far field caused by all other error sources. The approach taken toward evaluating the errors was to determine the upper bound on the errors as in Yaghjian.[1] These errors assume worst possible perturbations within the maximum bound. In the case of phase errors, Yaghjian compared his results with the errors resulting from using random perturbations with $1-\sigma$ values equal to his maximum bound. He found that he achieved a fairly close upper bound on the random error.

The size of the scan area required to ensure that limited scan errors were negligible was determined first. The upper bound on the error in electric field amplitude due to a finite scan plane is

$$E_s = \alpha \lambda L X g / (2A \cos \gamma)$$

---

[1] A.D. Yaghjian, "Upper-Bound Errors in Far-Field Antenna Parameters Determined From Planar Near-Field Measurements," NBS Technical Note 667, U.S. Department of Commerce, October 1975.

183

where E_s = the error normalized to 1 volt signal amplitude. For small values of E_s the error expressed in dB is approximately 8.7 times this value.[1]

α = a constant equal to the area of the antenna plane divided by the integral of the normalized illumination function (2.7 for a −40 dB Taylor illumination)

λ = wavelength

L = maximum width of the scan area[2]

X = largest amplitude of probe output at edge of scan area normalized to output at center of scan plane (it is a function of L and A)

g = normalized far-field amplitude in the direction for which the error is to be determined

A = area of the antenna plane

γ = maximum acute angle between the plane of the scan and any line connecting the edge of the aperture and edge of the scan area

Using this equation, the scan area necessary to ensure that the error caused by a limited scan is negligible was found. For a scan plane approximately 0.5 m in front of a 35 m diameter antenna operating at λ = 0.24 m , the scan must extend about 1 m beyond the edge of the antenna. The resulting error is about 0.01 dB and decreases very rapidly with increasing scan area. This implies that the scan plane must be about 12% larger than the antenna plane. Approximately 22,000 samples separated by $\lambda/2$ are required.

Reflection errors can also be made negligible. The equation for the upper bound on errors due to reflections is

---

[1] $20 \log(1 \pm \epsilon) \approx \pm 8.7\epsilon$ fc. $\epsilon \ll 1$.

[2] This analysis assumes a rectangular antenna and scan area. Comparable results should hold for other shapes.

$$E_r = W/2$$

where W is the peak-to-peak field variation in dB as the probe is moved away from the antenna. It can be shown[1] that the maximum value of W is given approximately by

$$W = 1/2(4\pi D)^2$$

where D is the distance of the probe from the antenna in wavelengths. Therefore, for $D \geq 2$ the maximum error is less than 0.01 dB, which is negligible.

The errors of primary concern are therefore the measurement errors. The upper bound measurement errors normalized to 1 volt signal amplitude are given as follows. The error in dB is approximately 8.7 times these values. The parameters are as defined earlier.

x-y Position Error

$$E_{xy} = \alpha\pi Pg/2L$$

where P is the in-plane position error.

z Position Error

$$E_z = 2\pi^2 z^2 g/\lambda^2$$

where z is the out-of-plane position error.

Measurement Amplitude Error

$$E_m = N(\alpha - 1)g$$

---

[1] Assuming a halfwave dipole for the probe and perfect reflection.

where N is the measurement nonlinearity in dB of measurement per dB of probe input.

Measurement Phase Error

$$E_\phi = \phi^2 g/2$$

where ϕ is the measurement phase error.

It should be pointed out that the measurement amplitude error is specified in terms of the measurement nonlinearity. A measurement also contains a random non-measurement-dependent term. However, for the highly tapered antenna illumination used, the error contribution due to this term is always negligible relative to the nonlinearity-induced error.

Figure 6.11 shows the effects of measurement errors on both the mainlobe (top scale) and a -40 dB sidelobe (bottom scale). As an example note that a 0.01 dB mainlobe error (or equivalently a 1 dB sidelobe error) results from either a 9.5 mm probe in-plane position error, a 1.8 mm probe out-of-plane position error, a 0.0007 dB/dB measurement amplitude nonlinearity, or a 2.7 degree phase measurement error. It can be seen that these requirements are stringent but not impossible.

6.5 CONCLUSIONS

A wide range of potential measurement techniques were considered. All of them showed some merit. The potential capabilities and accuracies as well as limitations were determined. None of them alone came close to satisfying the full range of testing needs. It is clear that a combination of techniques possibly including the SARF simulation will be necessary in order to fully satisfy all test requirements.
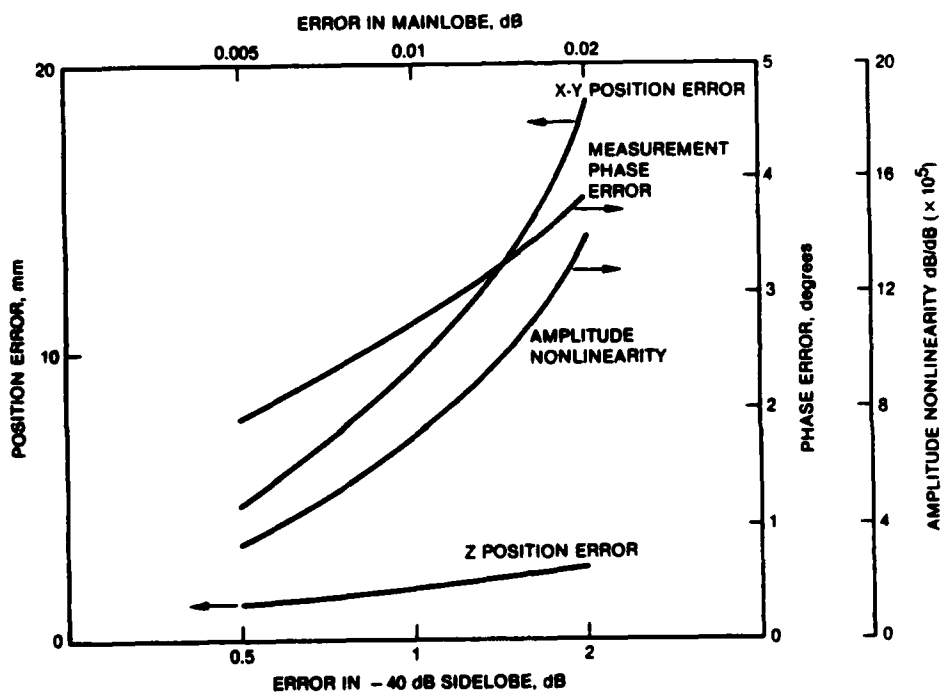
Figure 6.11.   Effect of Errors on Antenna Pattern

Far-field could be a useful technique if airborne or satellite probes can be used. This would introduce some additional complications or considerations to the testing program, but they should not be insurmountable obstacles.

Intermediate range with analytic correction could in principle provide for all of the parameter measurements, but it has several drawbacks. Chief among these drawbacks is that a moving probe must be used or the full antenna must be rotated. It is possible that this technique could be used in conjunction with some others such as frequency scale or test sections. In particular, this technique, in conjunction with the SARF simulation to provide the nominal correction terms, could substantially reduce the range size for the frequency scale or test section

techniques. This would reduce the magnitude of the scaling required in these techniques.

Near-field planar scan is also attractive in many respects, but it cannot be used to test adaptive null depth. Also, tight tolerances are required on the probe carriage. In spite of this restriction it offers so many advantages as discussed earlier that it should be seriously considered as one of the test methods.

Frequency scale was not considered in detail but it is one of the few techniques available for testing adaptive null depth. For this reason it also should be considered as a possible adjunct test method.

The key remaining issue is the feasibility of testing the structural design with the imposed gravity constraints. The cost for planar scan, intermediate range measurements must be evaluated. Also, the achievable fidelity of a scale model and/or SARF simulation model must be verified.

END

FILMED
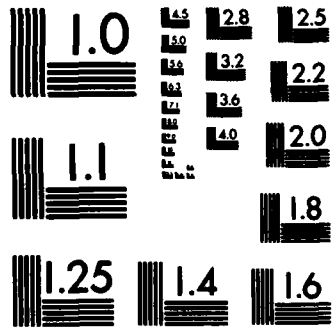
MICROCOPY RESOLUTION TEST CHART
NATIONAL BUREAU OF STANDARDS-1963-A

7   APPLICATION OF SBR FOR GROUND TARGET DETECTION

This task was undertaken with two principal objectives:

1. Assess the feasibility of using SBRs to detect tactical ground targets using Synthetic Aperture Radar (SAR) processing.

2. Examine the Grumman/Raytheon designs and determine how they might best be used in a SAR mode, and what modifications of frequency, beamwidth, bandwidth, altitude, etc., might be desirable to improve their SAR capabilities.

7.1   POTENTIAL FUNCTIONS

One of the potential high-payoff uses of space-based radars against ground (and some ocean) targets is to image the targets under conditions in which optical photography is not possible. A space-based synthetic aperture radar offers the possibility of obtaining high resolution images of regions of interest under all weather conditions. These images could be of military usefulness. Such images could show major terrain features such as mountains, lakes, and rivers. They would also show roads, bridges, buildings, and concentrations of vehicles or equipment. Successive images could be used to identify a buildup of military equipment or a change in deployment. The SAR is not effective in alerting one to approaching aircraft or the movement of ground targets. In fact, the images of many moving targets will be defocused or totally absent from the usual processed image. However, it is possible in special cases to reprocess the original data and recover the image of a moving target if its speed and direction of travel are known. Several potential military uses of a SAR are shown in Fig. 7.1. It should be noted that the potential uses shown which involve moving targets will require special processing, as previously mentioned.

7.2   RESOLUTION REQUIREMENTS

Two things are required in order to identify a target from a SAR image. First, the object of interest must have enough distinct radar

189
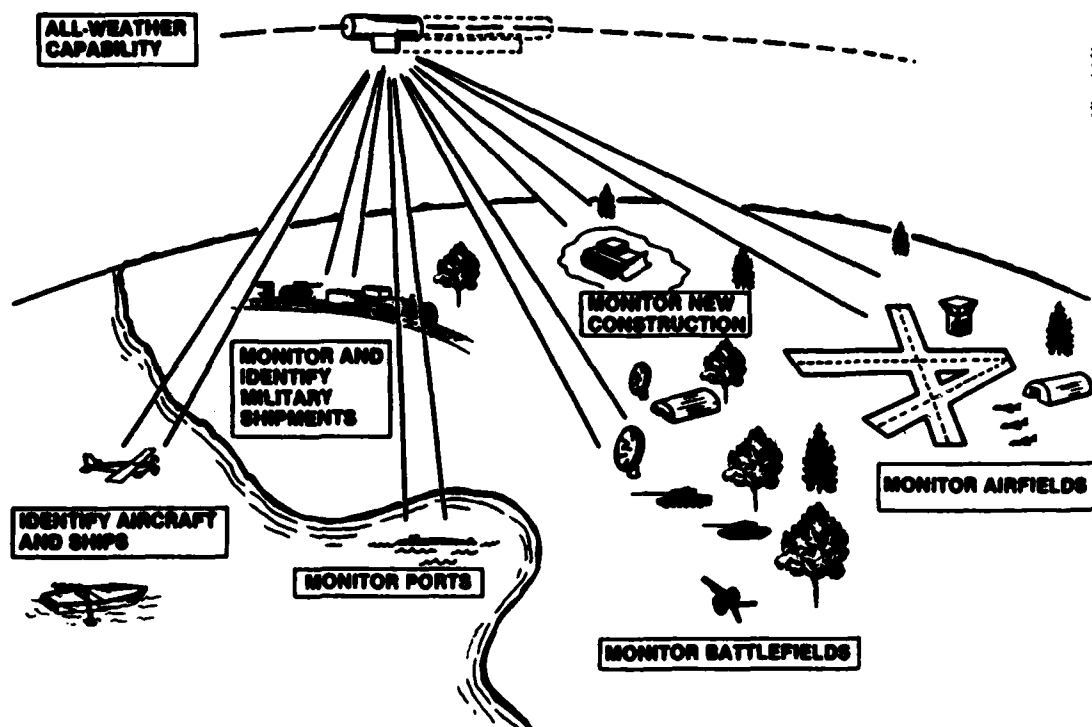
Figure 7.1. Potential Imaging-Radar Military Functions

scatterers for an interpreter to identify the object. Second, the SAR resolution cell must be small enough to separate those individual scatterers.

Although the images achieved from a synthetic aperture radar often seem similar to optical photographs, there are several important differences. In particular, in optical photographs the wavelength is much smaller than resolvable features of interest. Also, the light is generally a mixture of frequencies, incoherent and incident on the object from a number of directions. In a SAR the illumination is monochromatic, coherent, transmitted and received from one "synthetic aperture," and at a wavelength that is often large compared to the visually resolvable and recognizable features of objects. Therefore, whereas a photograph consists of a near continuum of spots of various brightness, a SAR image has usually only a few "hot" spots which emanate from possibly widely separated features of a target. These spots are due to (1)

190

scattering from smooth surfaces which have dimension and radius of curv-
ature large compared with the radar wavelength, and whose surface nor-
mals point toward the synthetic aperture, or (2) surfaces oriented rela-
tive to one another such that incident radiation is reflected back in
the same direction (e.g., a "corner reflector"). Because typical tar-
gets have few such scatterers at radar wavelengths, there is no guaran-
tee that improved resolution will lead to target identification.

It is possible to provide an estimate of the "necessary" as
opposed to "sufficient" resolution for target identification. This is
based on evaluation of the resolution required for optical identifica-
tion of targets.[1] The U.S. Army Night Vision Laboratories have devel-
oped a model for target recognition based on the ratio of resolution to
target dimension. They have defined recognition as follows:

> "Recognition is a level of discrimination between spe-
> cific objects. The class of objects may be all vehicles of
> military interest. The specific objects are tank, APC, etc.
> The difficulty of the discrimination level varies with the
> amount of detail needed to make a distinction between tar-
> gets, which in turn is a function of the number of objects in
> the class and the similarity of the objects. In typical Army
> surface-to-surface scenarios, the discrimination is usually
> between tank, APC, 2-1/2-ton truck, jeep, and man in the
> front, side, or three-quarters aspect. Surface-to-air recog-
> nition is between fixed wing and rotary aircraft. The Naval
> recognition task may correspond to a warship or a cargo ship
> distinction."

Their resulting criteria are shown in Table 7.1. For example, the
necessary resolution for a 95% probability of recognition of an object
10 m long would be 0.6 to 0.8 m. Therefore, if the object had a suf-
ficient number of scatterers, we could expect to recognize the object if
our SAR resolution was about 0.6 m or less.

---

[1] Night Vision Laboratory Static Performance Model for Thermal Viewing
Systems, U.S. Army Electronics Command, Night Vision Lab., ECOM-7043,
April 1975.

TABLE 7.1

PROBABILITY OF TARGET RECOGNITION

Probability of Recognition	Target Dimension/ Resolution
1.0	18-24
0.95	12-16
0.80	9-12
0.50	6-8
0.30	4.5-6
0.10	3-4
0.02	1.5-2

Clearly, the whole subject of target recognition is very complex. We do not intend to address it here in detail. For our purposes we will simply use Table 7.1 as a rule of thumb.

7.3 SYNTHETIC APERTURE CHARACTERISTICS

A synthetic aperture radar achieves its desirable accuracy with a very high resolution in range and one angle, the azimuth angle. The high resolution in the azimuth angle is achieved by forming a large effective horizontal aperture, and thus a very narrow effective azimuth beam by means of post processing of the reflected signal. The large effective aperture is obtained by moving the antenna while a coherent train of pulses is transmitted and received. The phase and amplitude of the pulses are stored and subsequently coherently processed as though they had been transmitted from one long array antenna. The effective beamwidth which results is $\lambda/(2L \sin \theta)$ where λ is the radar wavelength, L is the distance between the position of the actual antenna at the beginning and end of the data taking period, and θ is the angle between the antenna velocity vector in the middle of the data taking

period and the direction to the target at that time. In the usual situation θ is 90°. This is the side-looking strip mapping mode. The squint mode is when $\theta \neq 90°$. A common mode is the forward-looking SAR where $\theta < 90°$. In other modes of operation, the beam is scanned in order to increase the time of dwell and thus increase the synthetic aperture. This improves the resolution in some areas at the expense of reduced total coverage. In particular, one extreme is the spotlight mode where the beam remains fixed on a particular area as the radar passes. This mode produces a map which is the size of the beam footprint, but with resolution much better than that achieved in the strip mapping mode. The side-looking strip mapping and spotlight modes are illustrated in Figs. 7.2 and 7.3, respectively.

The resolution shown for the strip mapping mode is appropriate for aircraft or low-altitude satellite radars. For higher altitude satellites, the curvature of the earth becomes an important factor. Description of the actual resolution capability is, in general, complex and depends on the satellite altitude as well as the angle of incidence of the signal in the vicinity of the ground. For our purposes, a good first order approximation for the azimuth resolution is given by

$$\delta_{az} \approx \frac{D}{2(1 + H/r_e)}$$

where D = antenna horizontal dimension

H = satellite altitude

r_e = radius of earth

As can be seen for high altitudes, the resolution departs significantly from the low altitude value of D/2 . The satellite curved path also impacts many other of the standard SAR equations. A careful analysis should take this into account. For this review, we will restrict
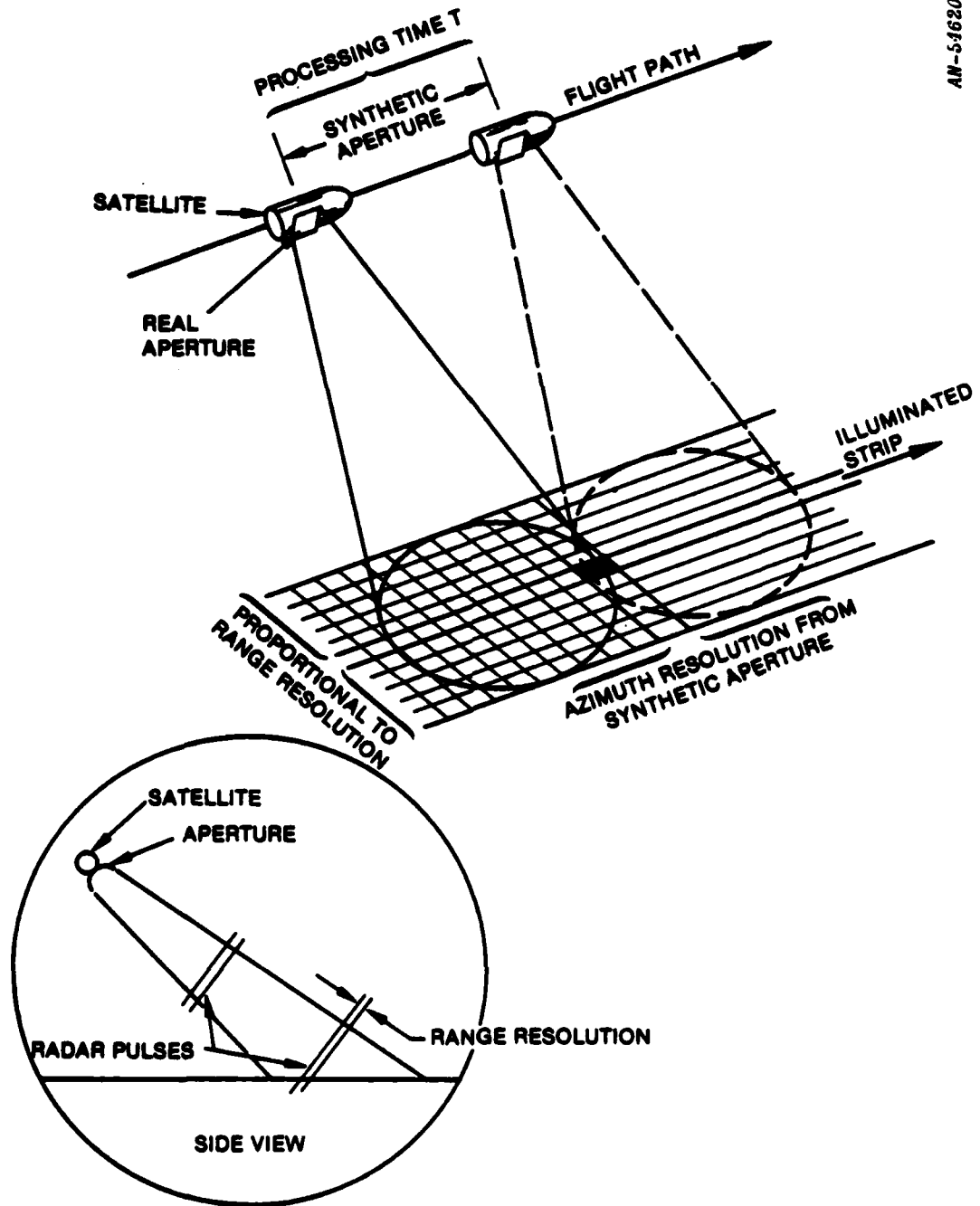
Figure 7.2. Synthetic-Aperture Strip Mapping

194
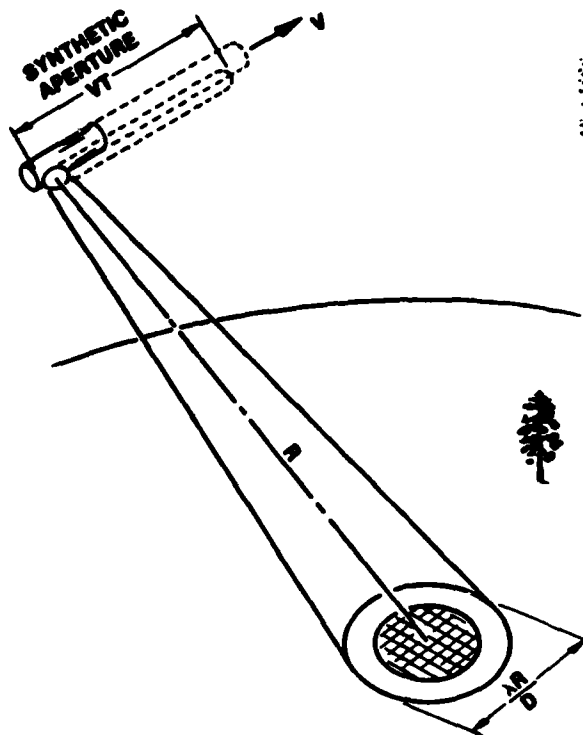
$$\text{RESOLUTION} = \left(\frac{\lambda R}{2V}\right)\left(\frac{1}{T}\right)$$

Figure 7.3. Synthetic-Aperture Spotlight Mapping

ourselves to low altitude (flat earth) approximations. In this case, the basic side-looking SAR equations[1-5] are given in Table 7.2.

It should be noted that bandwidth requirements are severe for high-resolution SAR. At a low grazing angle the bandwidth for 2-m resolution is approximately 75 MHz or better (depending on matched-filter

[1] L.J. Cutrona, "Synthetic Aperture Radar," Chapter 23 of Radar Handbook, M.I. Skolnik (ed.), McGraw-Hill Book Company, 1970.

[2] R.O. Harger, Synthetic Aperture Radar Systems, Academic Press, 1970.

[3] J.J. Kovaly (ed.), Synthetic Aperture Radar, Artech House, 1976.

[4] W.C. Curtis, J.J. Kovaly, and E. Brookner, "Synthetic Aperture Radar Techniques," Part 4 of Radar Technology, Eli Brookner (ed.), Artech House, 1977.

[5] J.J. Kovaly, "High Resolution Radar Fundamentals," Chapter 17 in Radar Technology, Eli Brookner (ed.), Artech House, 1977, pp. 248-249.

TABLE 7.2
BASIC SIDE-LOOKING SAR EQUATIONS

List of Symbols

c	Speed of Light	T_n	Noise Temperature
D_h	Real Aperture Width	V	Radar Speed
k	Boltzmann's Constant	δ_θ	Azimuth Resolution[*]
L	Losses	δ_r	Ground Range Resolution[†]
PRF	Pulse-Repetition Frequency	λ	Wavelength
R	Range	σ_o	Albedo
S/N	Signal-to-Noise Ratio	ψ	Grazing Angle

Parameter	Equation
Integration Time	$\lambda R/2V\delta_\theta$
Doppler Bandwidth (Minimum PRF)	V/δ_θ
Synthetic Aperture Length	$\lambda R/2\delta_\theta$
Range Ambiguity	$c\delta_\theta/2_V$
Bandwidth[§]	$c/2\delta_\theta \cos \psi$
Azimuth Angle Subtended	λ/δ_θ
Power Aperture[2]	$8\pi R^3 kT_n(S/N)V/\sigma_o\delta_r$

---

[*] For (focused) strip mapping, $\delta_\theta = D_h/2$.
[†] $\sigma_r = \Delta R \cos \psi$, where ΔR = range resolution .
[§] For square resolution ($\delta_r = \delta_\theta$).

weighting). At a high grazing angle such as used by Seasat-A (70 deg), the bandwidth required to achieve the resolution on the ground (rather than along the slant range) is about 220 MHz (75 MHz/cos 70°). Such a very wide bandwidth may be difficult to achieve in space-based phased array radars.

Other Issues. During the SAR integration period, the earth rotates under the satellite, causing a range migration. This migration of range-resolution cells, illustrated in Fig. 7.4, is highly sensitive to latitude, and thus a very precise knowledge of satellite attitude is needed to process out the effect. As an example, an S-band radar at an altitude of 500 n mi, which requires an integration time of 4.7 s to achieve a 2-m resolution in angle, will have a migration of 725 2-m range cells during the 4.7 s (at a latitude where the earth rotation rate is 600 kt).

As an alternative to knowing the satellite attitude very precisely, processing can be performed on the spectrum of the return signal to determine the earth rotation rate; this technique is used in Seasat-A processing.

On the other hand, satellite motion is very smooth compared to aircraft motion, so that satellite-based SARs do not experience the phase jitter problem encountered by aircraft SARs.
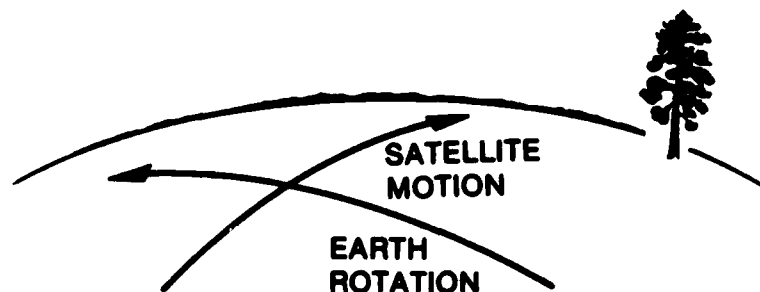
Figure 7.4. Range Migration Due to Earth Rotation

7.4 DATA PROCESSING

The SAR maps require a great deal of processing. This processing can be done on board or on the ground as illustrated in Fig. 7.5. Since the number of bits required to transmit the raw radar video is about the same as the number of bits required to transmit a processed image, there is no net communication advantage in either case. Because of the large amount of processing and the possibility of using adaptive processing to recover images of moving targets, there seems to be an advantage to ground processing.

On the other hand, one application where the processing might best be performed on board as depicted in Fig. 7.5 is where the image is to be transmitted directly to a number of users, either in a tactical situation, or to ships or aircraft. The ability to provide space-qualified real-time data processors for SAR applications is being addressed by the
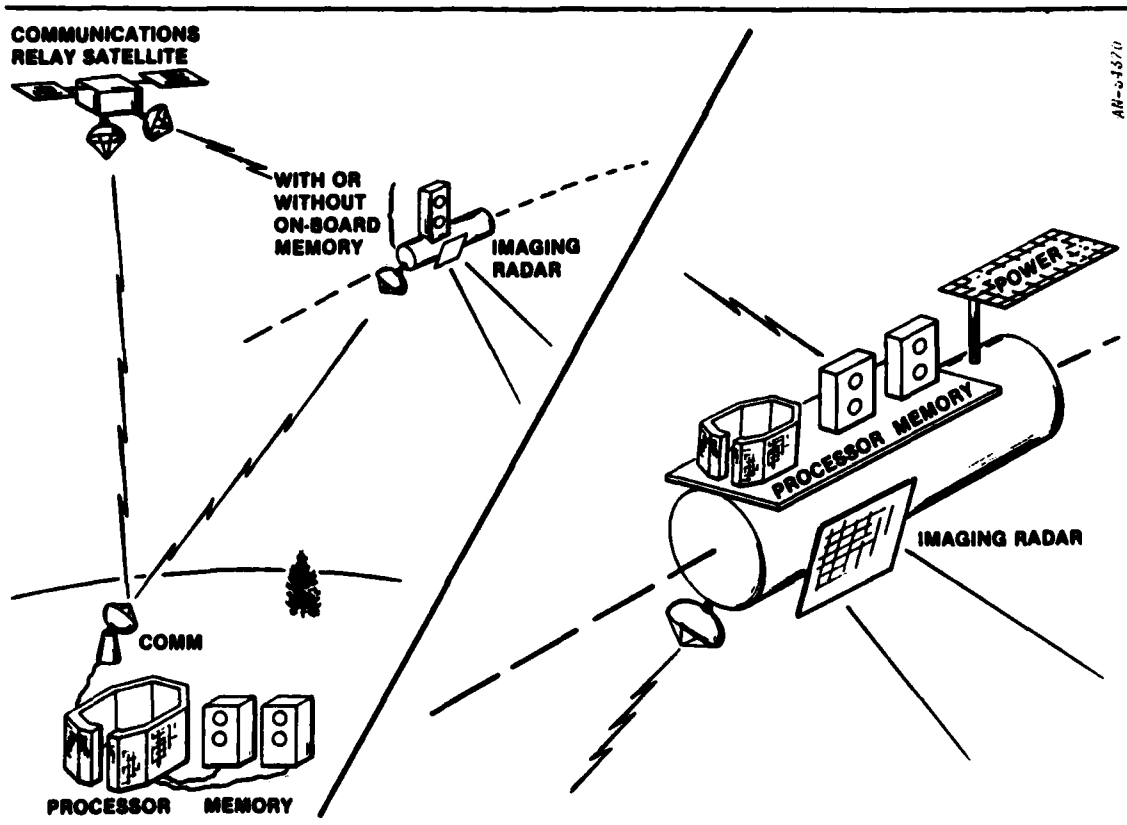

Figure 7.5. Satellite-borne Imaging Radar--Data Processing Options

ARPA-sponsored Advanced On-Board Signal Processor program being conducted by Raytheon. Although promising techniques are emerging from the program, it is not yet clear that sufficient long-term reliability can be achieved, considering the very large amounts of processing required.

A satellite-borne SAR might reduce its processing load by occasionally performing spotlight mapping of specific regions, and stretching the processing out over a much longer period of time (minutes) than it takes to collect the data (seconds). Spotlight mapping, however, because of its finer resolution, has additional processing problems over lower resolution strip mapping. The principal problem is that the scatterers being mapped do not remain in the same range-Doppler cell during the processing period, causing a smearing of the image. As a first approximation, the image aberrations caused by motion through the resolution cells are (1) cross-range-dependent astigmatism, and (2) a range-dependent cross-range focus error. These are sometimes called "range walk" and "variable range rate," respectively.

A solution to the problem is described by Jack Walker, head of the Technical Departments of Radar and Optics Division of the Environmental Research Institute of Michigan (ERIM), in his Ph.D. dissertation.[1] The return signal is stored in <u>polar format</u> (rather than the usual rectangular format) and the result is subsequently processed by a standard rectangular two-dimensional Fourier transform. Additional processing is required for interpolation in obtaining a rectangular set of points from a set of points stored in polar format.

Although there are many options for processing SAR data, Kirk[2] considered five likely algorithms and derived the bulk memory and total

---

[1] J.L. Walker, <u>Range-Doppler Imaging of Rotating Objects</u>, University of Michigan Report 671000-4-X, Ann Arbor Michigan, 1974.

[2] J.L. Kirk, Jr., "A Discussion of Digital Processing in Synthetic Aperture Radar," <u>IEEE Transactions on Aerospace and Electronic Systems</u>, May 1975.

arithmetic rate for each. These are given in Table 7.3. These relationships will be used in Sec. 7.6 when they will be applied to a potential modification of a currently proposed conventional space-based radar.

7.5 SEASAT-A

The feasibility of satellite-borne SAR has been demonstrated by the Seasat-A synthetic-aperture-radar satellite, developed by NASA and JPL.[1] The resolution of this radar--25 meters--is, however, insufficient to perform any of the defined military functions. An example image from this radar of the Santa Barbara (California) Channel is shown in Fig. 7.6. It is interesting to note that this image could have (and may have) been taken at night or on a completely foggy day. No clouds are shown in the image; the "clouds" over the ocean area are actually waves. This image took approximately 14 hours to process digitally.

The objective of the Seasat-A SAR system was to image ocean waves. The radar gathered data for three months during 1978 before the satellite malfunctioned. A large amount of data was obtained; by April 1979, about ten percent of this data had been processed into images.

Seasat-A had no on-board data storage or processing; the return radar signal was transmitted to ground-station networks on a 20-MHz-bandwidth analog data link. All signals were recorded for later non-real-time processing. Most of the processing has been optical, but some of it has been digital, which gives a slightly better resolution.

The Seasat-A actually has a resolution that is approximately four times better than the specified 25 m resolution. Four separate radar images are averaged to reduce the speckly nature of the radar images. The resulting image has a 25-m resolution.

---

[1] R. L. Jordan and D. H. Rogers, "The Seasat-A Synthetic Aperture Imaging Radar System," Wescon Technical Papers, Volume 20, 1976.

TABLE 7.3

SAR PROCESSING ALGORITHM SUMMARY

Algorithm	Bulk Memory	Total Arithmetic Rate
Correlator	$2k_a N_F N_R$	$N_F N_R f_r$
Prefilter Plus Correlator	$2k_a N_F N_R$	$N_F f_r + (K_{OS} K_S N_F^2 N_R / \Delta T)$
Multiple Prefilters Plus Correlator	$2k_a N_F N_R$	$2(K_{OS} K_S f_r / \Delta T)^{1/2} N_F N_R$
Prefilter Plus Two-Stage Correlator	$2k_a K_{OS} K_S N_R [M + (M + 3)N_F/2M]$	$N_R f_r + (2K_{OS} K_S N_R N_F^{3/2}/\Delta T)$
Prefilter Plus FFT	$2k_a K_{OS} K_S N_F N_R$	$N_R f_r + (K_{OS} K_S N_F N_R \log_2 K_{OS} K_S N/2\Delta T)$

where

N_F = number of Doppler filters

N_R = number of range cells

f_r = PRF

K_{OS} = prefilter oversample factor (~1.7)

K_S = synthetic array weighting constant (~1.2)

M = number of first-stage correlator filters

ΔT = coherent integration time

N = number of radar interpulse periods

NOTE: The number of amplitude bits k_a will vary slightly among the algorithms and, also, depending upon whether the storage is pre-correlator or in the integrator. The first three algorithms are for integrator storage and the last two are for precorrelator storage.
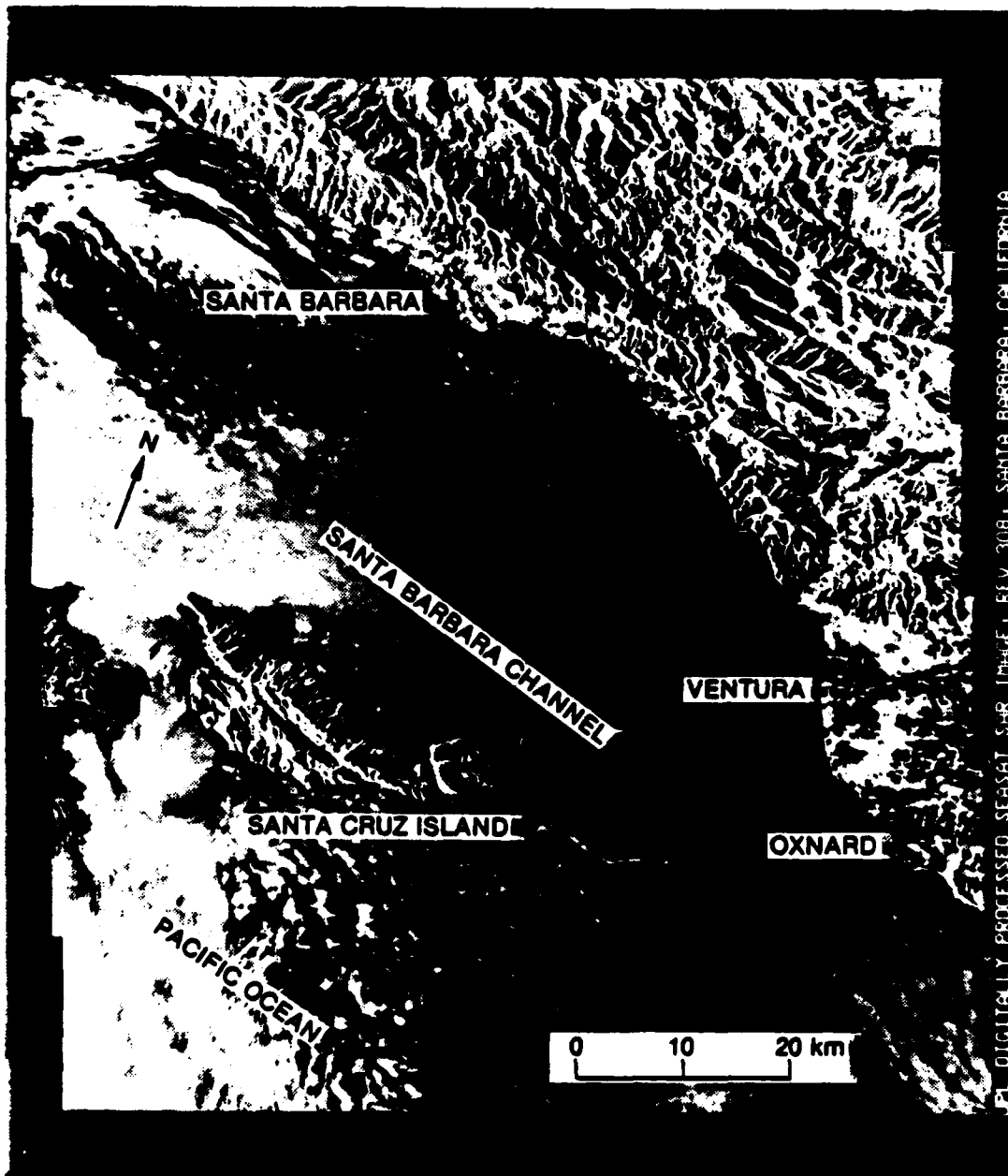
Figure 7.6. Seasat-A SAR Image of Santa Barbara (California) Channel.
Resolution is 25 meters. (Courtesy of Jet Propulsion
Laboratory)

The parameters of the Seasat-A SAR are listed in Table 7.4.

7.6   ADAPTATION OF REPRESENTATIVE DESIGN

Here we consider the implications of adapting a representative design for a conventional space-based radar to a SAR application. The system characteristics are given in Table 7.5.

The most obvious implication of the representative design from the point of view of a SAR application is its 1 MHz bandwidth. At a 45° ground inclination angle, the resulting ground cross-track resolution would be 212 m. The azimuth resolution for strip mapping would be given by

$$\delta_{az} = \frac{D}{2(1 + H/r_e)} = 4.8 \text{ m}$$

TABLE 7.4

CHARACTERISTICS OF SEASAT-A SAR SYSTEM

Satellite Altitude	800 km
Frequency	1.28 GHz
Wavelength	0.235 m
RF Bandwidth	19 MHz
Transmit Pulse Length	33.4 μs
Time-Bandwidth Product	634
Radar Transmitter Peak Power	800 W
Radar Transmitter Average Power	44 W
Data Recorder Bit Rate	100 megabit/s
Data Recording Pass Duration	10 min
Radar DC Power	500 W
Radar Antenna Dimensions	11 by 2.3 m
Radar Antenna Gain	35 dB

TABLE 7.5

REPRESENTATIVE SBR DESIGN

<u>Satellite</u>

Altitude	1,667 km (900 n mi)
Velocity	7 km/s
Period	2 hr
Orbit	Circular polar

<u>Radar</u>

Band	S
Wavelength	0.1 m
Power	
Peak	2.5 kW
Average	1.2 kW
Bandwidth	1 MHz
Antenna Diameter	12.2 m
Noise Temperature	410°K
Losses	10 dB
Communication Link Bandwidth	45 Mbit/s

The effect of unequal range and azimuth resolution on target recognition is not obvious. Most human visual experience has been with roughly equal resolution in two dimensions. However, a resolution of 212 m is inadequate for any military use, whereas 4.8 m could be of some military use. It would therefore seem that it would be desirable to reduce the range resolution cell to the order of the azimuth resolution cell. This would require an increase in the bandwidth to 44 MHz. The resulting resolution cell would be 4.8 m × 4.8 m.

From the discussion of Sec. 7.2 we know that in order to recognize a target with a probability of 80%, the target must typically be of a

length of about 10 resolution cells. Therefore, in this case we could expect to be able to recognize objects of dimension 48 m or more. Clearly, this would be of military use, but one would desire much finer resolution for most tactical applications. Finer resolution in azimuth could be achieved by use of the spotlight mode as discussed earlier. A comparable improvement in range resolution would require a further increase in the bandwidth.

From Table 7.2 we can write the expression for the signal-to-noise ratio as

$$S/N = \frac{PA^2 \sigma_o \delta_r}{8\pi R^3 2kT_n LV}$$

With $\delta_r = 4.8$ m , and using an earth albedo (σ_o) of -20 dB, the S/N is approximately 44 dB. This radar is clearly over-powered for the SAR application.

We now consider the data processing and communication require-ments. The first thing to do is to compute the coverage rate. The coverage swath width is given by the product of range times beamwidth divided by the sine of the incidence angle, or:

$$W_g = R\theta_b/\sin \theta$$

$$= (2.153 \text{ km})(0.008 \text{ rad})/\sin 45°$$

$$= 24 \text{ km}$$

The rate of coverage is the product of W_g and the ground velocity of the beam which is given by

$$V_g = 5.5 \text{ km/s}$$

The resulting coverage rate is $1.32 \times 10^8 \text{ m}^2/\text{s}$. For a square resolution element of 4.8 m the rate of resolution cells is $5.7 \times 10^6/\text{s}$. Assuming a 5-bit measurement, the data rate becomes 29 Mbit/s. This is considerably less than the postulated 45 Mbit/s communication capability.

The data processing requirements are determined by using Kirk's[1] algorithms. The most likely processor would be a prefilter with fast Fourier transform. In order to specify the memory capacity and arithmetic rate we must first determine the value of the PRF, the number of range gates, N_R, and the number of Doppler filters, N_F. The other constants are given by Kirk.[1]

The high PRF bound is given by the range ambiguity constraint

$$\text{PRF} < \frac{C}{2(R_F - R_N)}$$

where the far and near ranges of the beam to the ground R_F and R_N are 2,161 and 2,144 km, respectively. The result is

$$\text{PRF}_{high} < 8.8 \text{ KHz}$$

The low PRF bound is given approximately by twice the platform velocity divided by the antenna length

$$\text{PRF}_{low} < \frac{2V}{L} \approx 1 \text{ KHz}$$

For this example we use 6 KHz.

---

[1] J. Kirk, op. cit.

The number of range gates N_R is given by

$$N_R = \frac{W_2}{\delta_r \sin \theta_1} \approx 7 \times 10^3$$

The number of filters is equal to the azimuth compression ratio

$$N_F = \frac{L}{r_a} = 5 \times 10^3$$

The memory capacity which is given by

$$2K_a K_{OS} K_S N_F N_R$$

becomes 8×10^8 bits. The arithmetic rate which is given by

$$N_R f_r + (K_{OS} K_S N_F N_R \log_2 K_{OS} K_S N / 2\Delta T)$$

becomes $7.5 \times 10^8/s$. To put these numbers in perspective, the Raytheon Company is designing integrated array computing elements for DARPA and the Air Force under the Advanced On-Board Signal Processor program. These chips will be able to perform 4×10^7 arithmetic operations per second, with a prime power requirement of 0.5 W per chip. A small number of chips operating in parallel could easily meet the arithmetic requirement using only a few watts of prime power. The storage requirement of 8×10^8 is likewise large but certainly within current technology.

To summarize, in terms of the SAR mission, the representative space-based radar is adequate or over-designed in all areas except bandwidth, where it is woefully inadequate. In particular, since its expected S/N was shown to be approximately 44 dB, its power-aperture gain

product is of the order of 25 dB more than required. Data processing could be done on board or on the ground. This could easily be accomplished with the specified 4.8 m × 4.8 m resolution and appears to be within the near term state of the art for resolution cells of the order of 2 m × 2 m. The communication requirement for a 4.8 m × 4.8 m resolution strip mapping mode is 29 M bit/s, considerably less than the 49 M bit/s specified. Spotlight mode operation would offer more resolution with no increase in communication bandwidth because of the longer time available for transmission. The radar bandwidth required to achieve 4.8 m of resolution is 44 MHz. This is a factor of 44 times the current bandwidth. Such a change would have a major impact on the transmitter, receiver, and antenna.

It must be concluded that the representative space-based radar design is not an appropriate one for SAR applications.

MISSION
of
Rome Air Development Center

RADC plans and executes research, development, test and selected acquisition programs in support of Command, Control Communications and Intelligence (C^3I) activities. Technical and engineering support within areas of technical competence is provided to ESD Program Offices (POs) and other ESD elements. The principal technical mission areas are communications, electromagnetic guidance and control, surveillance of ground and aerospace objects, intelligence data collection and handling, information system technology, ionospheric propagation, solid state sciences, microwave physics and electronic reliability, maintainability and compatibility.

END

FILMED

11-83

DTIC